N-1835

NCEL

Technical Note

October 1991

By T.A. Shugar, T.J. Holland, and L.J. Malvar

Sponsored By Office of Naval Technology

ADVANCED FINITE ELEMENT ANALYSIS OF DRYDOCKS AND WATERFRONT FACILITIES - A TECHNOLOGY ASSESSMENT

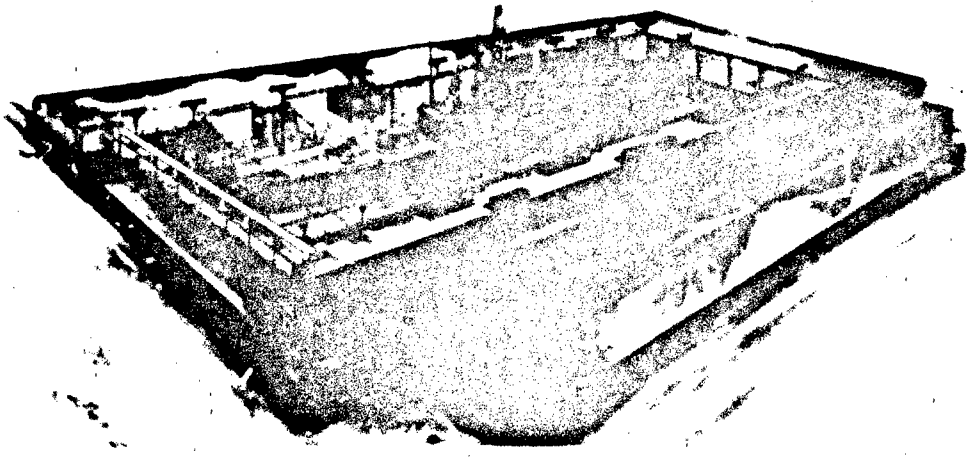

ABSTRACT Various models of Navy waterfront structures are presented and employed to assess their effectiveness in predicting the vulnerability of these systems to operational and earthquake loads. The emphasis is on application of three-dimensional finite element models to reinforced concrete structural analysis. Results indicate that dynamic analysis is important in the calculation of the structural response of both a drydock and a blocked vessel in drydock. The primary natural frequencies and natural mode shapes for a drydock are longitudinal deformation modes which cannot be predicted by current methodology based upon statically equivalent analysis of two-dimensional models. Further results from nonlinear analysis provide new insight into the behavior of the drydock/caisson seal for hydrostatic loads, which is dramatically different from that which underlies current design and maintenance procedures. Similarly, results from a three-dimensional nonlinear static analysis of a scale model of a reinforced concrete pier deck, subjected to punching shear failure loads, are shown to compare well with experimental data. Modern three-dimensional finite element technology is appropriate for analysis of waterfront structures.

NAVAL CIVIL ENGINEERING LABORATORY PORT HUENEME CALIFORNIA 93043-5003

METRIC CONVERSION FACTORS

Approximate Conversions to Metric Measures

Symbol	When You Know	Multiply by	To Find	Symbol
		LENGTH		
in	inches	*2.5	centimeters	cm
ft	feet	30	centimeters	cm
yd	yards	0.9	meters	m
mi	miles	1.6	kilometers	km
		AREA		
in^2	square inches	6.5	square centimeters	cm^2
ft^2	square feet	0.09	square meters	m^2
yd^2	square yards	0.8	square meters	m^2
mi^2	square miles	2.6	square kilometers	km^2
	acres	0.4	hectares	ha
		MASS (weight)		
oz	ounces	28	grams	g
lb	pounds	0.45	kilograms	kg
	short tons (2,000 lb)	0.9	tonnes	t
		VOLUME		
tsp	teaspoons	5	milliliters	ml
Tbsp	tablespoons	15	milliliters	ml
fl oz	fluid ounces	30	milliliters	ml
c	cups	0.24	liters	l
pt	pints	0.47	liters	l
qt	quarts	0.95	liters	l
gal	gallons	3.8	liters	l
ft^3	cubic feet	0.03	cubic meters	m^3
yd^3	cubic yards	0.76	cubic meters	m^3
		TEMPERATURE (exact)		
°F	Fahrenheit temperature	5/9 (after subtracting 32)	Celsius temperature	°C

*1 in = 2.54 (exactly). For other exact conversions and more detailed tables, see NBS Misc. Publ. 286, Units of Weights and Measures, Price $2.25, SD Catalog No. C13.10:286.

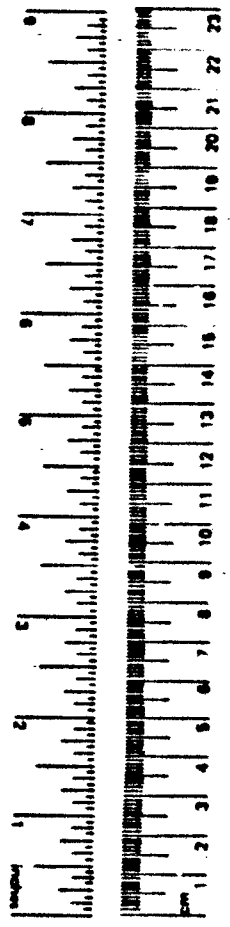

Approximate Conversions from Metric Measures

Symbol	When You Know	Multiply by	To Find	Symbol
		LENGTH		
mm	millimeters	0.04	inches	in
cm	centimeters	0.4	inches	in
m	meters	3.3	feet	ft
m	meters	1.1	yards	yd
km	kilometers	0.4	miles	mi
		AREA		
cm^2	square centimeters	0.16	square inches	in^2
m^2	square meters	1.2	square yards	yd^2
km^2	square kilometers	0.4	square miles	mi^2
ha	hectares (10,000 m^2)	2.5	acres	
		MASS (weight)		
g	grams	0.035	ounces	oz
kg	kilograms	2.2	pounds	lb
t	tonnes (1,000 kg)	1.1	short tons	
		VOLUME		
ml	milliliters	0.03	fluid ounces	fl oz
l	liters	2.1	pints	pt
l	liters	1.06	quarts	qt
l	liters	0.26	gallons	gal
m^3	cubic meters	35	cubic feet	ft^3
m^3	cubic meters	1.3	cubic yards	yd^3
		TEMPERATURE (exact)		
°C	Celsius temperature	9/5 (then add 32)	Fahrenheit temperature	°F

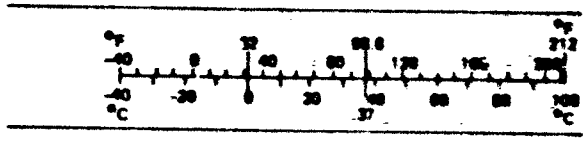

REPORT DOCUMENTATION PAGE

Form Approved
OMB No. 0704-018

1. AGENCY USE ONLY (Leave blank)	2. REPORT DATE	3. REPORT TYPE AND DATES COVERED
	October 1991	Interim: FY88 - FY90

4. TITLE AND SUBTITLE
ADVANCED FINITE ELEMENT ANALYSIS OF DRYDOCKS AND WATERFRONT FACILITIES - A TECHNOLOGY ASSESSMENT

5. FUNDING NUMBERS
PR - RM33F60-001-02-06-010
WU - DN668013

6. AUTHOR(S)
T.A. Shugar, T.J. Holland, and L.J. Malvar

7. PERFORMING ORGANIZATION NAME(S) AND ADDRESS(ES)
Naval Civil Engineering Laboratory
Port Hueneme, CA 93043-5003

8. PERFORMING ORGANIZATION REPORT NUMBER
TN - 1835

9. SPONSORING/MONITORING AGENCY NAME(S) AND ADDRESS(ES)
Chief of Naval Research
Office of Naval Technology
Arlington, VA 22217-5000

10. SPONSORING/MONITORING AGENCY REPORT NUMBER

11. SUPPLEMENTARY NOTES

12a. DISTRIBUTION/AVAILABILITY STATEMENT
Approved for public release; distribution unlimited.

12b. DISTRIBUTION CODE

13. ABSTRACT *(Maximum 200 words)*

Various models of Navy waterfront structures are presented and employed to assess their effectiveness in predicting the vulnerability of these systems to operational and earthquake loads. The emphasis is on application of three-dimensional finite element models to reinforced concrete structural analysis. Results indicate that dynamic analysis is important in the calculation of the structural response of both a drydock and a blocked vessel in drydock. The primary natural frequencies and natural mode shapes for a drydock are longitudinal deformation modes which cannot be predicted by current methodology based upon statically equivalent analysis of two-dimensional models. Further results from nonlinear analysis provide new insight into the behavior of the drydock/caisson seal for hydrostatic loads, which is dramatically different from that which underlies current design and maintenance procedures. Similarly, results from a three-dimensional nonlinear static analysis of a scale model of a reinforced concrete pier deck, subjected to punching shear failure loads, are shown to compare well with experimental data. Modern three-dimensional finite element technology is appropriate for analysis of waterfront structures.

14. SUBJECT TERMS	15. NUMBER OF PAGES
Finite element models, structural dynamics, structural analysis, drydocks, steel caissons, reinforced concrete pier deck, concrete material models, waterfront facilities	150
	16. PRICE CODE

17. SECURITY CLASSIFICATION OF REPORT	18. SECURITY CLASSIFICATION OF THIS PAGE	19. SECURITY CLASSIFICATION OF ABSTRACT	20. LIMITATION OF ABSTRACT
Unclassified	Unclassified	Unclassified	UL

CONTENTS

INTRODUCTION

Large structural/geotechnical systems generally represent a substantial capital investment and a substantial strategic resource for the Navy. They may also be classified as essential and/or high-risk facilities. Correspondingly, they require special attention in engineering design, hazard mitigation and maintenance measures, and vulnerability studies. At the same time, substantial technology in structural analysis capability exists due to advances in computational structural mechanics. Unfortunately, this existing technology is relatively untapped regarding approaches to design, analysis, and vulnerability assessment of the Navy's facilities. Experience in its application must be gained. This problem is addressed in this report.

OBJECTIVE

The objective of this study was to demonstrate the effectiveness of existing modern computer-based structural analysis methods by applying them to several current technical problems involving naval waterfront facilities.

BACKGROUND

Uninterrupted operation of drydocks and piers is essential to readiness of fleet combatants. During war, waterfront systems supporting repair of fleet combatants would be threatened by air forces and underwater swimmers. Global Wargame 86 indicated that fleet operational limitations could result from current graving drydock vulnerability. During peacetime, ship repairs can be catastrophically interrupted by damage incurred from a major seismic event. There is a 5 percent annual

probability of a major seismic event (>7 Richter scale) with the potential of severely damaging graving drydocks at Puget Sound, Mare Island, Pearl Harbor, Hunters Point, and Long Beach Naval Shipyards, and San Diego Naval Station. The minimum replacement cost for a small drydock has been estimated to be $140 million. The potential damage to docked ships and the impact of disruption of fleet overhaul cycles is incalculable.

For the sake of brevity, this report excludes consideration for the important problem of Naval Shore Facilities subject to blast loads. This is the subject of a separate report entitled, "Three-Dimensional Structural Analysis Methodology for Navy Explosive Safety Facilities - A Technology Assessment" (Shugar, et al., 1992).

STRUCTURAL ANALYSIS SUBSYSTEM MODELS STUDIED

One-dimensional continuous models of drydocks and their natural frequencies and mode shapes are discussed and demonstrated initially in this report. Studies of these preliminary models provide orientation and perspective on the behavior attainable from more complex three-dimensional finite element models.

An assessment is made of two-dimensional models of drydocks. These models may be said to be the present technical basis for structural engineering aspects of drydock certification. They are useful in providing needed experience in application of finite element technology. However, the assumptions upon which they are based are often not satisfied.

The safety of a blocked vessel in drydock is the paramount concern of the drydock certification process. It follows that, technology permitting, the blocked vessel be viewed as a drydock subsystem so that its dynamic response is coupled with the dynamic response of the drydock itself allowing the response to be calculated more accurately. A simplified two-dimensional lumped parameter model of a blocked vessel in drydock is presented and its dynamic response is computed relative to a simplified strong motion earthquake load to demonstrate this modeling concept.

To demonstrate their analytical effectiveness, three-dimensional finite element models of drydocks and drydock subsystems, particularly a steel caisson, are investigated. The effective construction of three-dimensiona finite element models is discussed.

A detailed three-dimensional finite element model of a drydock caisson subsystem was developed. Analyses using this model are presented. They include a study of the contact forces to which the seal is subjected due to typical hydrostatic load conditions. Also, natural vibrations of the caisson model are presented and discussed.

A simplified three-dimensional finite element model of a reinforced concrete drydock subsystem was constructed based upon plate bending finite elements. The model accounts for the variable thickness of the drydock's sidewalls and endwalls and also includes the steel caisson as part of the subsystem. In a study of the drydock subsystem's natural vibration characteristics, the first ten natural frequencies and natural mode shapes were calculated to demonstrate that the basic frequencies of response and modes of deformation likely to participate in any dynamic response to earthquake excitation are different from those predicted by two-dimensional models.

Other waterfront facilities that impact fleet readiness are piers and wharfs. A three-dimensional nonlinear analysis of a 1/3-scale laboratory model of a reinforced concrete pier was conducted. This analysis evaluates the ability of current finite element technology in accurately reproducing the behavior of highly nonlinear materials such as reinforced concrete. To this end, concrete and steel rebars were modeled separately in what is known as a discrete reinforcement model. The development of cracking in the concrete was followed, together with the associated stiffness degradation and nonlinear load-displacement history.

STRUCTURAL ANALYSIS SOFTWARE

Though the demonstration analyses described above are the primary subject of this report, they are regarded as preliminary to the development

of a specialized nonlinear structural analysis software system for selected large structural/geotechnical systems in naval facilities.

The overall goal is to adapt appropriate modern methods in computational mechanics and combine them with several more recent products from Navy-sponsored basic research in structural modeling to produce a special purpose, advanced nonlinear structural analysis system. Some of these basic research products and their transition potential were reviewed in "An Evaluation of Numerical Algorithms for the Nonlinear Dynamic Analysis of Large Soil Structure Systems" (Bayo, 1987).

The flexibility to effectively and expeditiously address and determine the essential structural behavior of any critical facility subjected to strong motion earthquake and severe blast loads is a desirable goal, and the proposed special purpose software system will facilitate achievement of that goal.

While commercially-available technology is potent, it very often does not strictly apply to complex Navy systems. As a result, the technical problem must inevitably be modified to accommodate the problem specification requirements of existing commercial structural analysis software products. These products have been developed for a very large market place in which the Navy is but a single customer. They provide a general purpose capability and hence, they often do not strictly apply to specific Navy problems. Experience has born this out. The contracting cycle is not suited to expeditious development and procurement of a new or modified commercial capability. Hence, timely acquisition of the required capability most often does not occur. It is also true that in nonlinear problems the required capability often cannot be well-defined until several attempts to solve the problem have been made. All this points to the need for enhanced response via a flexible capability in nonlinear structural analysis. A software framework designed to provide guidance toward achieving this capability was developed. Some of the issues considered are briefly summarized in the following paragraphs. A full description is presented in "A Software Development Specification for Nonlinear Structural Analysis" (Landers, 1990).

Structural engineers should exploit recent advances in computer science with regard to hardware and software. Existing batch oriented environments are conducive to creating inadvertent errors in input data which negate long costly analysis computer runs. Further, they make the development and testing of new methodologies and algorithms very difficult. Even with interactive text editors, the construction and debugging of new concepts and ideas often involves many iterations of the "edit-compile-debug" cycle.

Low-cost work stations equipped with powerful 32-bit processors, high-resolution graphic displays, and inexpensive networking facilities are appearing rapidly while the cost of raw processing power is dropping rapidly. Further, and significantly, vendors are beginning to come to a consensus on standards for the tools they provide for intermachine communication, graphics, and data bases.

Unfortunately, advances in structural engineering software development have not kept pace with the rapid changes in the computer market place. Some attempts are documented wherein existing, well-respected, monolithic finite element software systems traditionally run on large computers have been "down loaded" to workstation environments. However, little innovative software is available to the research and development community. This group requires a computational environment that is responsive to changes in the state of the art in computational mechanics and software development. Since new techniques and algorithms must be tested and debugged as they are implemented, a system that provides a high degree of flexibility and interaction is required.

A description of a software environment for application to structural engineering is provided in the Landers (1990) report. The system is primarily intended for the design and implementation of new methodologies and techniques in finite element analysis, but it can be extended to production situations as well.

DEMONSTRATION OF STRUCTURAL ANALYSIS MODELS

ONE-DIMENSIONAL CONTINUOUS BEAM MODELS OF DRYDOCKS

Since a drydock has a long slender shape, it is tempting to treat it as a continuous beam for purposes of a preliminary structural dynamics study. Indeed early design and analysis approaches for drydocks were based on elementary beam formulas (URS/John A. Blume and Associates, 1978; Woodward-Clyde Consultants, 1979; and Moffat and Nichol, Engineers, 1981). These early approaches were, however, static analyses where the drydock walls were treated as vertical cantilever beams. It is surprising that certain fundamental, readily available results for one-dimensional continuous beam natural frequencies and natural vibration mode shapes were not considered in these early studies. In this section, these data are presented to demonstrate their effectiveness in two respects. First, the longitudinal mode shapes of drydocks can be estimated by one-dimensional continuous beam models. Second, these data serve to guide the development of more advanced analyses based on three-dimensional finite element models of drydocks.

Three separate continuous beam models are presented and discussed, each increasing in complexity and scope. The data presented for the first and second models are essentially available in various reference books on structural dynamics such as those listed in the bibliography provided in Appendix A. The third model is a newly derived modification of the other models to account for the translational inertia of the drydock endwall and drydock caisson.

Properties for the one-dimensional continuous beam models are calculated based upon an idealized cross section of drydock No. 6 at Puget Sound Naval Shipyard (NSY). This particular drydock was selected because it is a relatively new drydock with a thin wall and a thin floor structural design. Its engineering design and construction is well documented in the open literature by Zola and Boothe (1960). The idealized cross section and associated data used are presented in Figure 1. The material model is linear elastic and the mass density, ρ_c, and modulus of elasticity,

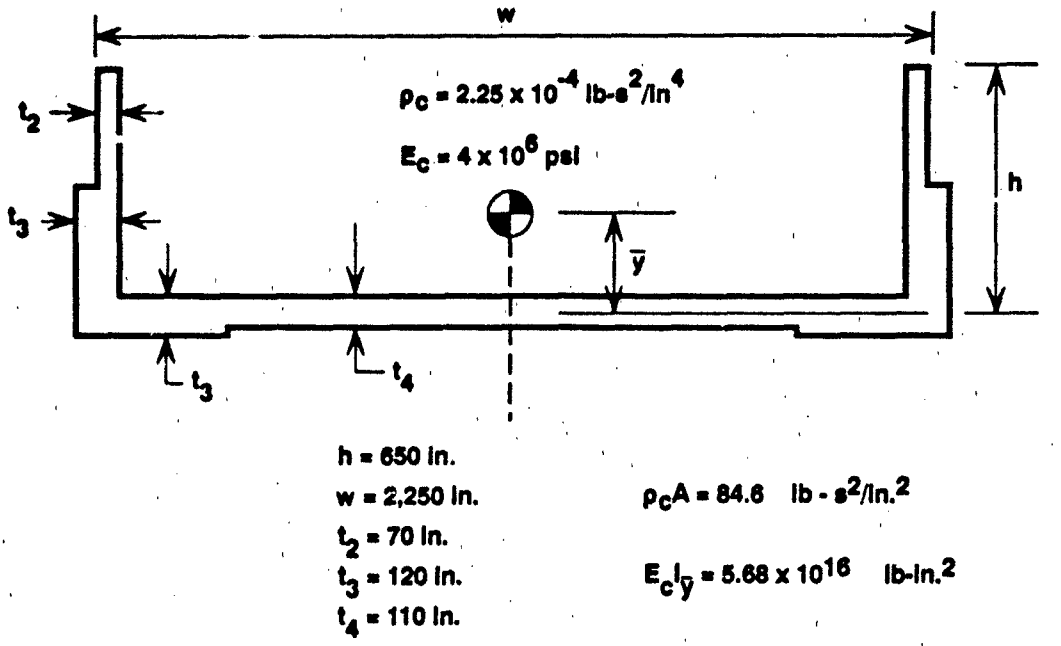

Figure 1. Idealized Cross-Section Properties of Drydock 6 at Puget Sound NSY.

E_c, are nominal values for concrete. The product of ρ_c and the cross-sectional area A represents the mass per unit length of the drydock, and the product of E_c and the second moment of area about the neutral axis I_y represents the longitudinal bending rigidity of the drydock.

Free-Ended Beam Model

In the free-ended beam model, the drydock is assumed to have free-end conditions. This is also sometimes referred to as a "flying beam" model. The effects on natural frequencies and mode shapes of the drydock due to the surrounding soil and foundation are ignored in this model.

A tabulation of natural frequencies and mode shapes for this model and other continuous beams can be found in the comprehensive reference by Blevins (1979). The results for the present drydock model are presented in Figure 2. Here L is the length of the drydock and f_n is the natural frequency for the n^{th} natural mode of vibration. The formula for this frequency is given in the figure. The first five

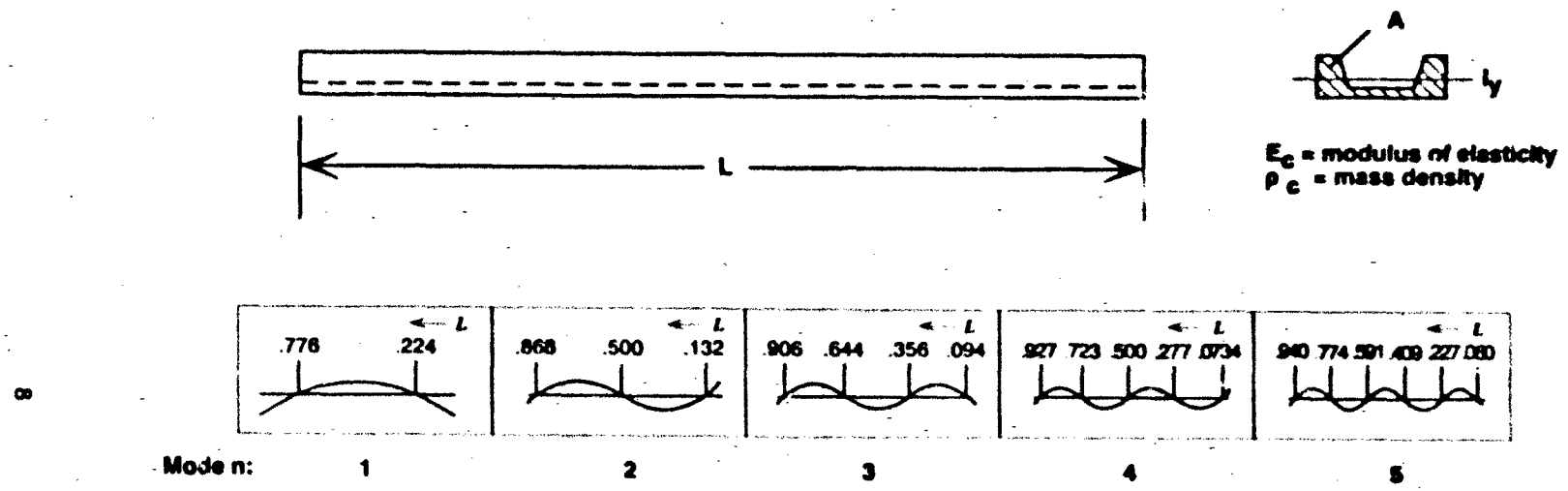

$$\lambda_n = \left(n + \frac{1}{2}\right)\pi$$

$$f_n = \frac{\lambda_n^2}{2\pi L^2}\sqrt{\frac{E_c I_y}{\rho_c A}}$$

Figure 2. Natural Frequencies and Modes for a Free-Ended Beam.

nonzero natural mode shapes are also depicted. These results naturally pertain to longitudinal bending in the drydock sidewalls and floor (as contrasted with vertical bending in the walls from a cantilevered wall model). The dynamic response for displacements and stresses in the drydock relative to a prescribed dynamic load can be calculated using a linear combination of these fundamental deformation shapes according to the modal superposition method in structural dynamics theory as described by, for example, Clough and Penzien (1975). The particular combination of mode shapes and the magnitude of the response depend on the frequency content and spatial distribution of the prescribed dynamic load.

In addition to neglecting the effect of the soil and foundation, these results are based on the assumption that vibration of the drydock is symmetrical about a vertical plane through the drydock longitudinal centerline. Consequently, other vibration modes such as torsional deformation modes (longitudinal twisting about the centerline) and bending modes in the horizontal plane (about the strong axis) are precluded from these data. To retain these modes, three-dimensional models must be considered. However, the effect of an assumed elastic foundation for the drydock is easily investigated by one-dimensional continuous beam models as shown in the next model.

Elastically-Supported Free-Ended Beam Model

In the elastically-supported free-ended beam model, the drydock is assumed to be continuously supported along its length by an elastic foundation as shown in Figure 3. The modulus of the foundation, E_f, has units of force per unit area, and the stiffness modulus, k_f, has units of force per unit length. The resulting natural frequencies and natural modes for this system are shown. These data are also taken from tabulations in Blevins (1979).

The natural frequencies of the system increase with the square root of the foundation modulus, E_f, as shown by the formula given in Figure 3 (note that this is the same as the formula in Figure 2 when E_f is zero). However, the natural mode shapes of the continuous beam-foundation model are identical with the natural mode shapes of the continuous beam model

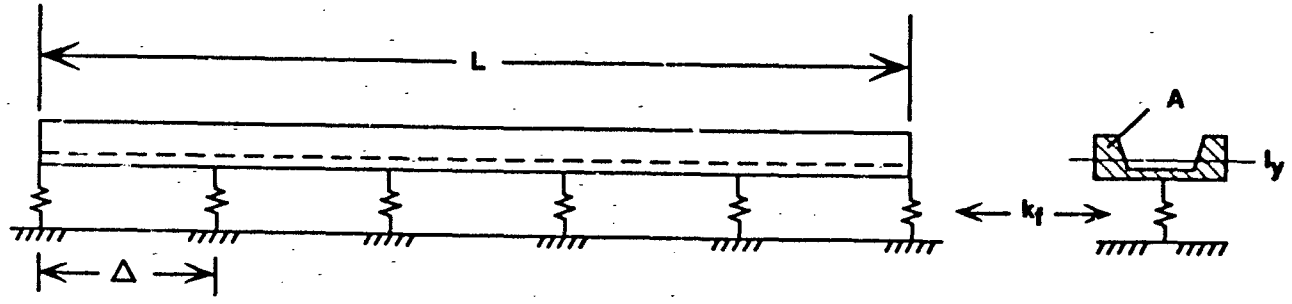

ρ_c = mass density of beam
E_c = modulus of elasticity for beam
$E_f = k_f/\Delta$, foundation modulus

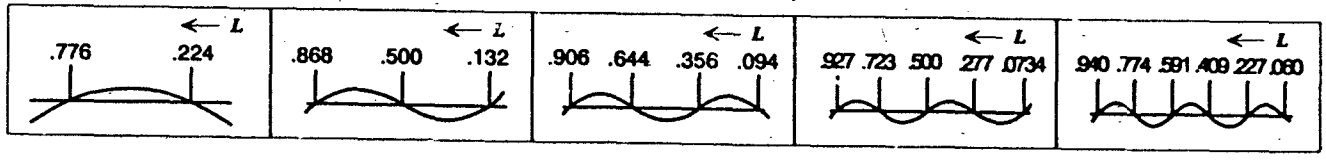

Mode n: 1 2 3 4 5

$$\lambda_n = \left(n + \frac{1}{2}\right)\pi$$

$$f_n = \frac{\lambda_n^2}{2\pi L^2}\left(1 + \frac{E_f L^4}{E_c I_y \lambda_n^4}\right)^{\frac{1}{2}}\sqrt{\frac{E_c I_y}{\rho_c A}}$$

Figure 3. Natural Frequencies and Modes for a Free-Ended Beam on an Elastic Foundation.

in the absence of the foundation. This well-known result was first published by Stafford (1967). Simply stated, the shapes of the natural longitudinal bending modes of the drydock are independent of the foundation modulus, according to this model.

Elastically-Supported Free-Ended Beam With Tip Masses

To account for the translational inertia of the drydock endwall and the drydock caisson, the previous continuous beam model was modified to include concentrated masses at either end of the continuous beam, m_1 and m_2, respectively. This model is shown in Figure 4.

From the previous model, it was seen that the presence of the elastic foundation caused an increase in the natural frequencies of the system in a very simple way. This is also true of the present model. It can be shown (see Stafford, 1967) that the natural circular frequency, Ω, of a beam on an elastic foundation can be determined by taking the square root of the sum of the squares of the "rigid body" natural circular frequency, given by $\sqrt{E_f/(\rho_c A)}$, and the natural circular frequency of the beam in the absence of the elastic foundation, ω. The relation is general and independent of boundary conditions and holds for any natural mode of vibration n. Thus,

$$\Omega_n = \sqrt{\omega_n^2 + E_f/(\rho_c A)} \qquad n = 1,2,\ldots$$

There are no published tabulated natural frequency data for the continuous beam model with tip masses. Therefore, the characteristic equation governing the natural frequencies and mode shapes and its solution are presented. The theory used to derive this equation is explicated well in Craig (1981), for example. The resulting characteristic equation is:

$$2 M_1 M_2 \lambda^2 \tanh \lambda L \tan \lambda L$$

$$+ (M_1 + M_2) \lambda (\tan \lambda L - \tanh \lambda L)$$

$$+ \frac{1}{\cosh \lambda L \cos \lambda L} = 1$$

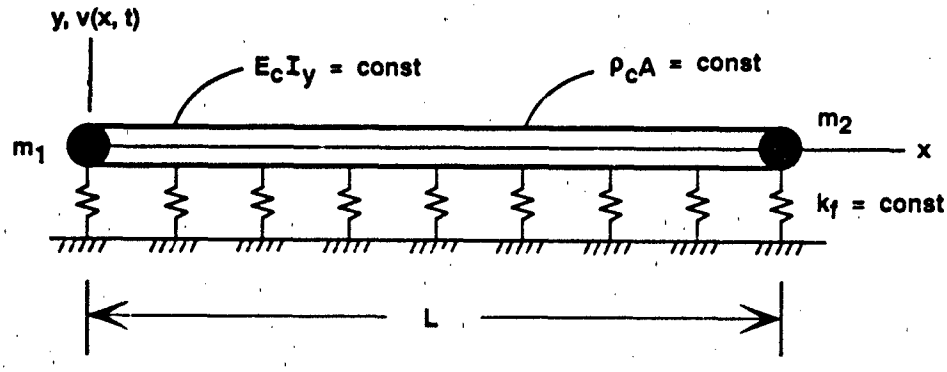

Figure 4. Elastically Supported Free-Ended Beam Model with Tip Masses: 1-D Drydock Model.

where: $M_1 = \frac{m_1}{\rho_c A}$ and $M_2 = \frac{m_2}{\rho_c A}$

and $\lambda^4 = \frac{\rho_c A \omega^2}{E_c I_y}$

The tip mass ratios, M_1 and M_2, are tip masses normalized on the mass per unit length of the beam. It is noted that when the tip mass ratios are zero, the characteristic equation for the "flying beam" is recovered from this equation. This equation is (see Rogers 1959, for example):

$$\cosh \lambda L \cos \lambda L = 1$$

The "flying beam" natural frequencies (indicated in Figure 2) are determined from the roots of this equation.

It is not the tip masses m_1 and m_2, but the tip mass ratios M_1 and M_2, that matter when determining the natural circular frequencies for the longitudinal bending modes of the drydock.

For purposes of solving the characteristic equation for its roots, let $a = \lambda L$. Then, the characteristic equation becomes:

$$\left(\frac{2\,M_1\,M_2}{L^2}\right)\ a^2\ \tanh\,(a)\ \tan\,(a) + \left(\frac{M_1 + M_2}{L}\right)\ a\ (\tan\,a - \tanh\,a)$$

$$+\ \frac{1}{\cosh\,(a)\ \cos\,(a)}\ =\ 1$$

For the case of drydock No. 6 at Puget Sound NSY, the above dimensionless coefficients are evaluated as:

$$\left(\frac{2\,M_1\,M_2}{L^2}\right) = 5.1176 \times 10^{-12}$$

$$\left(\frac{M_1 + M_2}{L}\right) = 4.1270 \times 10^{-6}$$

The solution, by numerical iteration, of the characteristic equation for the first root gives:

$$a_1 = 4.57565$$

or

$$\lambda_1 = \frac{4.57565}{L}$$

Therefore, the first (nonzero) circular natural frequency is:

$$\omega_1 = \sqrt{\frac{E_c I_y}{\rho_c A}}\ \lambda_1^2 = 6.5524\ \text{rad/s}$$

The graph of the iterative solution depicting the root a_1 is shown in Figure 5. The corresponding value when the tip masses are zero is (from Figure 2):

$$\omega_1 = \left(\frac{3/2\ \pi}{L}\right)^2 \sqrt{\frac{E_c I_y}{\rho_c A}} = 6.918\ \text{rad/s}$$

which is higher than the value when tip masses are included. Thus, inclusion of the tip masses in the continuous beam model causes a 6 percent decrease in the fundamental natural frequency.

$$y_1(a) = 5.1176 \times 10^{-12}\, a^2 \tanh(a) \tan(a) + 4.1270 \times 10^{-6}\, a\,(\tan a - \tanh a) + \frac{1}{\cosh(a)\cos(a)}$$

$$y_2(a) = 1$$

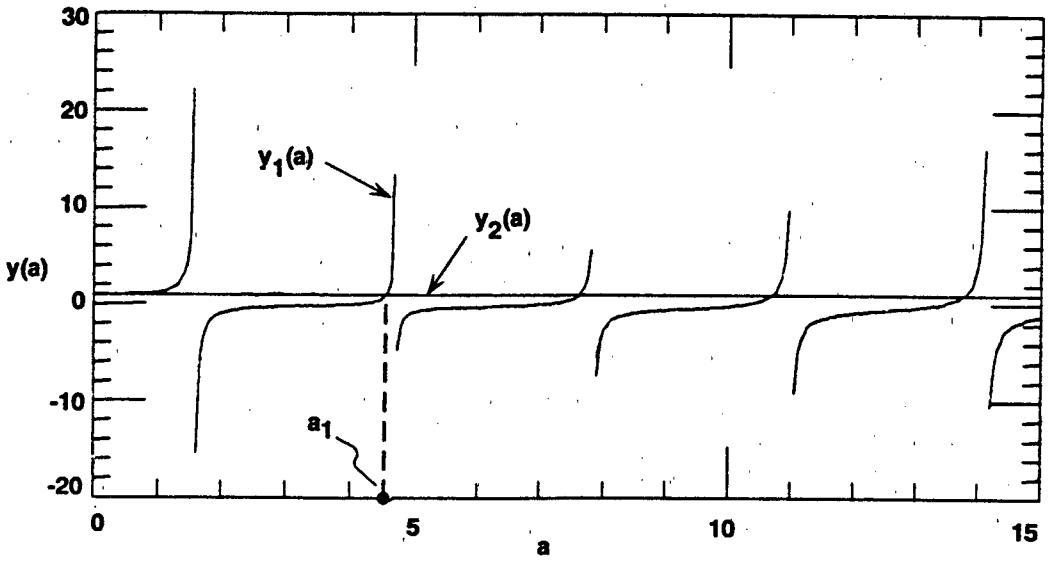

Figure 5. Graph of Iterative Solution of Characteristic Equation for 1-D Drydock Model.

Using the lower value of ω_1, the one-dimensional continuous beam model estimate of the first natural frequency of drydock No. 6 at Puget Sound NSY is:

$$f_1 = \omega_1/(2\pi) = 1.04 \text{ Hz}$$

This frequency is indeed close to the range of frequencies containing substantial energy in typical earthquake ground motion records. However, this value ignores the effect of the soil foundation.

Various values of the soil modulus, E_f, were compiled from Wu (1967) to demonstrate the effect on natural frequency of a range of typical soil stiffnesses. The increase in the first natural circular frequency with soil stiffness is graphed in Figure 6. The shape of the graph for ω_1 evidences the square-root relationship discussed earlier between natural circular frequency and soil modulus, E_f. Additional curves for

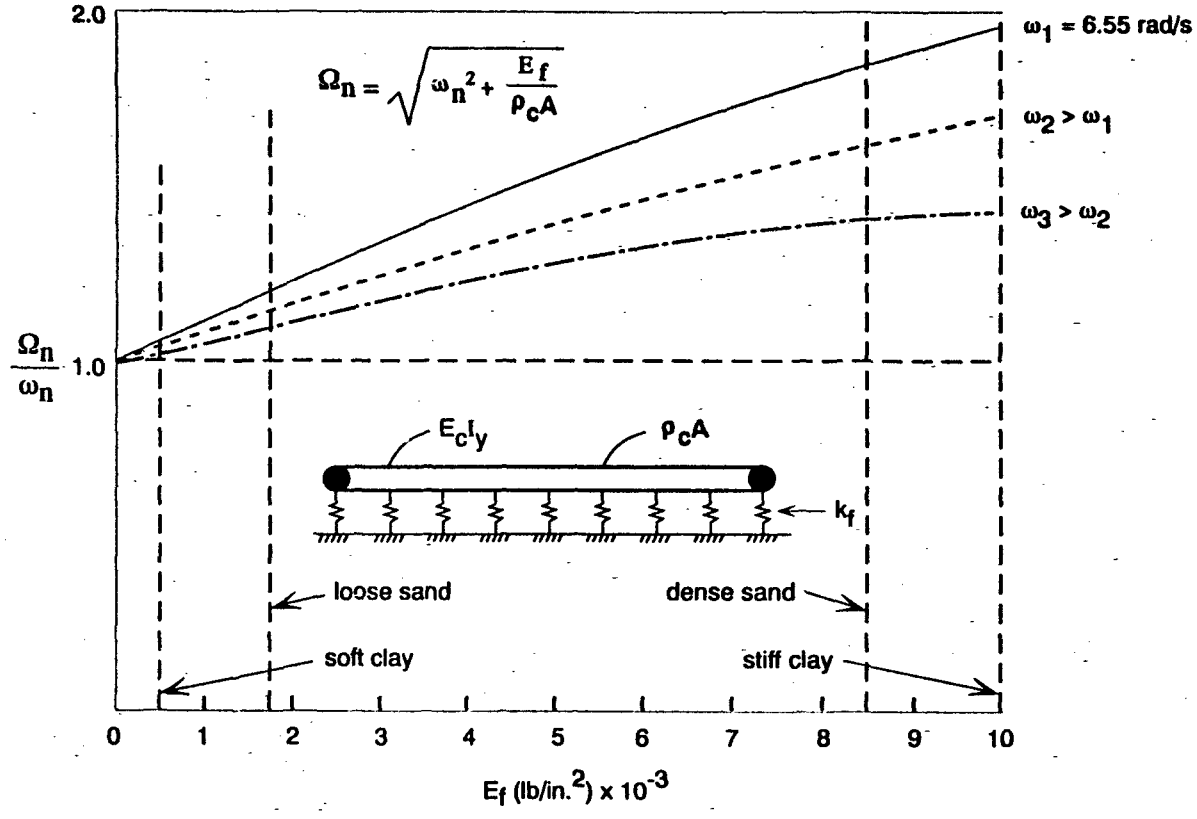

Figure 6. Increase in Natural Frequency with Soil Stiffness for 1-D Drydock Model.

the second and third natural circular frequencies are merely sketched in the figure to emphasize the diminishing effect of the soil stiffness on frequency for higher modes.

From these results, the value f_1 = 1.04 hertz would, therefore, appear to underestimate the value corrected for the presence of the soil foundation. That is, the actual first natural frequency including the effect of the soil stiffness could be substantially higher, perhaps closer to 2 hertz according to the graph. But these results account only for the added influence of the soil foundation's stiffness, and not for soil foundation's inertia. The inertial properties of the soil cannot safely be neglected particularly for embedded structures such as drydocks. The actual frequencies may well be similar to those calculated in the absence of soil, because the effect of neglecting soil inertia would appear to mitigate the effect of neglecting soil stiffness. However, more powerful soil-structure interaction numerical analysis models are generally required to also account for soil foundation inertia.

The preceding discussion serves to introduce the larger problem which is the understanding of the phenomenon of soil-structure interaction. Correctly computing soil-structure interaction effects when determining the natural vibration and dynamic response of drydocks subjected to earthquake loads is essential. Both frequency domain and time domain approaches, as described by Wolf (1985) and Bayo (1983, 1987), need to be considered in future earthquake analyses of Navy drydocks and waterfront facilities. Linear and nonlinear finite element models of these systems are generally recommended for such analyses.

TWO-DIMENSIONAL FINITE ELEMENT MODELS OF DRYDOCKS

The purpose of this section is to describe two-dimensional finite element structural analysis models of drydocks with particular emphasis on the engineering assumptions that are implied in these models.

Some new calculations of the natural frequencies and natural mode shapes for a two-dimensional finite element model of a drydock are presented and discussed. These data were prepared for a subsequent

comparison with three-dimensional finite element models which are presented in a later section. Two-dimensional finite element models are currently used to support the Navy's drydock certification program with respect to structural safety of the drydock. As defined by Yachnis (1985), drydock certification is an independent technical review of existing facilities, and a method for developing ways to insure the safety of the ship during docking and while the ship is being built or repaired. There are two points in this definition that the present discussion emphasizes: (1) the procedure is fundamentally a technical process, and (2) the procedure encourages the improvement of the engineering analysis methods used, since the drydock certification program is a continuous process.

It is noted that while the Naval Facilities Engineering Command (NAVFAC) has the responsibility for conducting certification studies of drydock facilities, the Naval Sea Systems Command (NAVSEA) has the ultimate certification authority. Thus, NAVFAC is a consultant to NAVSEA in certifying the safety of ships in drydock. Further, certification is to be conducted in accordance with MIL-STD-1625, "Drydocking Facilities Safety Certification Criteria for Docking U.S. Navy Ships" (Naval Sea Systems Command, 1984).

According to Wu (1985), there are over 50 graving drydocks that need to be certified in the United States. Naval shipyards are usually located in areas with unfavorable soil conditions. There have been many hydraulic fills that utilize uniform, fine sands which are subject to liquefaction. These drydocks were built during the past 20 to 50 years.

Drydock Loads and Failure Modes

Various load cases have been defined for structural analysis of drydocks.* However, the earthquake load case for drydocks located in seismic zones 3 and 4 is of primary concern. The earthquake load case includes the effects of dead load; ship blocking loads; soil and foundation loads; and earthquake-induced, equivalent static loads.

*It is noted that blast loads have not been addressed.

General failure modes envisioned by Yachnis (1985) and Wu (1985) include: foundation instability where the dock rotates, shifts, or uplifts and generally displaces as a rigid body; structural damage to the dock such as overturning walls; displacement of the caisson; failure of utility tunnels; and auxiliary failure modes such as ship blocking failures and overturning of cranes into the dock.

Failure modes may well be site-specific and include other modes as well. For example, buried pipelines, water tunnels, and pressure equalization systems which are critical to operation and safety are subject to strains due to both rigid body and relative motion (differential displacement) of the structural system (ASCE Committee on Seismic Analysis, 1983). However, there is evidence that heavy industrial facilities, provided they have been designed for seismic loads, will perform very well (ASCE Committee on Dynamic Analysis, 1987).

Linear Static Analysis of Drydocks for Earthquake Loads

According to Chelapati and Takahashi (1982), the earliest structural analyses conducted in support of drydock certification were quite simplified and based upon strength of materials theory (URS/John A. Blume & Associates, 1978; Woodward-Clyde Consultants, 1979; and Moffat and Nichol Engineers, 1981). The general conclusion was that much more can be done in applying available structural analysis technology. Most of the earlier studies did not vary parameters to obtain ranges of response, and the many assumptions made most likely lead to results that are too conservative. It was recognized that even a very simple, linear two-dimensional finite element model is a more accurate basis for structural analysis than elementary beam formulas from the theory of strength of materials.

Drydock certification has since been supported by structural analysis methods which are based on two-dimensional finite element modeling technology (Holland and Takahashi, 1984; and Wu, et al., 1984). This methodology for drydock analysis is reviewed next.

Two-dimensional finite element models of drydocks are based on the plane strain deformation assumptions from the theory of elasticity. A two-dimensional idealization of a drydock is shown in Figure 7. A typical idealization of an equivalent static earthquake load is included in the

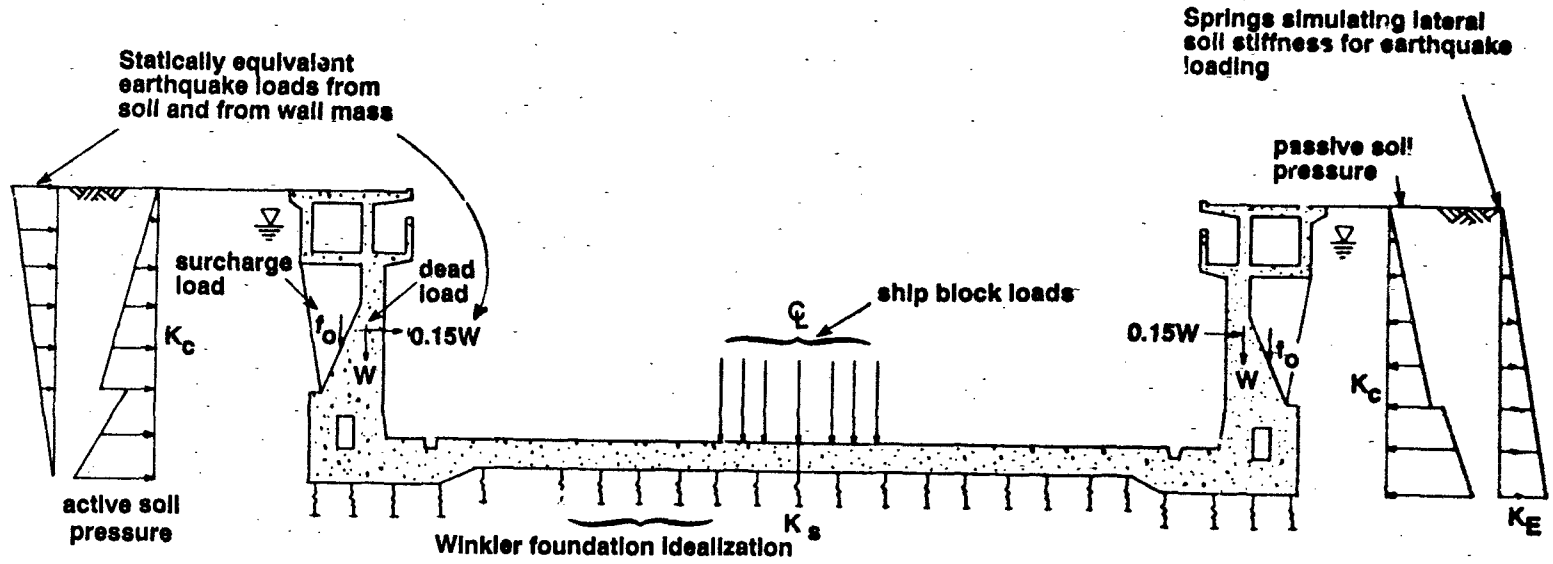

Figure 7. Typical 2-D Idealization of Drydock and Earthquake Load.

figure. The surrounding backfill and foundation structures are excluded from the model. These geotechnical structures are replaced with their idealized effects as indicated. For example, the triangular distributions of soil pressure loads shown represent the inertia effect of adjacent soil and wall mass.

Active, lateral soil pressure is assumed to increase linearly with depth according to Rankine's theory for the state of stress in granular soil. The intensity depends on the angle of friction and unit weight of the backfill material which varies according to whether it is dry, saturated, or submerged (Bowles, 1977). Further, a factor accounting for wall movement may also be introduced to increase the intensity. There is also a vertical component of soil loading which is termed the surcharge, and is represented in Figure 7 by the concentrated force acting downward on the sloping face of the drydock wall.

An equivalent static earthquake-induced lateral soil pressure is also included in Figure 7 which is assumed to decrease linearly with depth. It is calculated by the method discussed by Seed and Whitman (1970). This method is a very simple extension of the calculation method for the static, active soil pressure mentioned above. The total force (the area of the active pressure triangle) is multiplied by 3/4 of the horizontal ground acceleration. This product is the increase in total lateral force due to an earthquake. It is then distributed over the vertical wall as a triangular pressure distribution with the centroid located at 2/3 the wall height above the drydock base. An additional vertical component may be included to account for wall friction forces, and where combined with the lateral component the resultant equivalent static earthquake-induced pressure in the drydock wall is obtained (Wu, et al., 1984). Thus, on one side of the drydock, a static active soil pressure plus an equivalent static earthquake-induced pressure is imposed when simulating the earthquake load case.

On the opposite side, a passive soil pressure, which is generally understood to be greater than the at-rest active pressure, is imposed. Additionally, a continuous column of horizontal springs is included to simulate soil stiffness under earthquake loading. The stiffness modulus K_e is assumed to increase linearly with depth, as shown.

Beneath the drydock floor, the bearing stress of the soil is replaced by a Winkler foundation model which is a continuous layer of uniformly spaced vertical springs with modulus K_s. An elastic subgrade modulus is assigned to the springs and is determined according to soil bearing capacity under assumed static load conditions.

Soil friction forces on the drydock wall cannot be calculated in the current analysis procedure because they are statically indeterminant. Various load cases may be studied to bracket the response and, thus, to overcome this difficulty somewhat. However, the basic problem of indeterminacy remains because the soil backfill structure is excluded from the drydock model; that is, the basic problem of soil-structure interaction is simplified or decoupled in the present two-dimensional structural analysis procedure.

Discussion of Modeling Assumptions

The current two-dimensional finite element analysis procedure supporting drydock certification includes several fundamental assumptions as follows:

1. Plane strain conditions from elasticity theory apply.

2. Soil-structure interaction may be decoupled.

3. Soil constitutive properties are linear.

4. The structural response is independent of time.

These four assumptions are expanded and discussed below in the order listed.

Plane Strain Condition. Two-dimensional plane strain finite element analyses are often conducted for long, uniform, or prismatic structural/geotechnical systems such as lined tunnels and earthen dams. A typical length-to-width ratio of drydocks is approximately eight, which

means these structures are sufficiently long and slender as to certainly suggest that plane strain conditions could be appropriate. However, it is useful to analyze this assumption more closely.

The conditions under which the plane strain theory assumption of elasticity would be valid for drydock analysis are stated here with the help of Figure 8:

a. The geometry, the loading, and the boundary (support) conditions of the drydock do not vary with coordinate z along the drydock length.

b. The drydock displacement in the z-direction, w, is zero (i.e., the drydock does not develop axial strain).

These conditions, in the context of general two-dimensional, plane strain finite element analysis are discussed by Gallagher (1975).

The geometry of drydock sections at a pumphouse location and at stations near the caisson and endwall, for example, are indeed different from one another. So the geometry of the drydock does vary along its length. Therefore, the structural rigidity of a drydock sidewall will vary with coordinate z. Near the endwall, for instance, the huge in-plane or membrane stiffness of the endwall will have a large restraining effect on lateral displacement of the drydock sidewall. Clearly, results from the two-dimensional plane strain finite element analysis will not be applicable near the endwall. For similar reasons, the same is true near the caisson or pumphouse, or anywhere the drydock cross-sectional geometry changes dramatically.

The depth of the water table and backfill material in many cases will also vary along the drydock length. Therefore, the associated loads due to hydrostatic pressure and earthquake-induced soil pressures do vary with coordinate z. It is clear that condition (a), which is required for valid application of plane strain finite element analysis to drydocks, does not strictly apply. The error which is introduced because of this must be shown to be acceptable. One way to do this would be to conduct a three-dimensional analysis and assess the error.

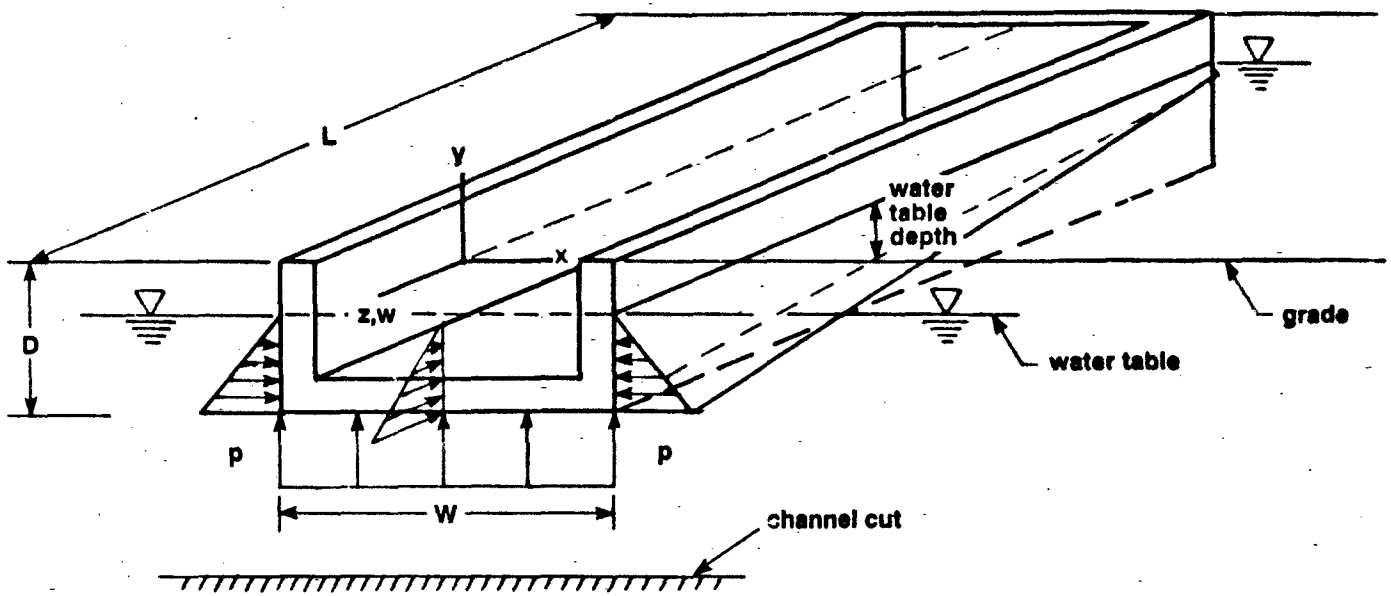

Figure 6. Analysis of Plane Strain Theory Assumptions for a Drydock.

Moreover, two-dimensional finite element models cannot account for the dynamic torsional response of structures and for the response for nonvertically incident seismic waves. The intrinsic geometrical symmetry of two-dimensional models raises serious doubts as to their applicability to three-dimensional configurations in general, as stated by Luco (1982). The approach to calculating a drydock's dynamic response to strong-motion earthquakes should, therefore, be based on a three-dimensional analysis if torsional and longitudinal bending stresses are to be considered.

Soil-Structure Interaction. Decoupling of the soil-structure interaction effects assumes fundamentally that the structure's motion at the soil interface does not influence the motion of the adjacent backfill and foundation materials, and vice versa. For example, this assumption would neglect the affect of soil liquefaction on the structure, and the effect of the structure's presence on soil liquefaction. A more accurate approach would be to model both the drydock and soil together employing coupled soil-structure interaction analysis. This approach would eliminate the current necessity for the many assumptions relating to soil pressure and friction acting on the drydock walls and floor. Dhatta, et al. (1985) show that the modulus of the elastic springs that simulate soil stiffness next to the structure under earthquake loads are a function of excitation frequency. This frequency dependence is clearly not included in the present methodology. The properties of the equivalent elastic foundation are assumed constant and are based on static soil properties. To determine the significance of the error, parametric studies varying the elastic spring moduli are needed. Alternatively, dynamic analyses in the frequency domain may be appropriate (Wolf, 1985) where nonlinear effects are minor.

Soil Constitutive Properties. Invoking the assumption that foundation materials behave linearly, forecloses on model predictions of failure states within the backfill and foundation materials, or permanent plastic deformation of the foundation materials. Foundation instability cannot be predicted directly by the current linear procedure. To retain the

capability of predicting foundation failure, modern nonlinear soil constitutive models must be used for the backfill and foundation structures. The importance of a properly operating backfill relief system is emphasized by Zola and Boothe (1960) for fully relieved drydock designs.

Structural Response. The assumption that the structure's response is independent of time ignores the possibility of resonance or amplified response in the drydock when the earthquake excitation frequency matches the drydock system's natural frequency. Resonance effects would seem to be particularly important to the dynamic response of blocked ships, drydock cranes, and other similar "superstructures" in contact with the drydock itself. These considerations bear directly on ship safety, which is the primary goal of the drydock certification program.

Other Considerations. Other considerations which foretell the need for dynamic analysis of drydocks are as follows. Amplification of ship blocking loads could be calculated by a dynamic analysis procedure. It is neglected in the current procedure. A dynamic analysis would capture the effects of radiation damping in the soil foundation, which is currently believed to be an important energy dissipation mechanism during dynamic events. This reinforces the need for dynamic soil-structure interaction models.

The technical problems associated with current two-dimensional finite element models of drydocks are summarized in Table 1. A correct procedure for earthquake analysis of drydocks would be based upon a three-dimensional, nonlinear dynamic analysis of the drydock including the surrounding backfill and foundation structures.

Natural Frequencies and Mode Shapes

Future dynamic analysis of drydocks would necessarily be preceded by an eigenvalue analysis of the finite element model to determine the natural frequencies and the natural mode shapes of the drydock. This section presents and discusses the results of such an analysis for a two-dimensional model. The two-dimensional finite element model in this

Table 1. Technical Problems With Current Two-Dimensional Finite Element Analysis of Drydocks

1. 2-D PLANE STRAIN CONDITIONS DO NOT APPLY
• Torsional and longitudinal bending response cannot be replicated.
2. SOIL-STRUCTURE INTERACTION IS NOT INCLUDED
• Drydock and foundation response is inaccurate.
SOIL CONSTITUTIVE PROPERTIES ARE NOT LINEAR
• Foundation material failure cannot be detected.
4. STATIC ANALYSIS CANNOT DETECT RESONANCE
• Predicted response may not be conservative.

case is a one-element-thick slice of a three-dimensional model of drydock No. 6, Puget Sound NSY. Natural frequencies and mode shapes for a three-dimensional model of this drydock will also be presented and discussed in a subsequent section of this report. Results for the two-dimensional model and the three-dimensional model will be compared to determine differences in the fundamental dynamic properties of the two modeling approaches.

To obtain a two-dimensional model with plane strain behavior, displacements in the long direction of the drydock for the one-element-thick three-dimensional model are constrained to be zero. This imposes condition (b) for plane strain behavior given in the previous section. Condition (a) is tacitly assumed to hold. Thus, the model presented here and used for calculating frequencies and mode shapes would be equivalent to a natural vibration analysis of drydock No. 6 based on the current two-dimensional plane strain modeling practice.

In this case, the two-dimensional finite element model exploits symmetry about the centerline of the drydock, as shown in Figure 9. A consequence of this is that all natural frequencies and mode shapes associated with modes of vibration that are antisymmetrical about the centerline will not be admitted in the calculation. Only natural mode

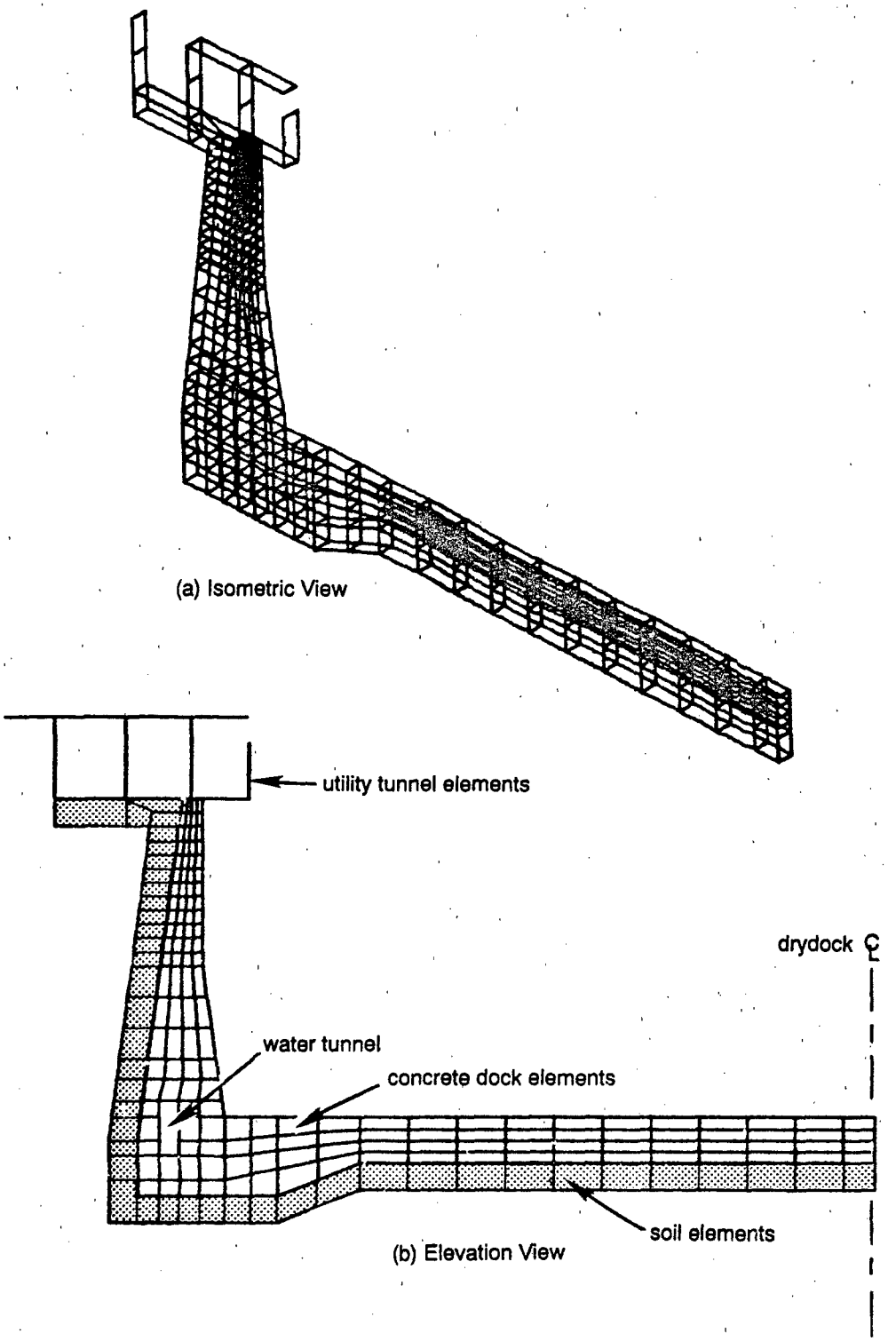

Figure 9. Two-Dimensional Finite Element Model of a Drydock.

shapes that are symmetrical with respect to the drydock centerline will result from this analysis. To obtain all modes, symmetrical and anti-symmetrical, would be straightforward, but a full two-dimensional slice of the drydock would have to be modeled. Nonetheless, the results from the present symmetrical two-dimensional model are a sufficient basis for subsequent comparison with the results from both one-dimensional and three-dimensional models.

Other features of the model are indicated in Figure 9(b). A single row of soil elements represent the effect of the surrounding soil foundation. The drydock material model and foundation material model are assumed to be isotropic and linear elastic. An equivalent modulus of elasticity and Poisson ratio of the foundation were calculated from a typical value for soil bearing modulus.

The first five symmetrical natural mode shapes and frequencies are shown in Figures 10(a) through 10(e). Only the concrete drydock portion of the model is shown in these figures; the utility tunnel and the row of soil foundation elements are omitted from the graphics presented.

These results show that the first mode shape is a floor bending mode and the second mode shape is a cantilevered wall bending mode. Subsequent modes are higher order combinations of these two deformation mode shapes. The equivalent static analysis procedure discussed in the previous section effectively assumes a deformation mode shape that is similar to a combination of these first two mode shapes. Thus, it may be concluded that the current equivalent static analysis procedure effectively neglects any contribution from modes of deformation beyond the second.

The lowest natural frequency calculated for the two-dimensional plane strain finite element model is 2 hertz. This might appear high compared to that which was calculated for the one-dimensional models in the previous section, which was about 1 hertz. However, the values are not directly comparable because they are fundamentally different mode shapes from fundamentally different models. In the present case they are lateral vibration modes, while in the former case they are longitudinal vibration modes. In a dynamic analysis with an input ground motion having a prominent 1-hertz energy component, use of this two-dimensional

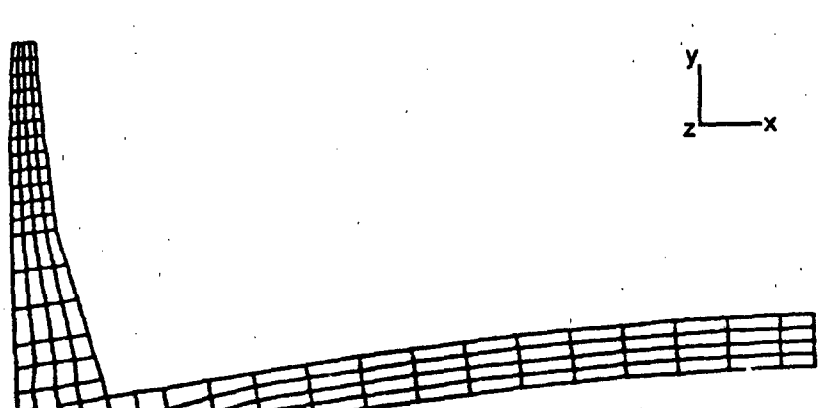

(a) MODE 1, 2.063 Hz

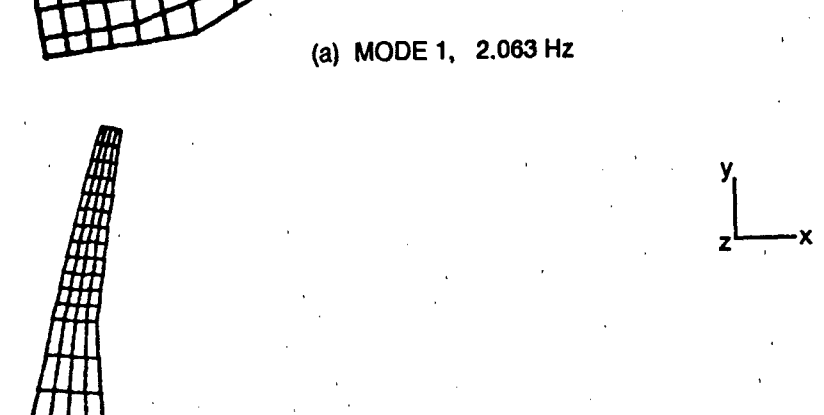

(b) MODE 2, 2.333 Hz

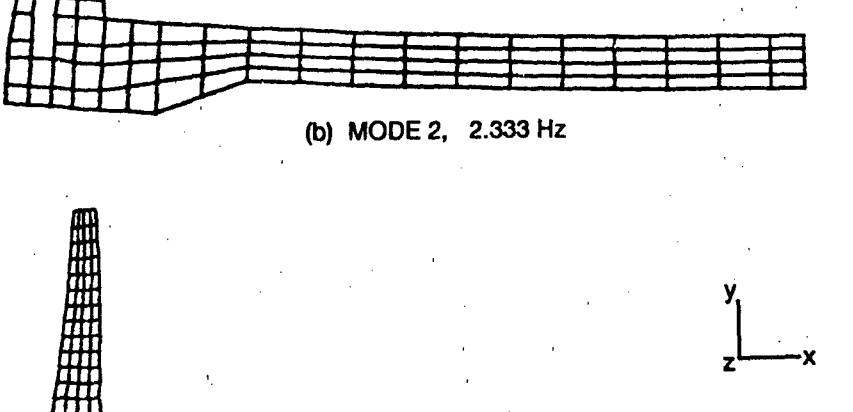

(c) MODE 3, 3.004 Hz

Figure 10. Symmetric Natural Mode Shapes and Frequencies: 2-D Drydock Model.

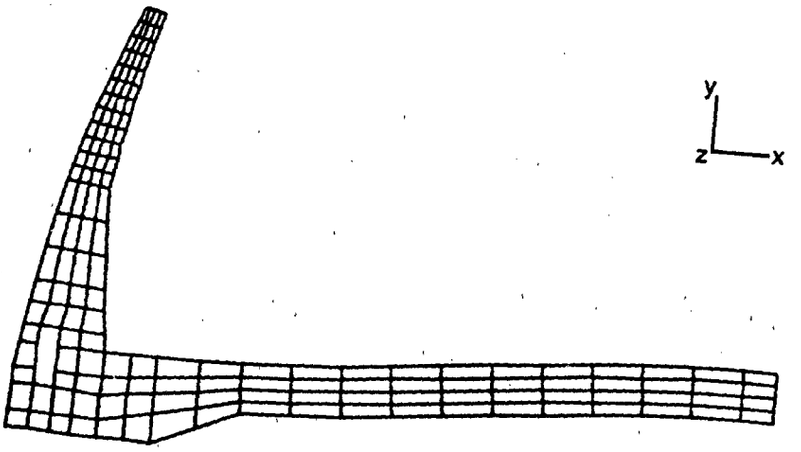

(d) MODE 4, 4.395 Hz

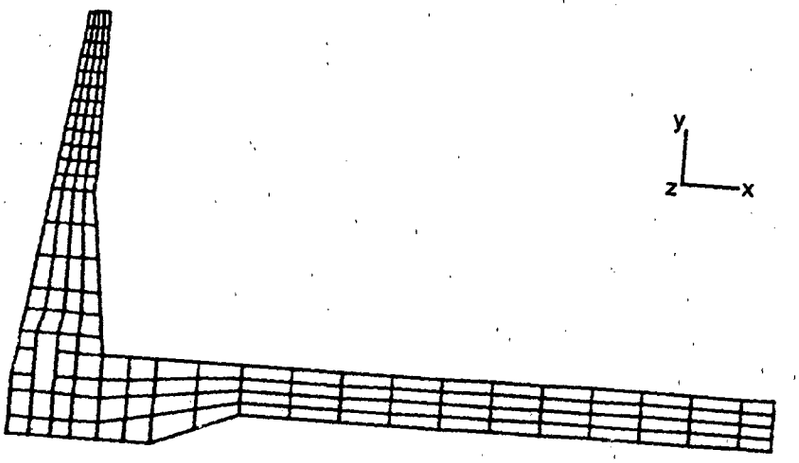

(e) MODE 5, 6.497 Hz

Figure 10. Continued.

model would lead to results having minimal resonance behavior. However, the one-dimensional model would respond with strong resonance. Thus, depending on which model was being used, dramatically different conclusions on the importance of basic dynamic behavior could be drawn from their results. The one-dimensional model considers only longitudinal bending modes and the two-dimensional model considers only wall and floor bending modes in a transverse plane.

Another observation from these results is that the wall bending modes are high-frequency modes (i.e., greater than 2 hertz). This is a result of the very large bending stiffness of the wall and floor sections, particularly where they meet at the base of the vertical cantilever. As a result, the walls would rarely be expected to bend in modes higher than, for example, the third because most strong motion earthquakes do not contain strong energy components beyond 5 hertz. The first two modes of wall deformation are effectively subsumed by the present equivalent static analysis procedure for earthquake loads. Thus, the equivalent static procedure may be a good approximation to the two-dimensional dynamic analysis. However, the sidewalls will also bend in longitudinal vibration modes which are of course precluded in the two-dimensional model approach.

Two-dimensional finite-element models of drydocks normally include a Winkler model (a row of linear elastic springs) for representing the effect of the soil foundation. To study the difference between the effects of using a row of two-dimensional finite elements and a row of one-dimensional springs, the latter model was also considered in this study. The first ten natural frequencies and mode shapes using an equivalent Winkler model for the drydock foundation were calculated. The results for both soil foundation models were very similar. The mode shapes were basically the same as those presented in Figure 10 and, therefore, are not presented. The natural frequencies were also similar, particularly for the more important lower modes. The natural frequencies for the first ten modes calculated with both foundation models are graphed in Figure 11. Thus, it does not seem to matter greatly which type of model (Winkler or finite element) is used to account for the foundation when considering the use of two-dimensional finite element models of drydocks.

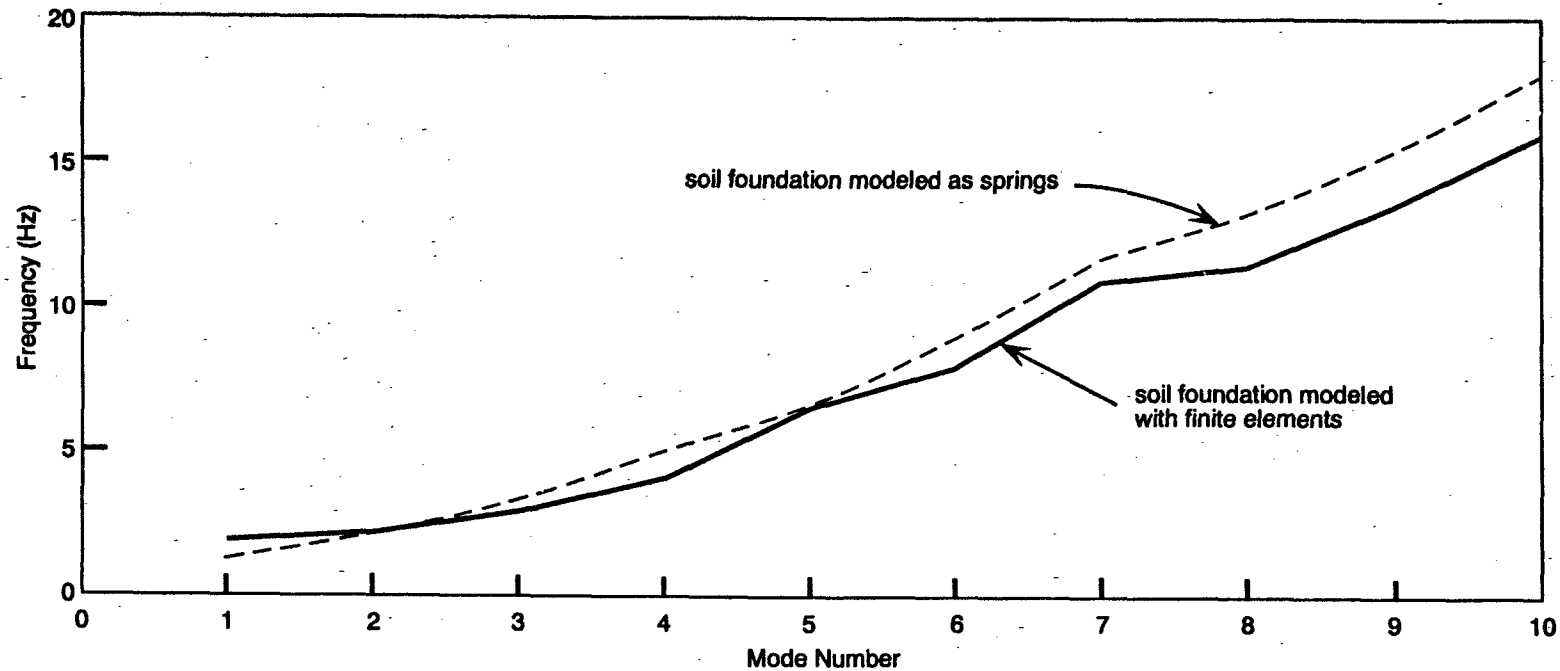

Figure 11. Natural Frequencies for Two-Dimensional Finite Element Model of a Drydock.

TWO-DIMENSIONAL LUMPED PARAMETER MODEL OF BLOCKED VESSEL

A principal goal of the Navy Drydock Certification Program is the establishment of the safety of the docked vessel. One important aspect that can arise is consideration of the safety of a blocked vessel relative to earthquake loading.

The need for earthquake analysis of drydocks has been questioned technically on the basis that a drydock is an embedded structure having no superstructure, as compared with a high-rise building, for example. However, a blocked vessel may be considered a subsystem of the entire drydock system, no differently than, for example, a pumphouse subsystem or a caisson subsystem. In this sense, a blocked vessel may indeed be viewed as a "superstructure" that responds dynamically to input base motion from the drydock floor. Further, the analysis of a complete drydock system, blocked vessel included, is in principle within the capability of modern structural dynamic analysis technology. There are various modeling approaches that could be applied in this regard, some more complex and possibly more accurate than others. However, it is believed that the dynamic interaction of a blocked vessel with the drydock floor could be calculated with modern methods to obtain accurate data on the dynamics of the vessel, blocking system, and drydock floor. The purpose of this section is to demonstrate this using a simple, two-dimensional lumped parameter model.

Construction of a fully three-dimensional subsystem model of a blocked vessel is possible. However, for the present demonstration, a two-dimensional, lumped parameter model of a blocked submarine was developed and analyzed for its dynamic response relative to a simulated drydock floor excitation. The model used here was inspired by Hepburn, et al. (1988), a study which was sponsored by NAVSEA. This publication also gives an account of the concern for the safety of blocked Navy vessels relative to earthquake loads. It develops a considerable amount of engineering data demonstrating that a blocked vessel model can be analyzed using the methods of structural dynamics to obtain accurate blocking system design data. The importance of knowing apriori the floor excitation imposed by the drydock system is also emphasized. To the extent that a drydock responds to an earthquake as a deformable body

rather than as a rigid body, it will modify the ground motion to which the blocked vessel is otherwise exposed. Specification of this modified ground motion is required for successful dynamic analysis of the blocked vessel. This is achievable by conducting soil-structure interaction analyses, as discussed earlier in this report.

Lumped Parameter Model of a Blocked Submarine

The drydock is assumed to be a rigid body that excites the blocked vessel simultaneously in both a horizontal and vertical direction. The lumped parameter model is shown in Figure 12 where a cylindrical mass, representing a submarine, is spring-mounted to the drydock floor and walls. In a lumped parameter model the system's inertia and elastic properties are assumed to be concentrated at discrete points. For simplicity, the submarine is assumed to be a uniform solid, circular cylinder. It has radius, r, mass, m, and mass moment of inertia about its center of gravity, I_{cg}. The blocking system is assumed to consist of keel blocks, side blocks, and horizontal braces representing a proposed wale shoring system consisting of rubber-tipped steel beams cantilevered out from the drydock sidewalls. These support elements are represented by linear elastic springs having moduli k_1 through k_4, as shown.

In this case, the lumped parameter model has three degrees of freedom. The variables u, v, and θ represent the absolute displacement components of the submarine's center of gravity in the horizontal and vertical directions, and the rotational displacement about the center of gravity, respectively. Instead of absolute displacement components, u and v, the displacements of the center of gravity relative to the drydock may be used. These are indicated by the variables x and y (see Figure 12). The relative displacement components are generally more useful when the excitation is base motion. Therefore, the displacement variables used in this demonstration are x, y, and θ. The prescribed input base motion is represented by x_b and y_b which are assumed to be simple harmonic functions representing, respectively, the horizontal and vertical displacements of the drydock.

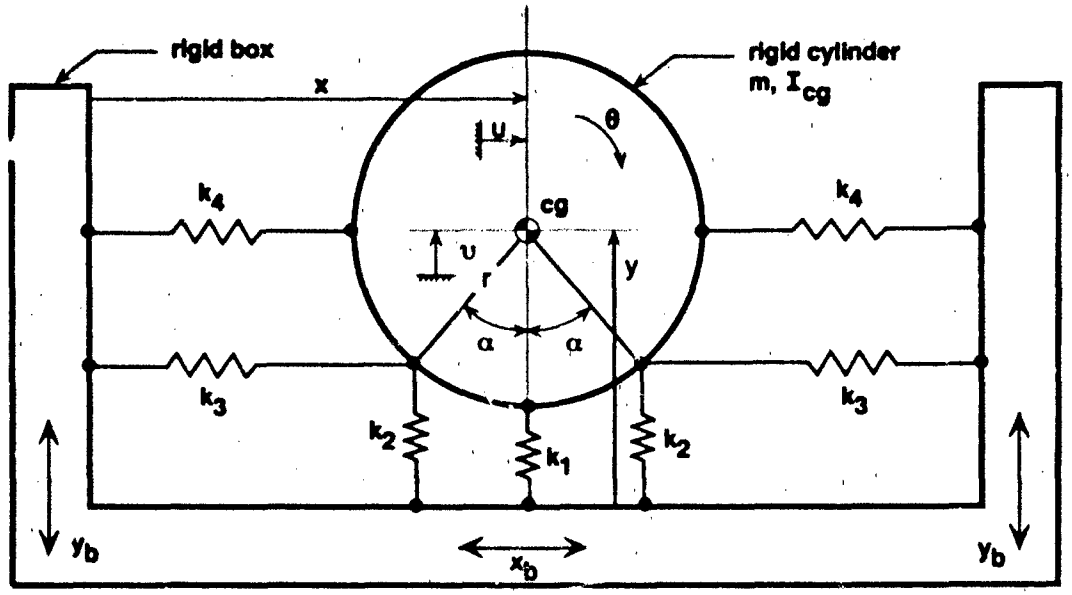

Figure 12. Two-Dimensional Lumped Parameter Model of a Blocked Submarine in Drydock.

The values used for the submarine's mass and rotational inertia are calculated based upon a displacement of 3,570 long tons. Fourteen identical blocking stations, of the type described, were assumed to support the vessel along its length. Thus, the values used for m and I_{cg} represent physical properties "per blocking station," and are suitable for use in the proposed two-dimensional or planar model (Figure 12).

The elastic properties used for the blocking system were calculated, in some cases roughly, from data presented by Hepburn, et al. (1988). Individual blocks are often composed of multiple materials including concrete, rubber, and oak and fir timber components. The methods for calculating equivalent elastic spring moduli, especially for the lateral spring moduli of the side and keel blocks, can be complex when accounting for both shear and axial deformation, as well as for the many materials involved. Yet, accurate analytical results do depend on accurate input data for these and other elastic properties of the model. The use of resilient isolator blocking systems (i.e., elastomeric bearings) would eliminate this uncertainty, but otherwise a field measurement program

is needed to obtain reasonably accurate data for the elastic properties of current blocking materials and systems. Values used for the parameters of the present lumped parameter model are listed in Table 2, and are sufficiently accurate for this demonstration.

Table 2. Parameters for Blocked Submarine Model

$k_1 = 5.30 \times 10^4$ lb/in.	r = 180 in.
$k_2 = 5.10 \times 10^4$ lb/in.	m = 1.480×10^3 in-s^2/in.
$k_3 = 3.0 \times 10^3$ lb/in.	I_{cg} = 2.397×10^7 lb-s^2-in.
$k_4 = 6.0 \times 10^4$ lb/in.	$\alpha = 30°$

Equations of Motion

The equations of motion for the lumped parameter model are conveniently derived by applying either Newton's Laws or Lagrange's equations of motion to the model of Figure 12. The results are a set of three, second order differential equations in time. In matrix form, the equations of motion are:

$$\begin{bmatrix} m & 0 & 0 \\ 0 & m & 0 \\ 0 & 0 & I_{cg} \end{bmatrix} \begin{bmatrix} \ddot{x} \\ \ddot{y} \\ \ddot{\theta} \end{bmatrix} + \begin{bmatrix} 2(k_4 + k_3) & 0 & -2k_3C \\ 0 & (k_1 + 2k_2) & 0 \\ -2k_3C & 0 & 2(k_3C^2 + k_2S^2) \end{bmatrix} \begin{bmatrix} x \\ y \\ \theta \end{bmatrix} = \begin{bmatrix} -m\ddot{x}_b \\ -m\ddot{y}_b \\ 0 \end{bmatrix}$$

or,

$$\underset{\sim}{m}\,\ddot{\underset{\sim}{x}} + \underset{\sim}{k}\,\underset{\sim}{x} = \underset{\sim}{Q}$$

The right-hand side term $\underset{\sim}{Q}$ is the force vector and it includes the terms $-m\ddot{x}_b$ and $-m\ddot{y}_b$, which are referred to as effective forces. They represent the system's excitation for any prescribed ground acceleration components, $\ddot{x}_b$ and $\ddot{y}_b$. The terms C and S denote the constants r cos α and r sin α, respectively, which define the position of the side blocks.

In this demonstration, a strong-motion earthquake is simulated by specifying the ground accelerations to be a sinusoid as follows:

$$\ddot{x}_b = \ddot{y}_b = 0.25g \sin(2\pi/T)t$$

where g is the acceleration of gravity, and T is the period of the simple harmonic motion. A value of 1 second was used for T. This excitation simulates a substantial earthquake with a 0.25g peak acceleration and a frequency of 1 hertz.

In the equations of motion, it is noted that the second equation is uncoupled and may be solved independently. This is due to the tacit assumption of small displacements in the blocked submarine's response, and the symmetry of the blocking system. Motion in the y-direction can exist independently of motion in the other directions. Further, because the forcing function is elementary, this equation can be solved analytically. That leaves the other two equations of motion to be solved simultaneously, because they are elastically coupled. Motion of the submarine in the x-direction cannot exist without motion in the θ-direction, and vice versa, according to this model. Despite the coupling, the remaining two equations can also be solved analytically. For more complex formulations, the equations of motion can be solved numerically using either the mode superposition solution method or the direct numerical integration solution method, as described by Craig (1981), for example.

Natural Frequencies and Natural Mode Shapes

Before determining the dynamic response, it is useful to determine the fundamental natural frequencies and natural mode shapes of the model to enhance understanding of its dynamic properties and behavior. These data are obtained by solving the eigenvalue problem:

$$(\underset{\sim}{k} - \omega^2 \underset{\sim}{m})\, \underset{\sim}{\phi} = \underset{\sim}{0}$$

for the natural circular frequencies ω and the natural mode shapes ϕ. Since there are three degrees of freedom (three displacements), the system correspondingly has three frequencies and three mode shapes. It's worth noting that the eigenvalue solution can also be obtained analytically since only two of the three equations are coupled in the above matrix eigenvalue equation. Otherwise, a microcomputer system may be used with a microcomputer program such as CAL80 (Bayo and Strubb, 1988), which has the capability to solve the eigenvalue problem as well as to solve for the dynamic response of small to medium structural models. In this case, both methods were used to verify accuracy of the computer solution and both methods yielded virtually identical solutions.

The results of the calculated natural frequencies and natural mode shapes are presented in Figure 13. The first calculated natural frequency is 1.01 hertz, and therefore a substantial resonance in the first mode of vibration will occur in the dynamic response since, in this demonstration, the prescribed excitation frequency was chosen to be 1 hertz. The first mode shape sketched is coupled, but its vibration is primarily rotational. This is a result of the very large rotational inertia of the submarine. The sketch of the mode shapes indicates the coupling that exists between horizontal vibration and rotational vibration in both modes 1 and 2, whereas mode 3 is uncoupled and consists of vibration solely in the vertical direction. Thus, it may be expected that for an earthquake which tends to cause horizontal floor motion, the blocked submarine will have a tendency to vibrate rotationally about its center of gravity in addition to vibrating horizontally. However, for an earthquake that tends to cause vertical floor motion primarily, the blocked submarine will tend to vibrate primarily in the vertical direction.

Dynamic Response to Simplified Earthquake Load

To obtain the dynamic response of the blocked submarine subjected to the simplified earthquake, the mode superposition method of solution was employed. The solution was calculated using the CAL80 computer program and also by hand as an analytical check on the computer solution of the dynamic response. The two dynamic response results were again virtually identical.

Natural Frequencies:

$\omega_1 = 6.325$ rad/s $\quad$ $\omega_2 = 9.256$ rad/s $\quad$ $\omega_3 = 10.233$ rad/s

$f_1 = 1.01$ Hz $\quad$ $f_2 = 1.47$ Hz $\quad$ $f_3 = 1.63$ Hz

Mode Shapes (mass normalized):

$$\underset{\sim}{\phi}_1 = \begin{Bmatrix} 0.2842 \times 10^{-2} \\ 0 \\ 0.2030 \times 10^{-3} \end{Bmatrix} \qquad \underset{\sim}{\phi}_2 = \begin{Bmatrix} 0.2584 \times 10^{-1} \\ 0 \\ -0.2233 \times 10^{-4} \end{Bmatrix} \qquad \underset{\sim}{\phi}_3 = \begin{Bmatrix} 0 \\ 0.2599 \times 10^{-1} \\ 0 \end{Bmatrix}$$

Sketch of Mode Shapes:

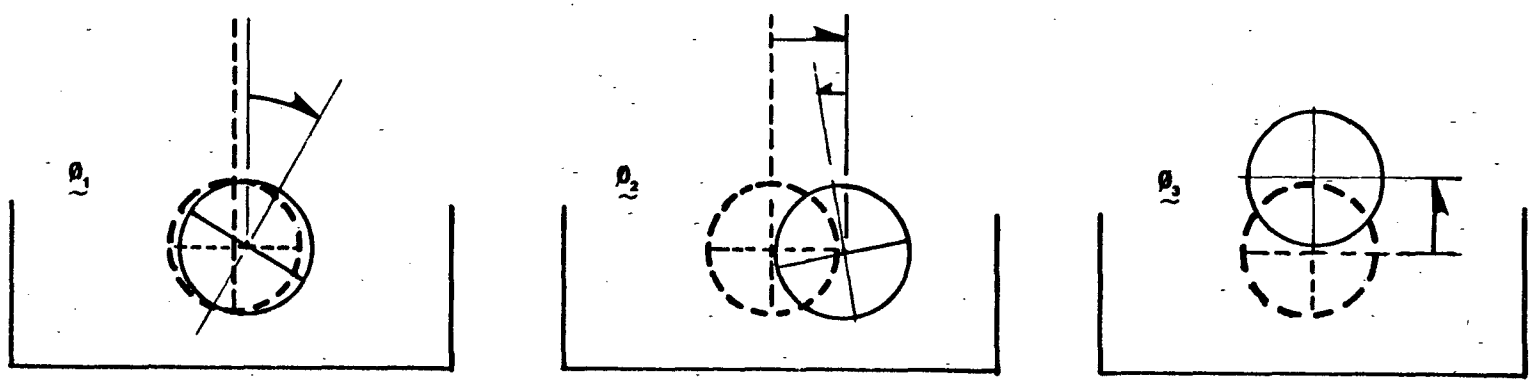

Figure 13. Natural Frequencies and Mode Shapes for a Blocked Submarine in Drydock.

The dynamic response results for the three displacement-time histories x(t), y(t) and θ(t) are shown graphed for a duration of almost 4 seconds in Figure 14(a). The drydock floor excitation is juxtaposed with the response data in Figure 14(b). The results show the rotational vibration growing due to a resonance condition in the absence of any assumed damping components in the blocking system as modeled. This is essentially the mode 1 resonance condition which was anticipated, and it predicts large rotational oscillations. For example, after shaking for 3 seconds the rotation amplitude has increased to 0.02 radians which amounts to about 3.6 inches of tangential displacement on the submarine hull's surface. Also, during the first 3 seconds of shaking, the maximum displacements of the hull center of gravity relative to the drydock are, respectively, 3.5 inches and 2.5 inches, in the horizontal and vertical directions.

Though an effort was made to make the model parameters in this demonstration as realistic as possible, these results are meant only to illustrate how the dynamic characteristics of a blocked vessel during drydock shaking can be calculated. The interaction between the vessel and the drydock is important to the understanding of the force and displacement effects for the vessel as well as the dynamic forces acting on the drydock floor. More attention must be given to an accurate description of the prescribed model parameters, and the prescribed acceleration of the drydock floor.

Measured Earthquake Response of Drydock

On 1 October 1987, a magnitude 5.9 earthquake with a 0.45g maximum acceleration occurred at Whittier Narrows in the Los Angeles Basin. The epicenter was approximately 42 km to the northeast from drydocks 1, 2, and 3 sited at the Long Beach NSY. Figure 15 shows the relative locations of these drydocks to each other. Strong-motion accelerograph instrumentation placed at two points on both drydocks 1 and 2 recorded the responses of the drydocks.

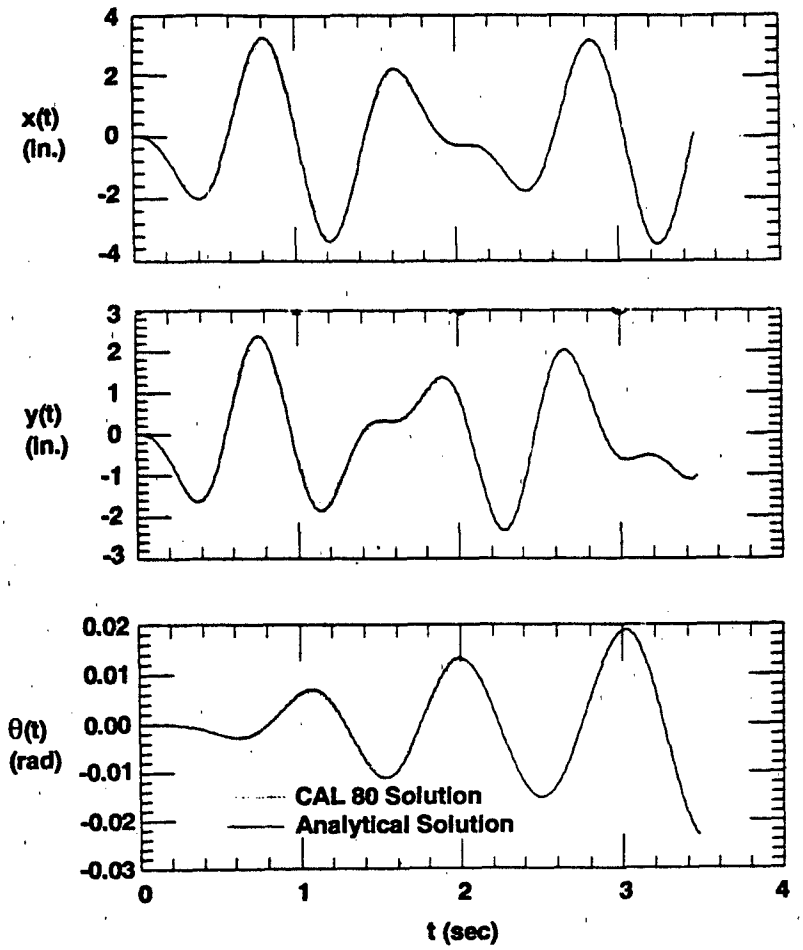

(a) Dynamic Response

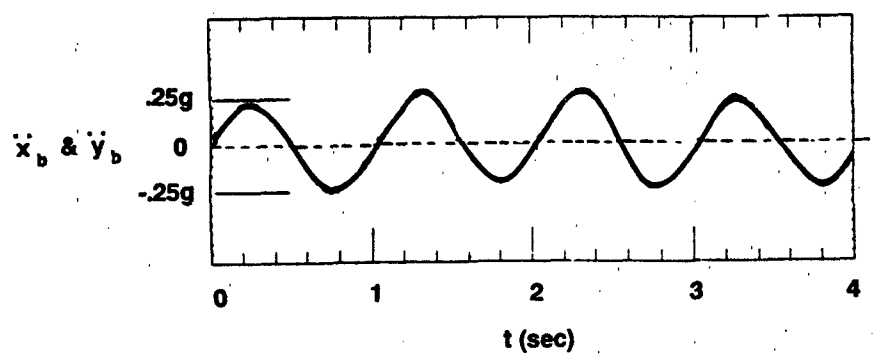

(b) Excitation

Figure 14. Dynamic Response of a Blocked Submarine in Drydock.

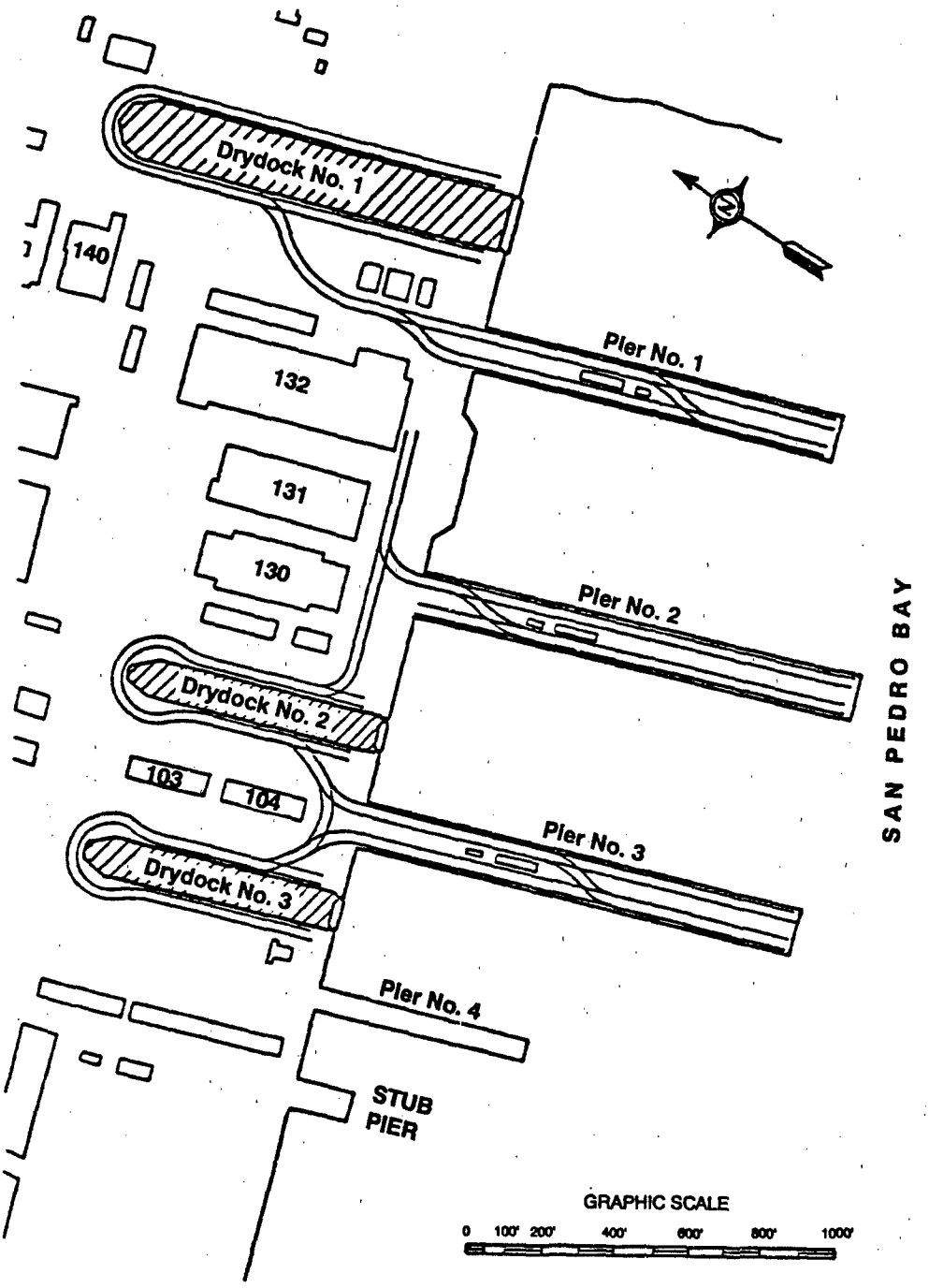

Figure 15. Location of Drydocks at Long Beach NSY.

The USS LEAHY (CG-16) was blocked in drydock 3 during the event, and sustained sufficient motion to cause permanent shifting of the hull relative to the side blocks. The relative displacements were recorded photographically, and discussed in the paper by Hepburn, et al. (1988). It is believed the drydock sustained only a 0.05g maximum acceleration during the event. Hepburn, et al. (1988) also describes a study in which post-predictions from a lumped parameter model of the blocked vessel successfully matched the recorded pattern of blocking movement. The purpose of this section is to provide a summary analysis and discussion of the corrected time histories of motion from the accelerograph traces which were compiled at the Naval Civil Engineering Laboratory (NCEL) by Lew (1988), and used in the model study by Hepburn, et al. (1988).

Accelerographs recorded the motion of drydock 1 at two stations, 580 feet and 875 feet from the caisson, along the length of the drydock. The time histories of the transverse component of the motion at the two locations are presented in Figures 16(a) and 16(b). The peak values of the motion are indicated in these figures. While the peak values of the motion at the two locations are not equal, they do occur at the same time. Further, the time histories for the two locations are remarkably similar. This can be observed by juxtaposing the two sets of graphs in Figure 16(a) and 16(b). Two points 295 feet distant had virtually the same kinematics in the transverse direction. The similarity is strongest for the acceleration. Some deterioration in this similarity is noted for the velocity and displacement (this is expected from the smoothing inherent in single and double integration of corrected acceleration data, from which these graphs are obtained). These data are clear evidence that drydock 1 responded essentially as a rigid body rather than as a deformable body in the transverse direction during the Whittier Narrows earthquake.

Similar conclusions can be drawn from an analysis of the data for the vertical and longitudinal components of the motion of drydock 1. Thus, it is believed that drydock 1, Long Beach NSY, responded as a rigid body to the 1 October 1987 Whittier Narrows earthquake.

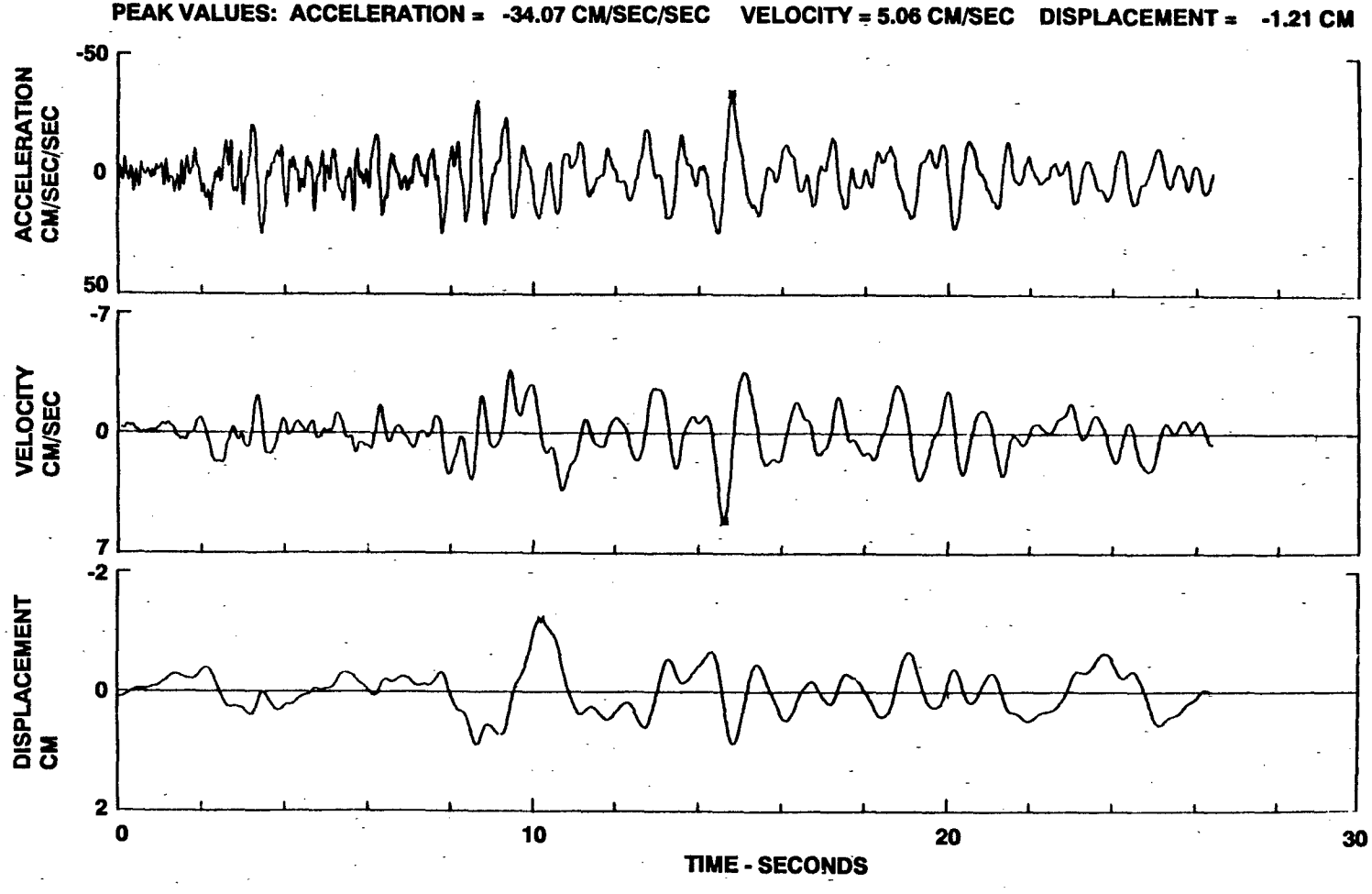

(a) Measured at 580 feet from caisson

Figure 16. Whittier Narrows Earthquake - Induced Motion of Drydock 1, LBNSY, Transverse Direction.

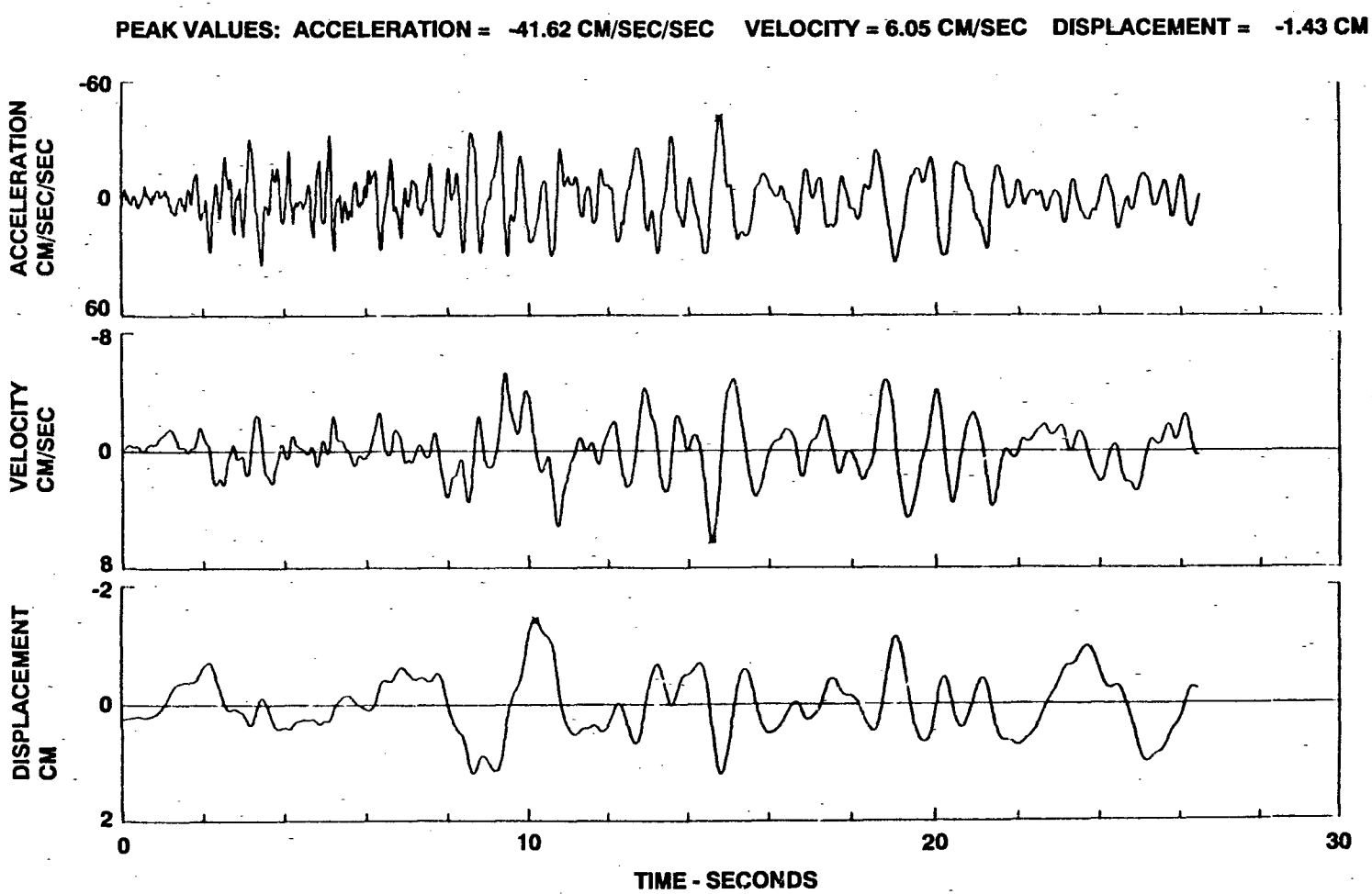

(b) Measured at 875 feet from caisson

Figure 16. Continued.

The data recorded for drydock 2 were neither as extensive nor as conclusive. There was some correlation between the longitudinal and transverse acceleration time histories. Again, correlation diminishes for velocity and displacement. There was no apparent correlation between the vertical acceleration time history and the transverse or longitudinal time histories.

An estimate of the natural period of the motion for drydock 1 can be obtained by the number of zero crossings in the displacement graphs of Figure 16 for a specified duration. The result is an estimated natural period of 1 second, or an estimated natural frequency of 1 hertz, for the excitation of drydock 1.

Since it is believed that this is rigid body motion, this natural frequency must also exist for the soil system in which the drydock is founded. At this particular site, the soil is soft hydraulic fill and beneath this are alternating layers of silts, sands, and clays which in turn overlay an aquifer. Scale model tests of the effects of embedment length on simple foundations conducted by Jennings and Wu (1984) tend to show the foundation and soil move as a rigid body for deep foundations.

Actual field data for the response of a large Navy drydock to earthquake loads are valuable. In this case, the drydock response is believed to be rigid body motion and the frequency of motion is influenced by the soil column upon which drydock 1 is sited. The input acceleration is, however, remarkably small, and does not qualify as strong-motion acceleration. Thus, the meaning of these data is limited in regard to the response of drydocks to strong-motion earthquakes. Nonetheless, however small the excitation, it was sufficient to cause damage to the blocking system supporting a ship.

THREE-DIMENSIONAL FINITE ELEMENT MODELS OF DRYDOCKS

Solids Modeling

Construction of three-dimensional finite element models requires substantial computer resources almost equal to those required for the actual analysis of the model. Computing power and computer storage are

required to manipulate and maintain large data files of information on geometry, large numbers of nodes, and the connectivity or relationship of elements to one another. As the data base grows, simple commands like inserting a single nodal point during model generation may take minutes, much to the chagrin of the user who is constructing the model.

The ease of constructing three-dimensional finite element models is dependent on the type of geometric model needed. Three-dimensional geometric models fall into three categories: (1) wireframes, (2) surfaces, and (3) solids. A brief discussion on how each pertains to finite element modeling is presented in Appendix B.

Substructure Modeling

Managing the complexity of a large three-dimensional finite element analysis of a drydock system could be greatly facilitated by substructure modeling procedures.*

Substructure theory is a generalization of the static condensation procedure in matrix structural analysis or in the finite element method where, for example, the nodal variables for an unattached internal node of a quadrilateral element are eliminated in terms of the nodal variables for the four corner nodes. In substructure modeling, the selection of the internal variables or degrees of freedom (dof) which are to be eliminated is arbitrary, so that a large structural/geotechnical system may be subdivided into substructures arbitrarily, and the dof internal to each substructure may then be eliminated, while retaining only the dof at the substructure interface level. The theory of substructure modeling in the context of drydock systems is reviewed in Appendix C.

Substructure modeling is but one approach to overcoming limited computer resources (speed and memory) when working with very large structural models. For effective use, analysts should be very familiar with the substructure modeling source code. Substructure modeling, while simple in theory, is difficult to implement in large-scale computer programs. A certain degree of substructure capability is included

*Przemiencki (1968) provides a classic introduction to the theory of substructures, while Furuike (1972) provides a more topical treatment of the method in the context of large-scale finite element problems.

in some commercial computer programs such as ADINA (ADINA Engineering, Inc., 1985), ABAQUS (Hibbitt, Karlsson and Sorensen, Inc., 1988), and GIFTS (CASA/GIFTS, Inc., 1988).

In practical application, there are three good reasons why substructure modeling is employed:

1. The same substructure repeats itself. When many substructures are identical, the method becomes computationally efficient.

2. Nonlinear behavior confined to a small part of the structure. Computational efficiency derives from reducing the size of expensive nonlinear calculations.

3. Organization of large-scale modeling of complex structures. For example, office A addresses the concrete drydock, office B addresses the pump house, and office C addresses the steel caisson.

Drydock Substructure Models

The construction of a three-dimensional finite element model of drydock 6 located at the Puget Sound NSY was attempted based upon the idea of substructure modeling. The model was to be built using eight-node solid brick elements for the walls and floor of the drydock, four-node plate elements for the utility tunnels atop the sidewalls, and elastic springs for the utility tunnel supports and surrounding soil. The material properties of the concrete and the steel rebar would be "smeared" to yield an effective material stiffness for the concrete dock. This is referred to as a smeared reinforcement model. No consideration was given to modeling various discontinuities (i.e., stairwells, etc.) or the shear/construction joints of the drydock.

The drydock was broken into seven substructures. These were the right main sidewall, the left main sidewall, the right end closure, the left end closure, the pumphouse, the head end, and the caisson. The level of discretization of the substructure was decided upon using the criteria that the aspect ratio of any element could not exceed 4.0 to

promote adequate accuracy in computed stresses, and the minimum number of solid elements through a cross section was to be four so that bending moments could be minimally captured. The computational size of the substructures was balanced against the computational size of the main system model by keeping the dof and bandwidth of the main model comparable to the dof and bandwidth of any substructure. Examples of the resulting substructure models are presented in Figures 17(a) through 17(f).

All of the substructures were created on a ComputerVision (Prime Computer, Inc., 1986) CAD/CAM system using finite element modeling software. This software was chosen because of its familiarity, ease of translation of data files for use with ADINA (the analysis program to be used), and it had graphics suitable for presentation requirements. However, this CAD/CAM system proved to be inadequate for large-scale modeling. It had two serious shortcomings. First, execution of the software was very slow. Predictably, as the number of solid elements in the drydock model increased the speed decreased. However, the system required 2 hours to generate four repeated slices of 250 elements in a sidewall substructure, and it required up to 10 minutes to renumber 200 nodes. Second, the capability of making parametric changes during construction of the substructure models was not supported by this system. Data for the nodes and foundation spring elements (approximately 1,000 each) had to be input one at a time. The times required to finish some of the substructures are listed in Table 3.

Table 3. Time Invested in Drydock Substructure Model Construction

Substructure	Time to Complete (weeks)
Right and left main sidewall	5
Right and left end closure	12
Caisson	6
Head end (not completed)	4
Pump house (not started)	--

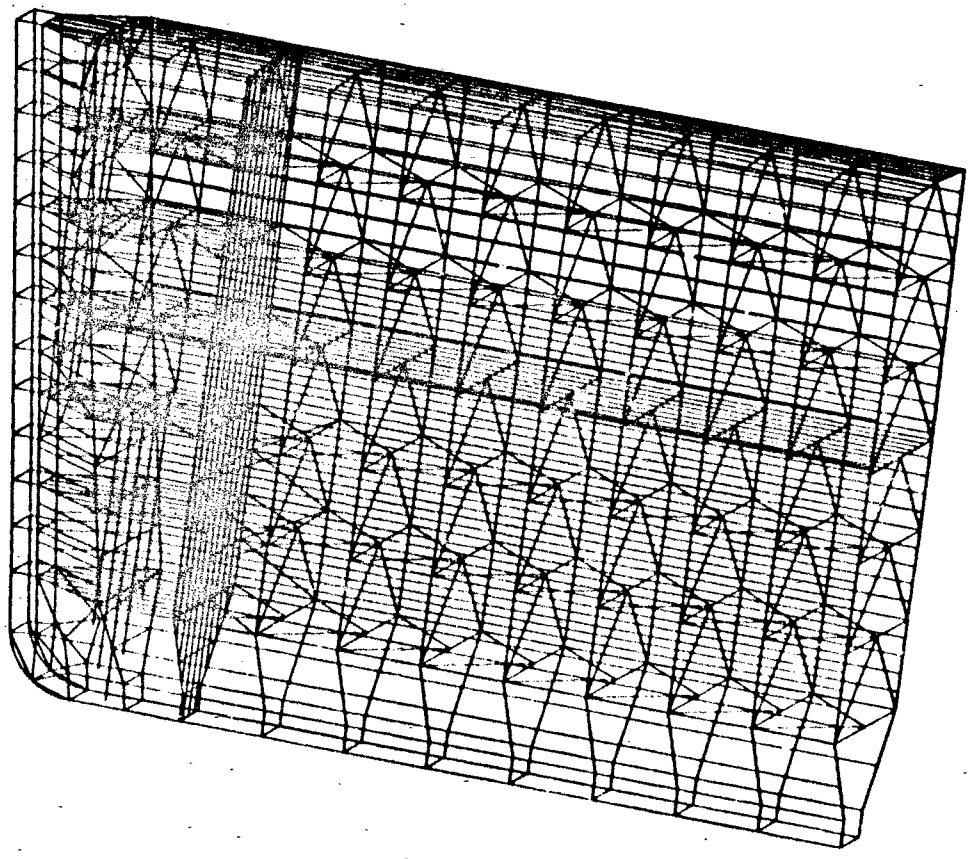

(a) Steel Caisson - Half Model

Figure 17. Drydock Substructure Models.

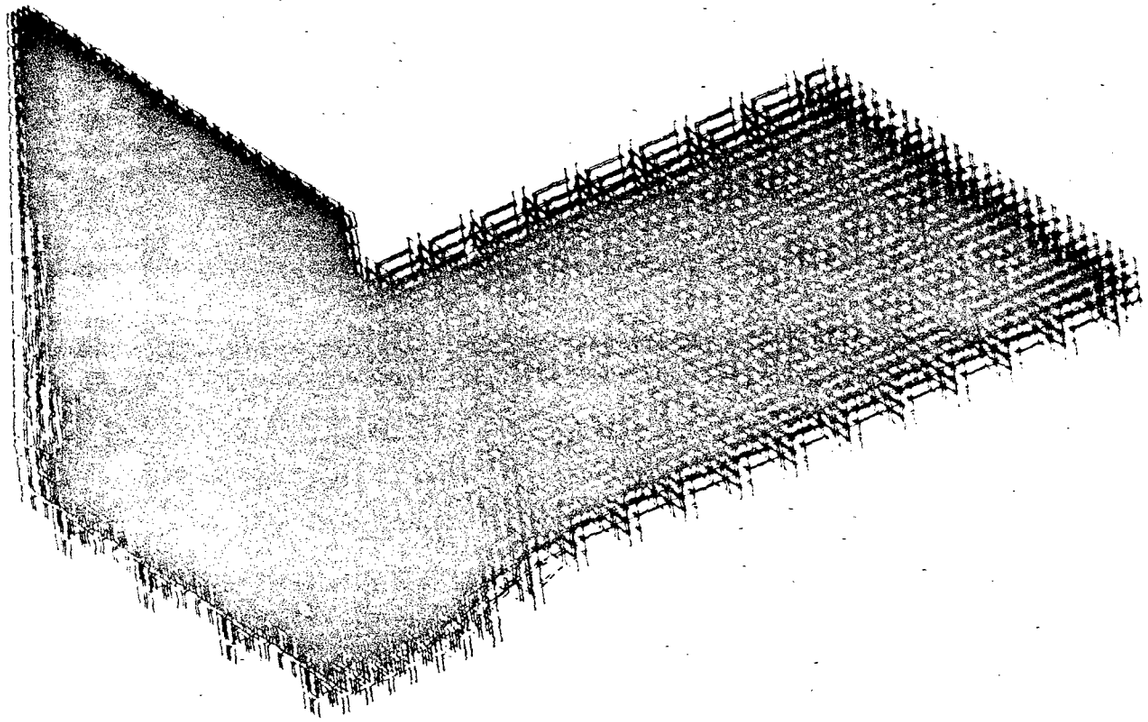

(b) Right Main Sidewall - Half Model

Figure 17. Continued.

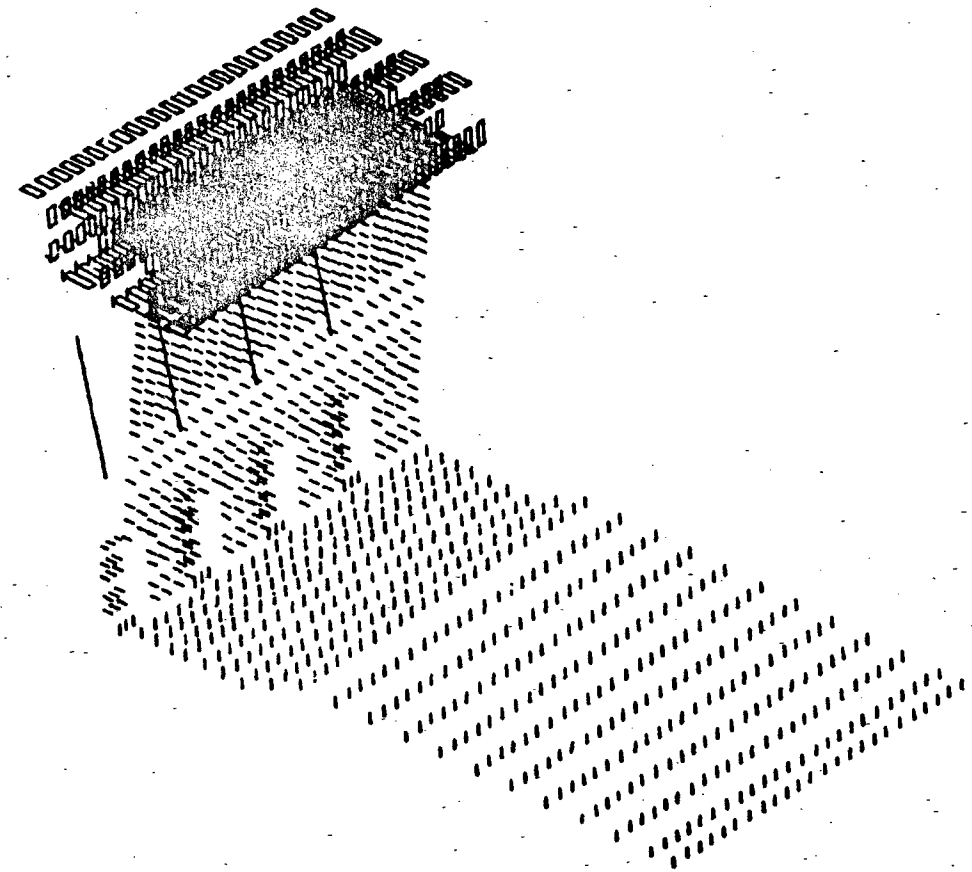

(c) Elastic Soil Foundation and Utility Tunnel for Right Main Sidewall - Half Model

Figure 17. Continued.

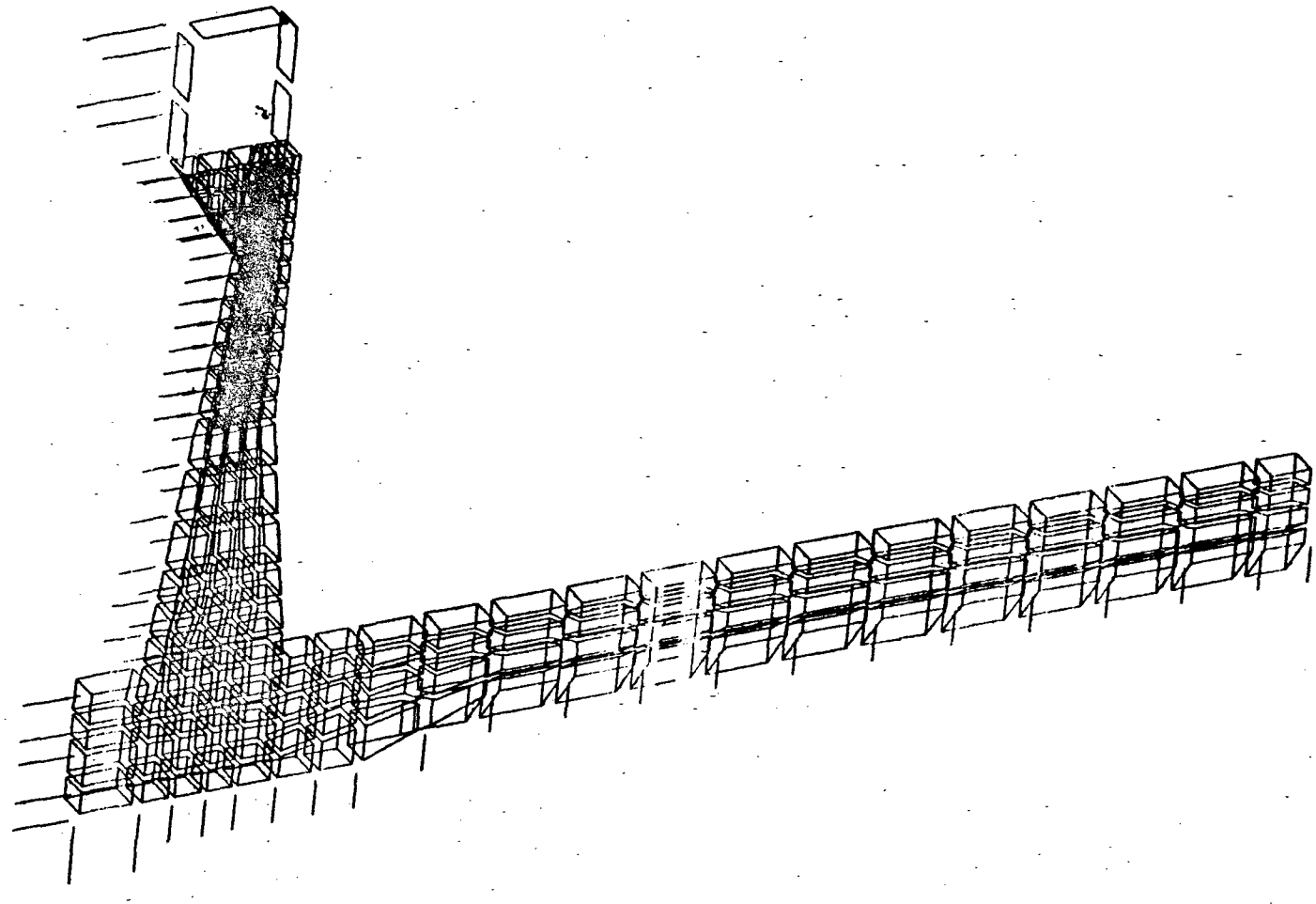

(d) Single Slice of Right Main Sidewall - Half Model

Figure 17. Continued.

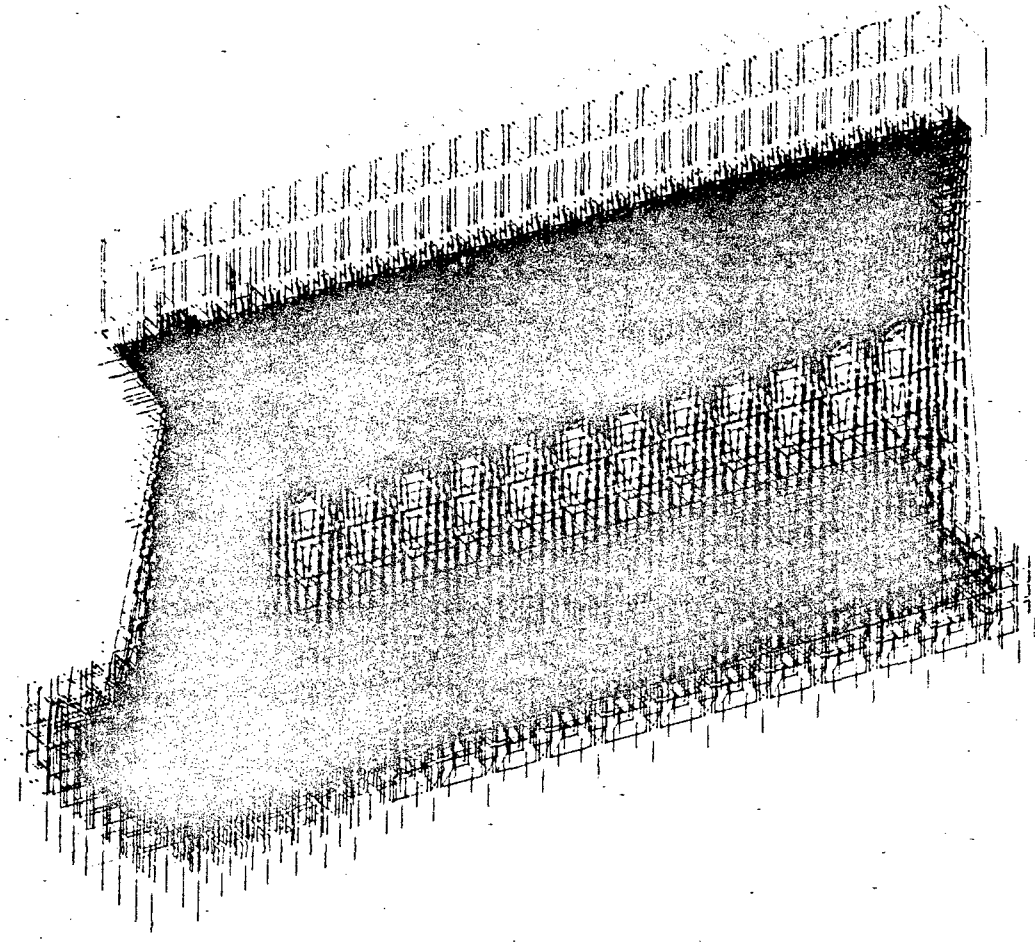

(e) Right Endwall - Half Model

Figure 17. Continued.

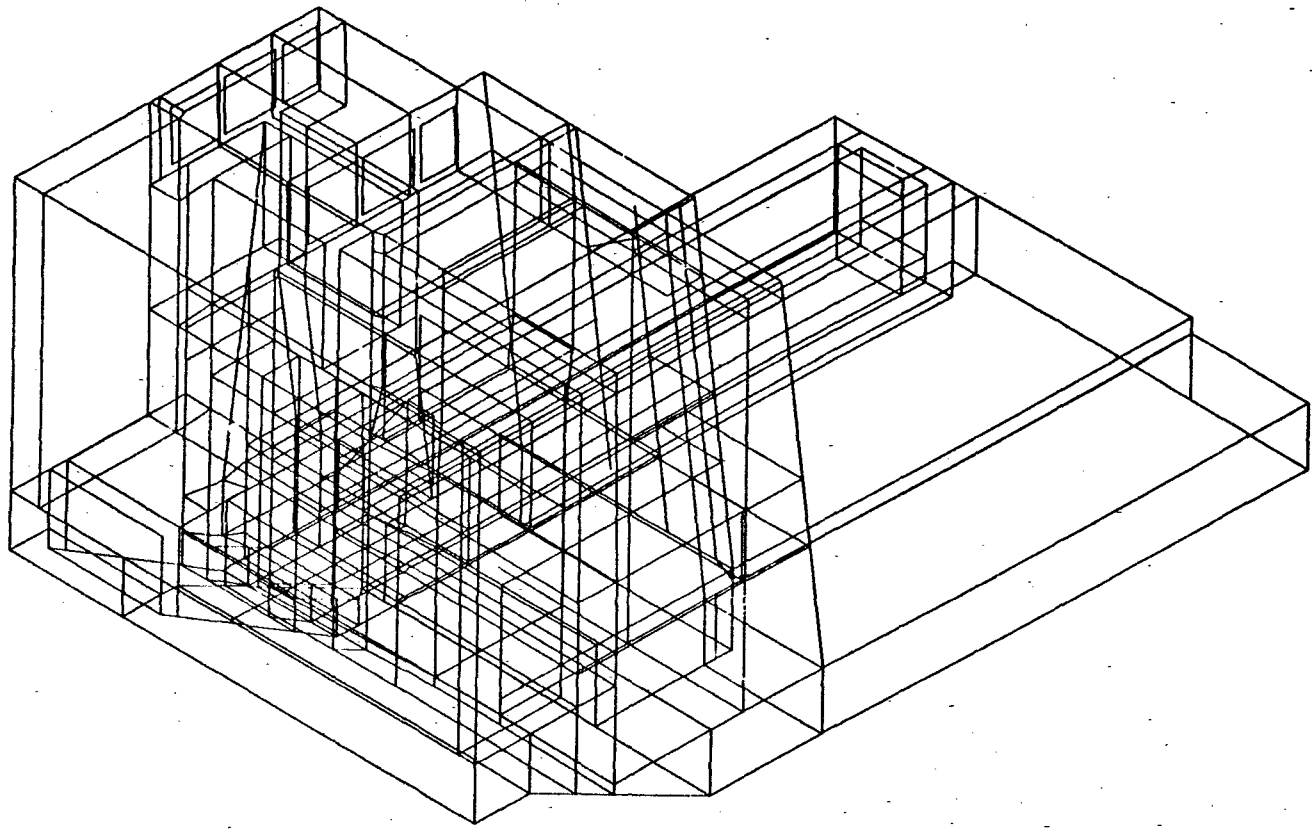

(f) Preliminary Box Model of Head End - Half Model

Figure 17. Continued.

It was later decided to switch the analysis package used from ADINA to GIFTS. This was done because ADINA did not have a usable substructuring capability that suited our problem. To use GIFTS, the model data files had to be translated from ComputerVision to GIFTS format. A FORTRAN program was written to do this. It required 8 weeks to write the file translation computer code, translate the files into GIFTS format, and verify the models. This was all done on the PC version of GIFTS. Another 6 weeks was devoted to using the GIFTS equation solver on each set of substructure equations to verify that the substructure model was valid.

An attempt was made to eliminate the internal nodes of the right main sidewall substructure using GIFTS. However, after a significant effort, it was found that the GIFTS substructure reduction capability could not cope with constrained nodes or springs on the boundaries of the sidewall. Analyzing the drydock using substructure modeling with GIFTS became impossible because it could not model the constrained nodes in the main model without assigning the main model all the dof of the substructures combined. This would defeat the idea of substructure modeling. Then it was decided to at least make a simpler "free-free" (i.e., no restraining nodes and no soils modeled) model for purposes of mode shape analysis using the substructure technique. However, problems were found in the GIFTS implementation of the substructure reduction algorithm for eigenvalue analysis. They were documented and forwarded to GIFTS support engineers.

A frequency analysis of the sidewall modeled as an independent structure, with soil foundation and boundary constraints included, was performed for a single one-element slice of the right main sidewall substructure model. Two versions of the model were employed (see Figure 9); one used solid elements to represent the soil and the other used spring elements to represent the soil. The eigenvalue analysis was completed on these two models using GIFTS. (The resulting natural frequencies and mode shapes were presented in the previous section of this report where two-dimensional models were discussed, see Figure 10.)

Large-scale analysis of a fully three-dimensional solid element model of the drydock using the substructure concept was not possible, due to the various problems and limitations with commercial software products mentioned above involving substructure modeling. Instead, a

much simplified three-dimensional model of the drydock as an independent structure was constructed using plate bending finite elements exclusively. Then using GIFTS, the eigenvalue analysis for the natural frequencies and natural mode shapes for this three-dimensional drydock model was easily completed. (The results are presented and discussed in a later section, Drydock Model Study.)

In summary, the ComputerVision CAD/CAM system did not provide sufficient hardware and software capability for construction of large, complex three-dimensional finite element models within any reasonable length of time and cost. The specific problems are:

- Hardware speed is too slow.
- Wireframe and solids modeling algorithms are inadequate.
- Combinations of solid and structural elements cannot be processed.
- Substructure combinations cannot be processed.

It is anticipated that new developments in the solids modeling industry as reflected in the latest version of the PATRAN Plus (1988) computer program or the MOVIESTAR computer program recently developed at Brigham Young University under Navy sponsorship, for example, will overcome the above problems and provide the necessary software capability to develop fully three-dimensional, substructured models of Navy drydocks.

Had the three-dimensional drydock system model envisioned here been successfully developed, it would have possessed several hundred thousand degrees of freedom. It is apparent that commercial finite element analysis software will have to improve substantially if the substructure theory approach is to be employed to manage the associated large-scale computational burden.

Caisson Model Study

Various finite element modeling approaches for analyzing the steel caisson of drydock No. 6, Puget Sound, are considered and demonstrated. Emphasis is given to caisson seal reaction loads assuming mainly that the seal is rigid.

Equivalent Flat Plate Finite Element Study of Caisson. To develop a preliminary understanding of the behavior of the caisson, calculations were made on an equivalent plate which is simply supported on three sides. This equivalent plate can be modeled via analytical methods in Timoshenko and Woinosky-Krieger (1959) or via numerical finite element methods. In both cases, the simply supported sides and the hydrostatic loads can easily be defined. The analytical model, however, is generally limited to rectangular plates and assumes classical boundary conditions so that the caisson seal will incorrectly carry tension. Alternatively, the finite element model allows for other than rectangular shapes (most caissons are trapezoidal) and more sophisticated boundary conditions including unilateral contact conditions or gapping. Either method, however, requires establishment of an equivalent plate thickness. The calculations for the equivalent plate thickness of the caisson are given in Appendix D. The result used for the study was determined to be 58.1 inches.

The symmetric half of the (176-foot 4.5-inch by 62-foot 10.5-inch, width versus depth) caisson was modeled as a rectangular plate. Numerical calculations were made using an equivalent flat plate finite element model of the caisson. (The analytical flat plate solutions were also considered, although they are omitted here for brevity.) Initial numerical tests were made to determine convergence rates of various finite element models of a rectangular plate simply supported on three sides and subjected to a hydrostatic load. The criteria used to evaluate the accuracy of the models is the centerline deflection at the top of the caisson and the boundary reaction loads on the caisson seal. The boundary supports are assumed to be rigid. The four-node shear flexible plate/shell elements in the ABAQUS finite element program were used.

The first series of tests, used to check the number of elements which are necessary for accurate solution convergence, employ the following caisson models: (1) model 1 uses a 4 by 10 element mesh, (2) model 2 uses a 28 by 20 mesh, and (3) model 3 uses a 42 by 30 mesh. Key results are shown in Table 4 and the seal responses are shown in Figures 18 through 20, respectively.

Table 4. Results of Finite Element Plate Model Convergence Study

Caisson Model No.	Mesh	Centerline Deflection (in.)	Seal Loads		
			Top Corner (lb/in.)	Bottom Corner (lb/in.)	Centerline Bottom (lb/in.)
1	10 x 4	1.633	-41,066	20,593	-9,678
2	28 x 20	1.633	-62,277	30,837	-9,736
3	42 x 30	1.633	-77,203	36,486	-9,750

It is noted that the seal response shows a large concentrated compression at the top corner and a large concentrated tension at the bottom corner (see Figures 18 through 20). The seal response along the vertical side shows an increase with depth as expected with a hydrostatic loading. The responses along the bottom show a very slight increase toward the centerline, but is relatively constant. As the mesh gets finer the responses at the corners tend to get more concentrated. The finite element solution is converging to what the linear theory of plates suggests, an infinite concentrated load at the corner of the free and supported edges. The centerline deflection and response of the seal along the bottom, however, show little change with mesh size. The 28 by 20 mesh was chosen for further analysis based upon these results.

Caisson model 4 is a 28 by 20 symmetric half of a mesh that is trapezoidal vice rectangular. The width across the top and the depth are unchanged, but the width across the bottom is smaller. The total hydrostatic load is correspondingly reduced by 8 percent. Results are presented in Table 5 and compared with those from model 2. The seal responses are shown in Figure 21.

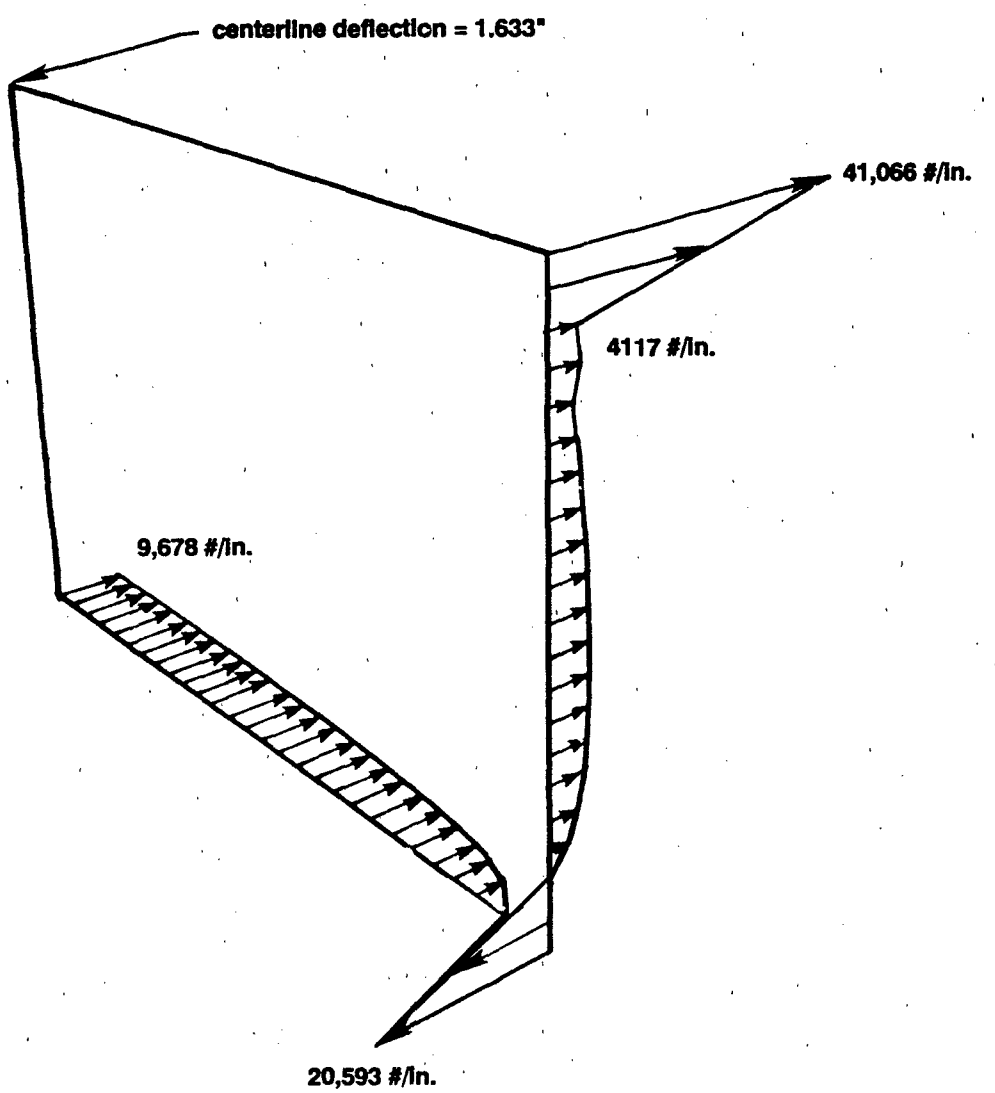

Figure 18. Rectangular Plate 10 x 4, Seal Reactions.

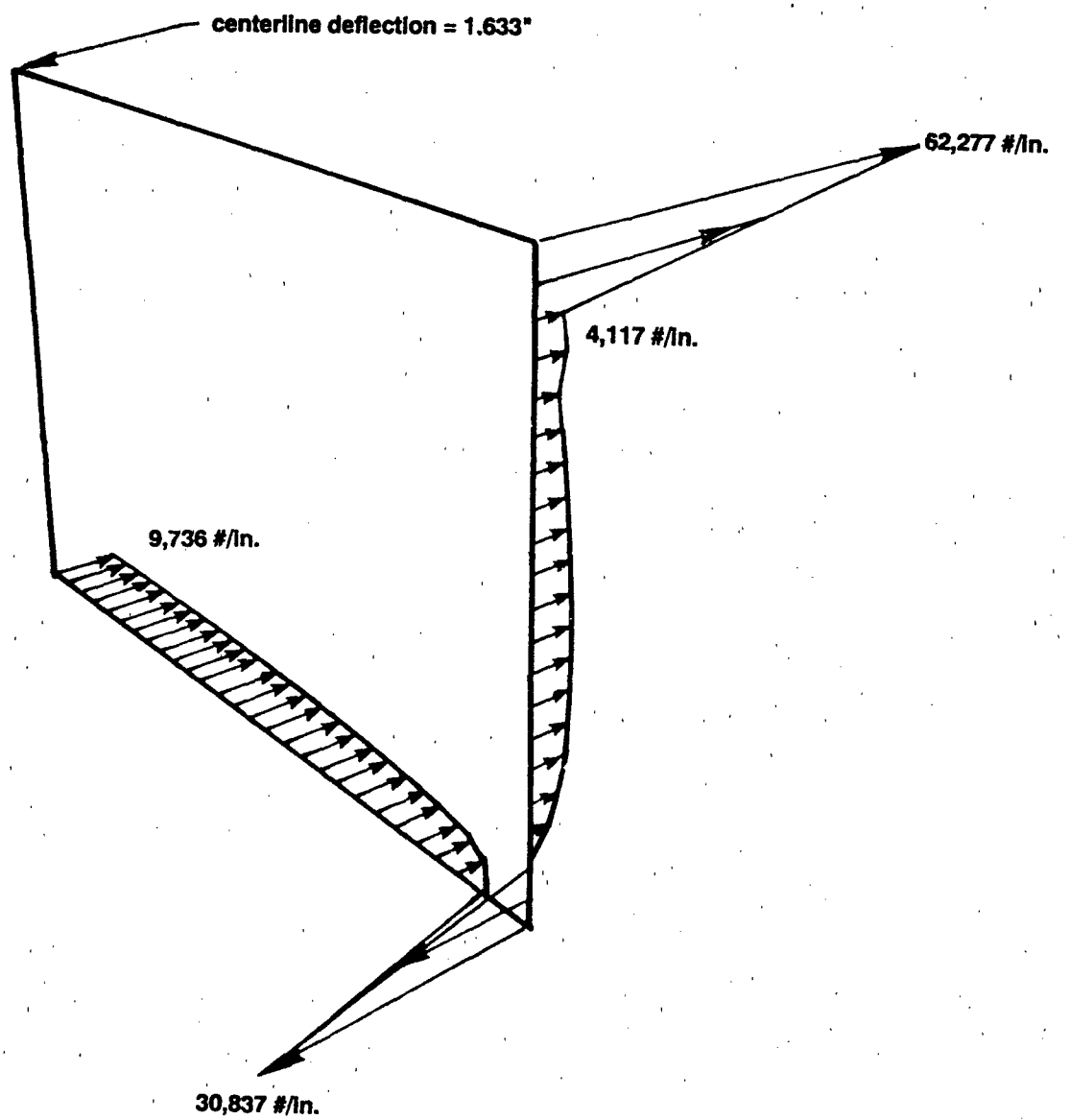

Figure 19. Rectangular Plate 28 x 20, Seal Reactions.

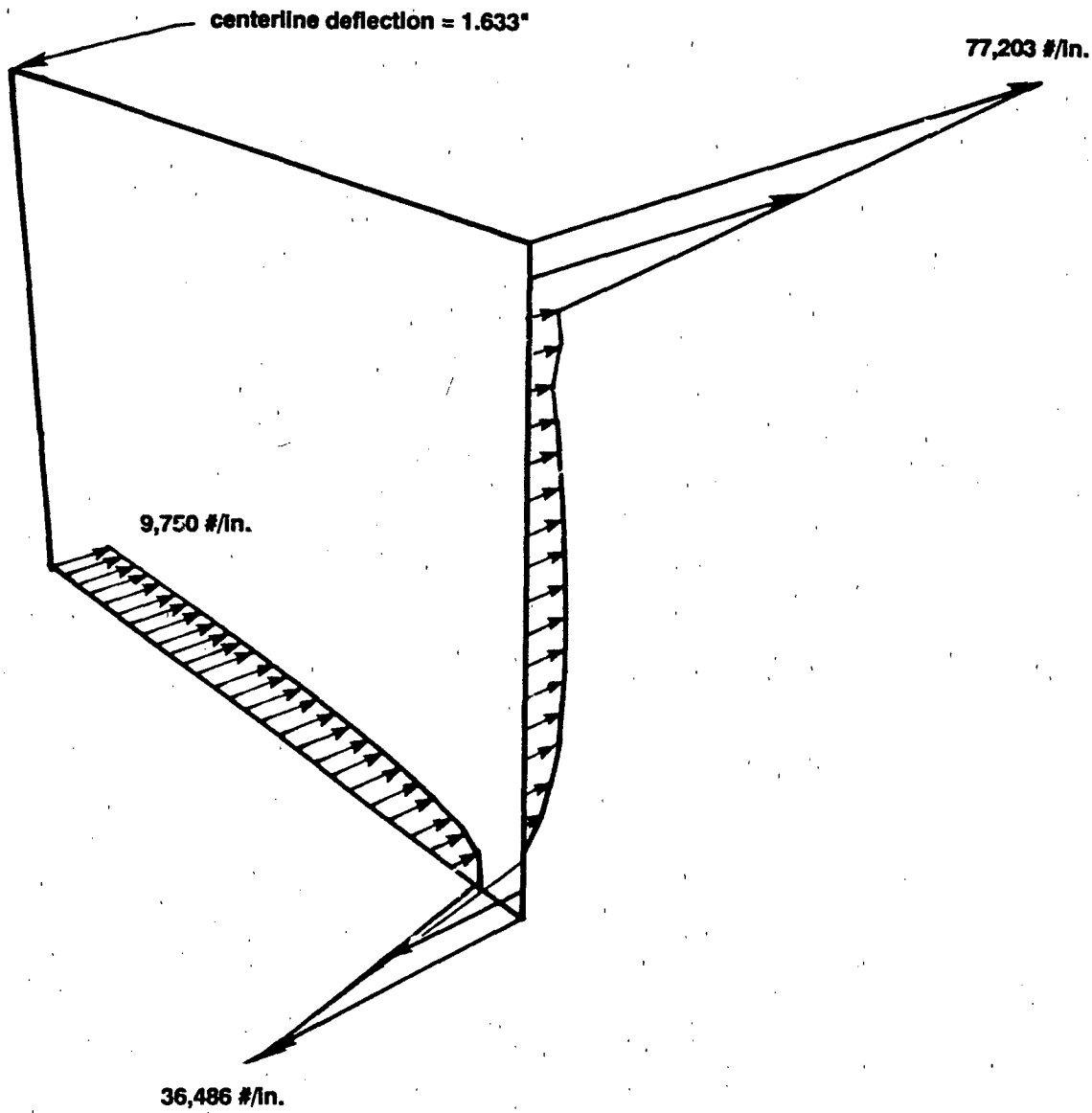

Figure 20. Rectangular Plate 42 x 30, Seal Reactions.

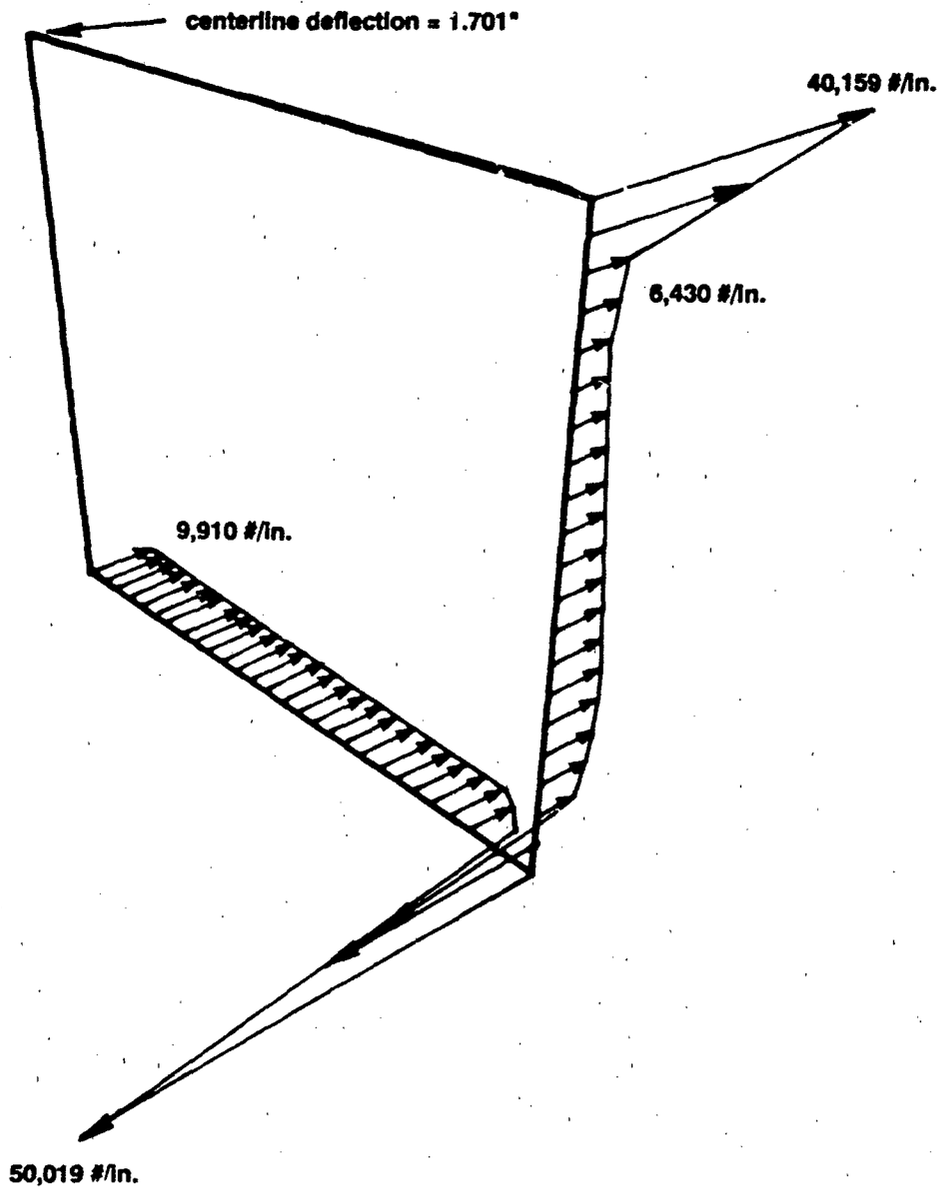

Figure 21. Trapezoidal Plate, Seal Reactions.

A slight increase in centerline deflection is noted for the trapezoidal shape. The compressive seal loads decrease significantly at the top corner and increase slightly at the bottom near the centerline. Also, the tension at the bottom corner increases significantly. Figure 21 indicates that although the magnitude of the peaks change, the basic behavior is the same.

Table 5. Results of Plate Model Geometry Study

Caisson Model No.	Mesh	Centerline Deflection (in.)	Seal Loads		
			Top Corner (lb/in.)	Bottom Corner (lb/in.)	Centerline Bottom (lb/in.)
2	28 x 20 Rectangular	1.633	-62,277	30,837	-9,736
4	28 x 20 Trapezoidal	1.701	-40,159	50,019	-9,910

Caisson model 5 is nonlinear because it allows gapping (or tension not allowed) along the seal. The results are shown in Figure 22. They illustrate how gaps may tend to form between the caisson and seal near the bottom corner (this area was in tension in previous models). Further, the compressive load acting on the seal is more concentrated. The length of seal that has released from the support is 74 feet of the total 142-foot width with a maximum gap of 0.276 inches at the corner. Additional results are given in Table 6.

In summary, the nonlinear caisson model shows an increase in maximum deflection and an increase in compressive loads on the seal. The maximum compression occuring along the bottom is of particular interest. In the linear model, the maximum compression along the bottom occurs at the centerline. The nonlinear model results show the maximum compression occurring near the separation point. Similar behavior is seen along the vertical edge of the seal.

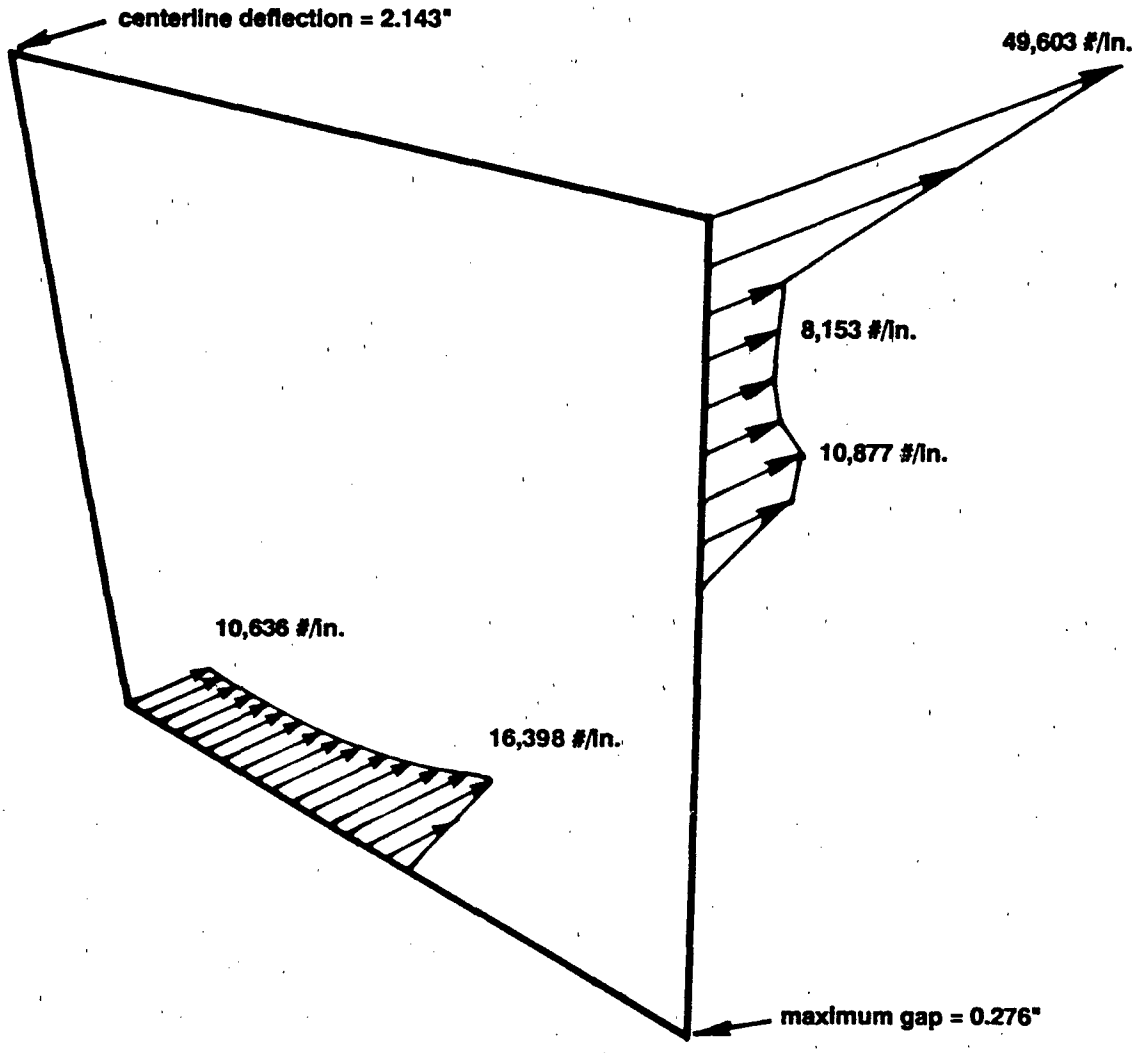

Figure 22. Nonlinear Analysis - Trapezoidal Plate/Seal Reactions.

Table 6. Results of Linear Model Versus Nonlinear Gapping Model

Caisson Model No.	Analysis	Centerline Deflection (in.)	Seal Loads	
			Top Corner (lb/in.)	Maximum Bottom[a] (lb/in.)
4	Trapezoidal linear	1.701	-40,159	-9,910
5	Trapezoidal nonlinear	2.143	-49,603	-16,397

[a]Maximum for the nonlinear run does not occur at the centerline (see Figure 22).

Three-Dimensional Finite Element Model Study of Caisson. The symmetric half of the caisson for drydock No. 6, Puget Sound, was modeled using detailed three-dimensional finite element technology. The internal frame was modeled beam for beam as shown in Figure 23. The plate structure consists of the external plates that are stiffened with small angle members and internal plates (bulkheads) that are used for stiffening the caisson and separating compartments, and these are modeled as shown in Figure 24. The external plates are modeled approximately with plates of equivalent thickness. The caisson is supported along the outside edge of the seal and is subjected to gravity and hydrostatic loads.

Model 6 incorporates the internal frame and shell structure of the caisson as described and also includes the stiffness of the concrete placed in the bottom of the caisson for ballast. The computed seal loads are shown in Figure 25. The concrete stiffness removes the compression spike near the bottom corner, but increases the tension carried at the corner. Key results of model 6 are compared with the equivalent plate model trapezoidal (model 4) in Table 7

Model 6 shows a significant reduction in deflection and in the seal loads. The maximum compression along the bottom is nearly unchanged, but the location predicted by the equivalent plate model was at the centerline whereas model 6 predicted a location between the bottom corner and the centerline.

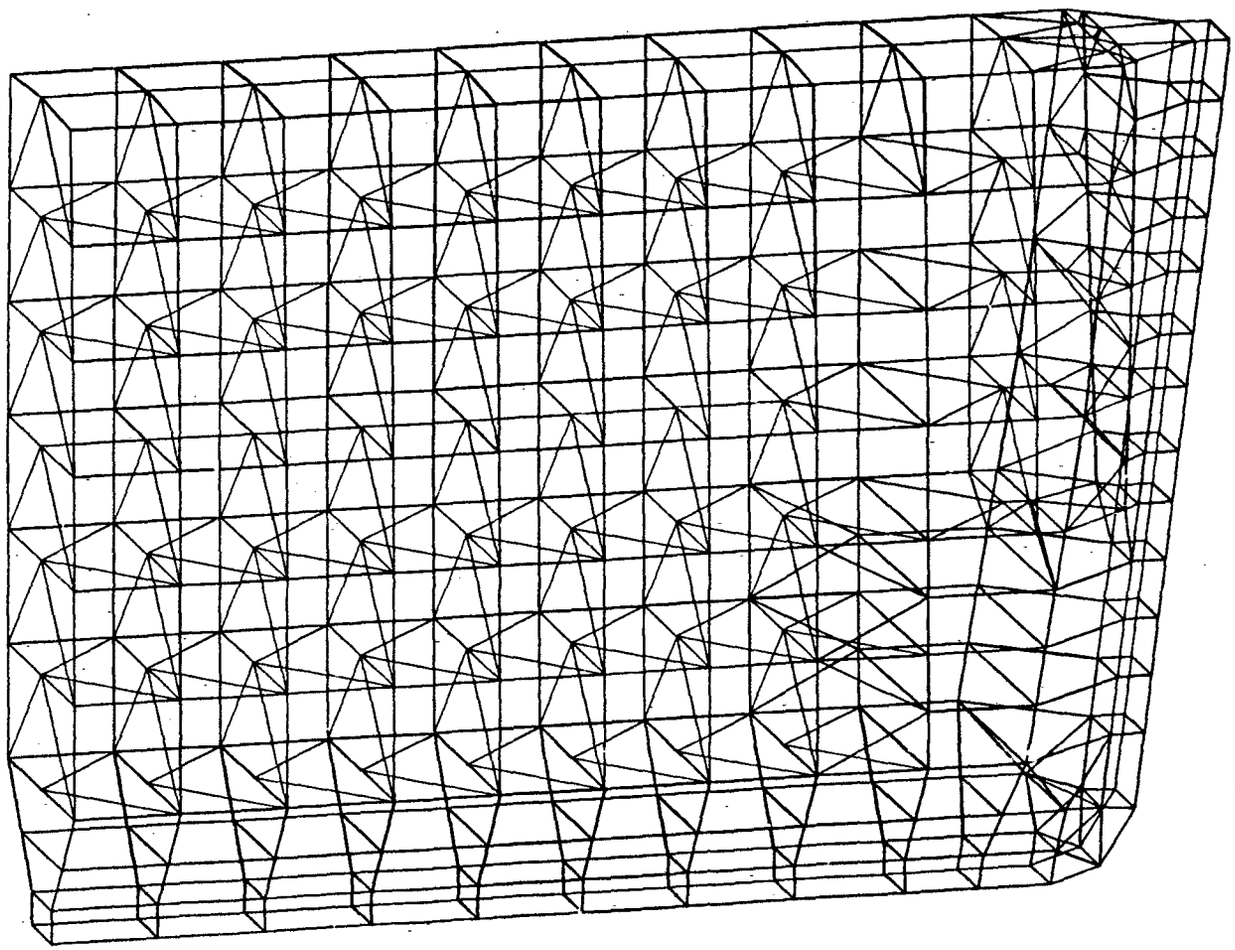

Figure 23. Internal Beams of Caisson (Symmetric Half).

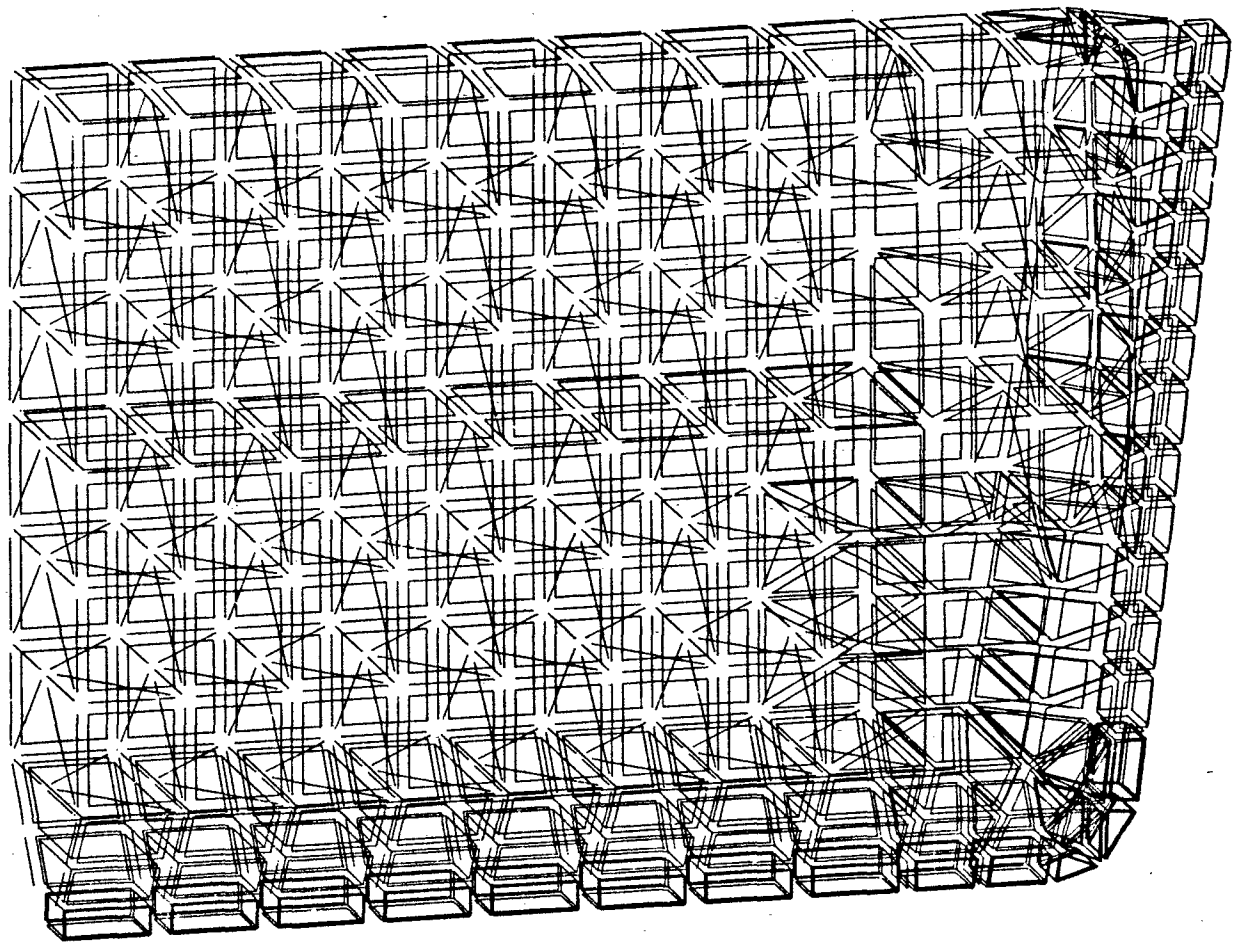

Figure 24. Plate Structure of Caisson (Symmetric Half).

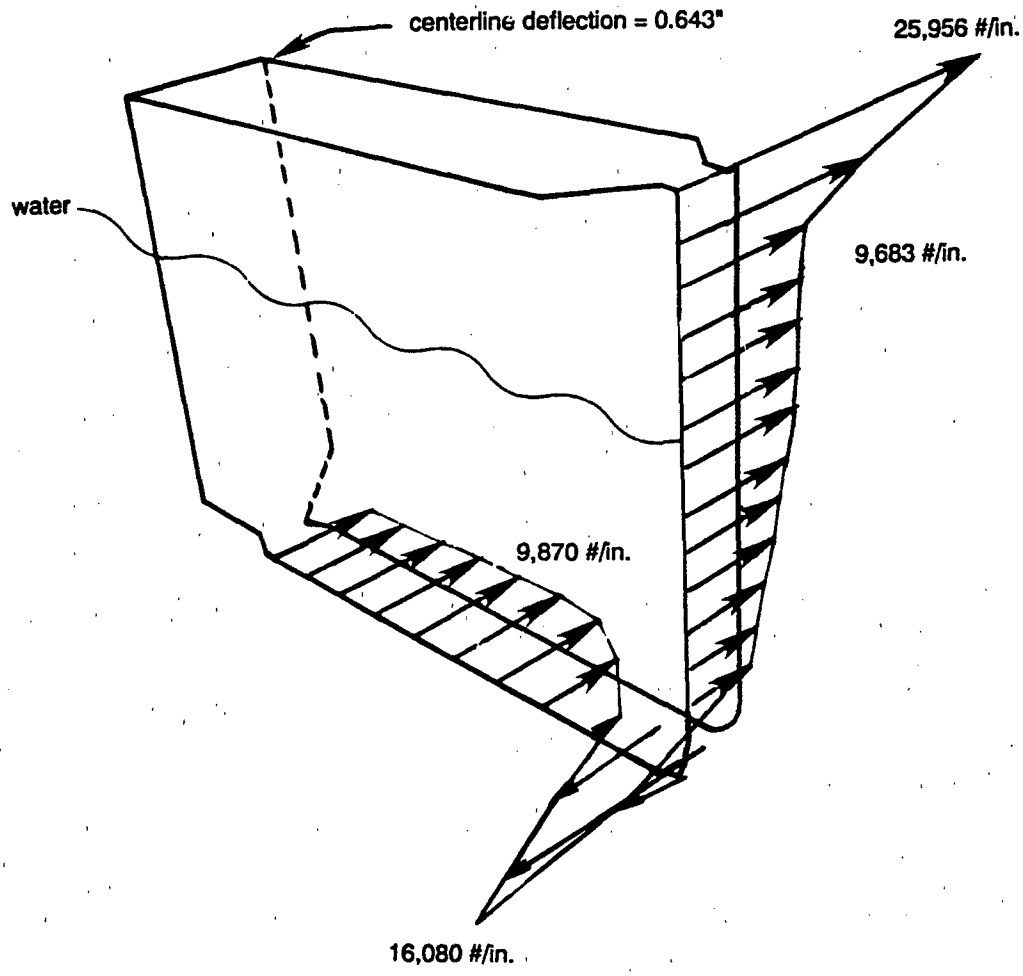

Figure 25. Seal Reactions - Linear Calculation.

Table 7. Results Comparing Equivalent Plate and 3-D Finite Element Models of Caisson

Caisson Model No.	Model Type	Centerline Deflection (in.)	Seal Loads		
			Top Corner (lb/in.)	Bottom Corner (lb/in.)	Maximum Bottom[a] (lb/in.)
4	Equivalent Plate	1.701	-40,159	50,019	-9,910
6	3-D	0.643	-25,956	16,080	-9,870

[a]Maximum for the nonlinear run does not occur at the centerline (see Figure 25).

Model 7 is a nonlinear analysis version of model 6 that allows gapping. The seal response is shown in Figure 26. Results from the nonlinear equivalent plate trapezoidal model (model 5) are compared to model 7 in Table 8.

Table 8. Results Comparing Nonlinear Equivalent Plate and Nonlinear 3-D Finite Element Models of Caisson

Caisson Model No.	Analysis	Centerline Deflection (in.)	Seal Loads		
			Maximum Gap (in.)	Top Corner (lb/in.)	Maximum Bottom[a] (lb/in.)
5	Equivalent Plate	2.143	-0.276	-49,603	-16,397
7	3-D	0.763	-0.102	-31,381	-10,713

[a]Maximum for the nonlinear run does not occur at the centerline (see Figure 26).

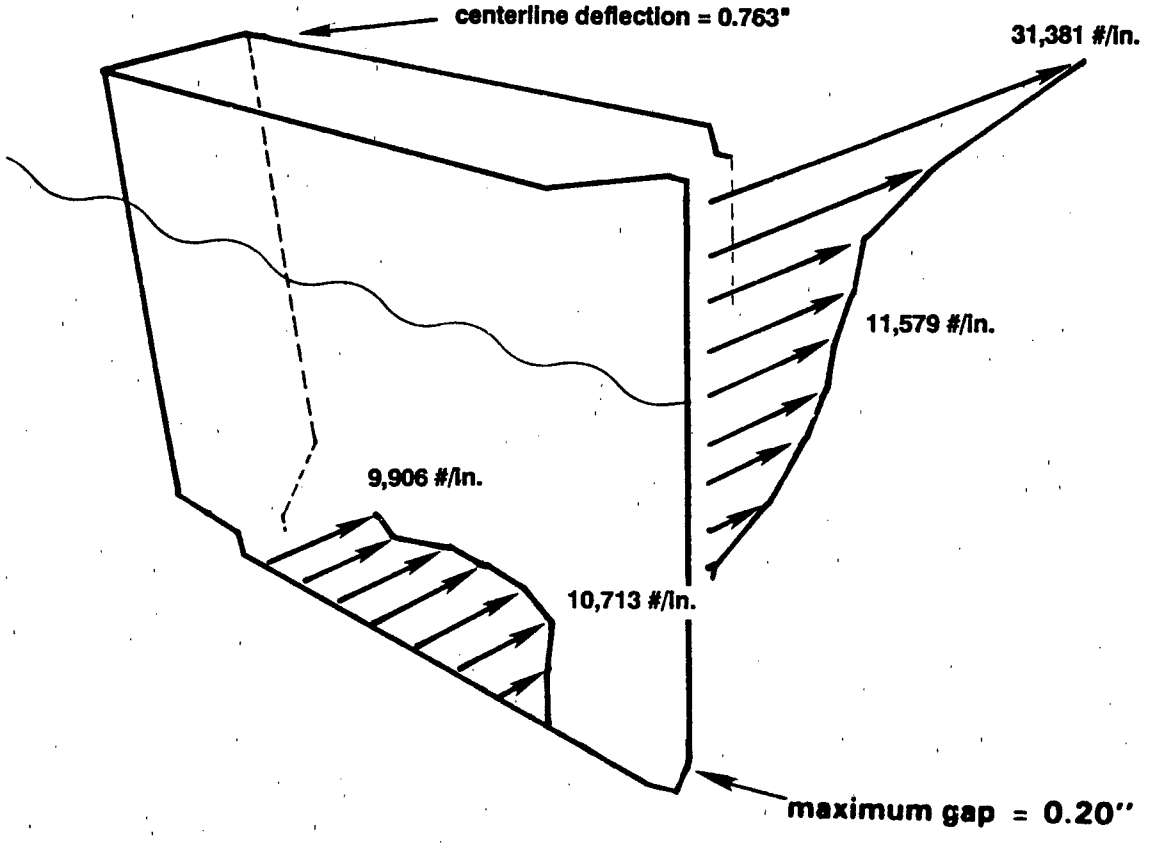

Figure 26. Seal Reactions - Nonlinear Calculation.

Model 8 estimates the behavior of the caisson bearing against a flexible seal. The flexible seal is implemented in a crude fashion via linear springs. The results from model 8 show that a flexible seal distributes the load uniformly. Further, there is no gapping. The centerline deflection is 2.445 inches. Deflections at the top corner and the bottom centerline are 1.451 and 0.669 inches, respectively. These results are shown in Figure 27.

Natural Vibration Analysis of a Caisson

A natural vibration analysis considering the symmetric half model of the caisson (Figures 23 and 24) was performed. The natural frequencies and periods for the first five symmetric modes are given in Table 9. The corresponding natural mode shapes are shown in Figures 28(a) through 28(e).

Table 9. Caisson Natural Frequencies and Periods

Mode No.	Frequency (Hz)	Period (sec)
1	9.041	0.1106
2	20.579	0.0486
3	24.904	0.0402
4	24.911	0.0401
5	24.918	0.0401

The first mode shape of vibration (Figure 28a) is similar to the shape the caisson would take when subjected to a hydrostatic load. It would be expected to be the dominant mode in the dynamic response to an earthquake load or to a uniform blast load. The second and third modes (Figures 28b and 28c) are similar in shape in the vertical direction to higher modes of a vertical cantilever wall. The fourth mode (Figure 28d) is a local deformation mode in the hull, as is the fifth mode (Figure 28e) which also contains a global horizontal deformation mode.

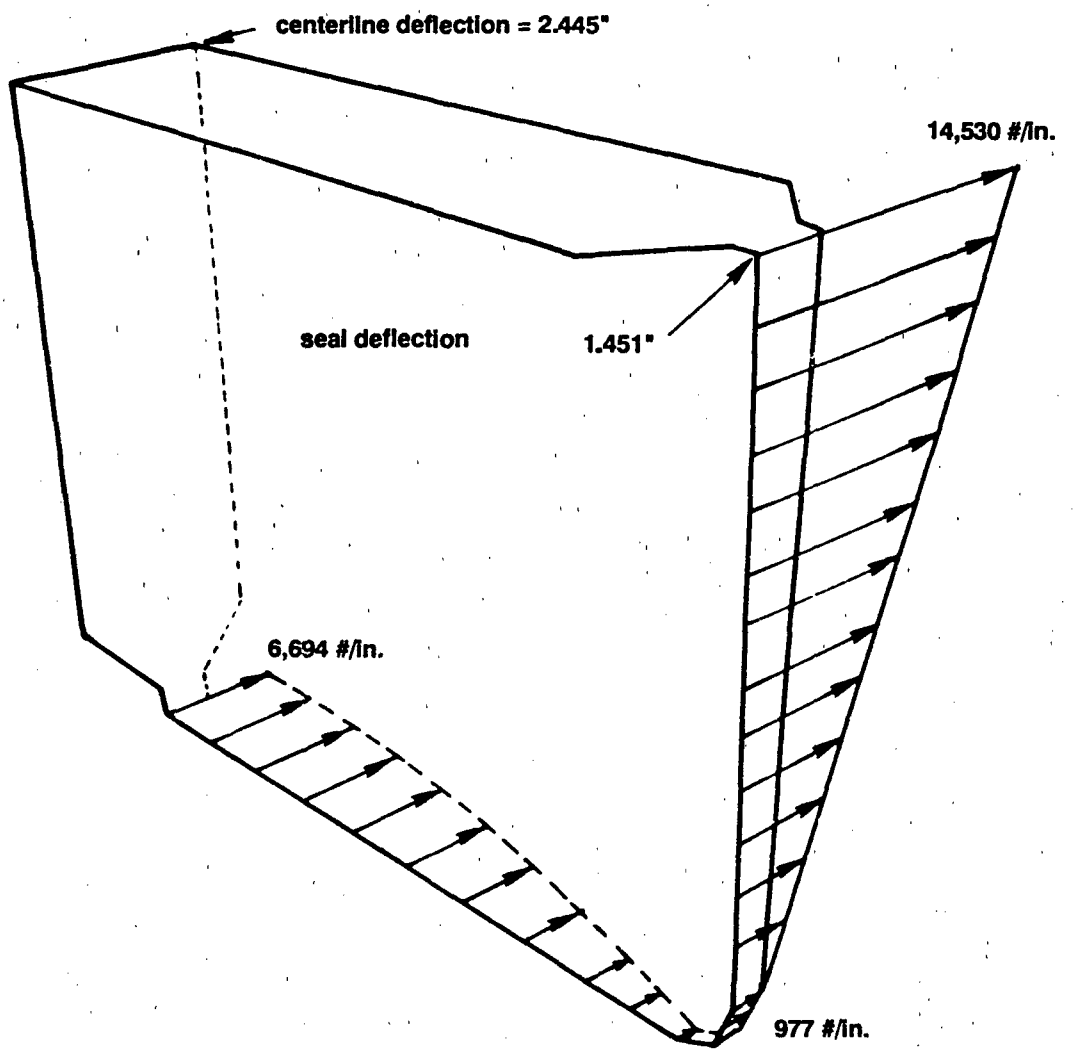

Figure 27. Seal Reactions, Nonlinear Calculation - Flexible Seal.

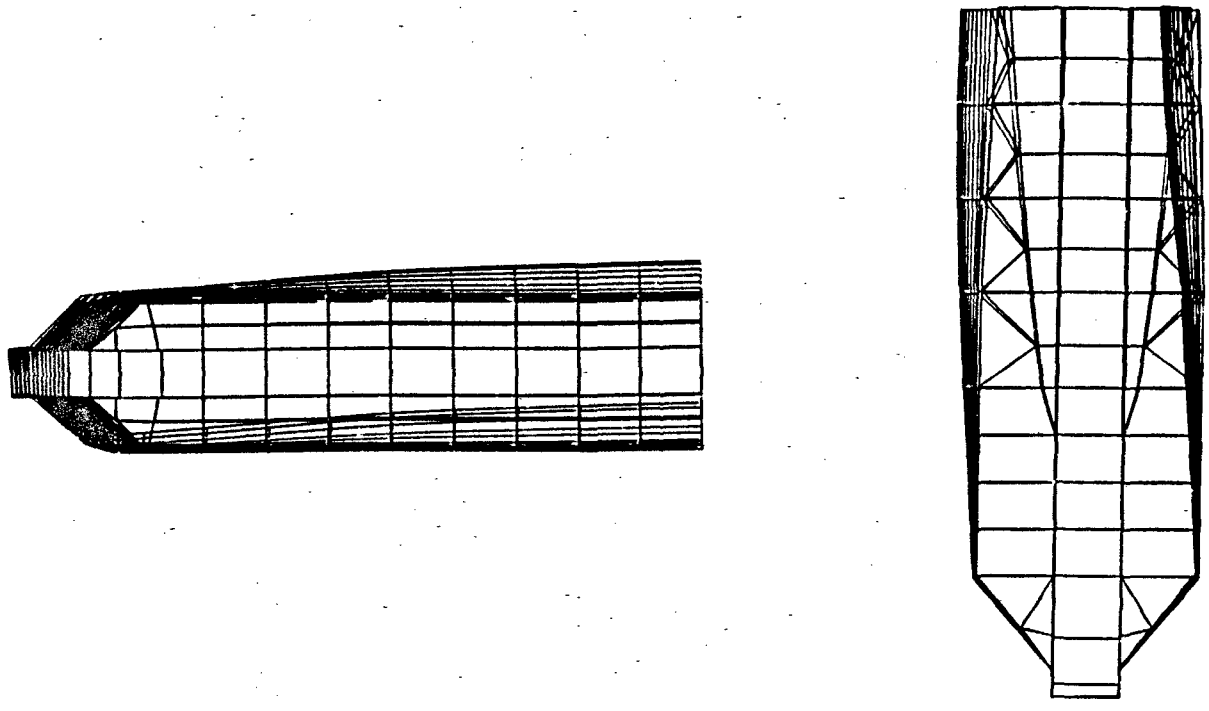

(a) MODE 1, 9.04 Hz

Figure 28. Natural Frequencies and Mode Shapes - 3-D Steel Caisson Model.

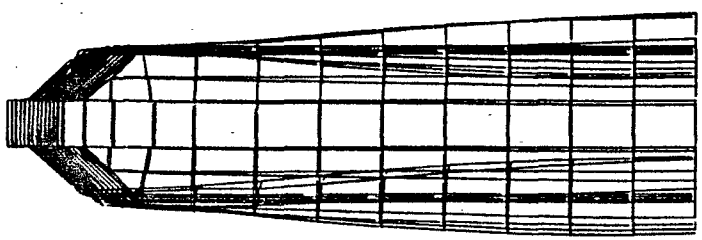

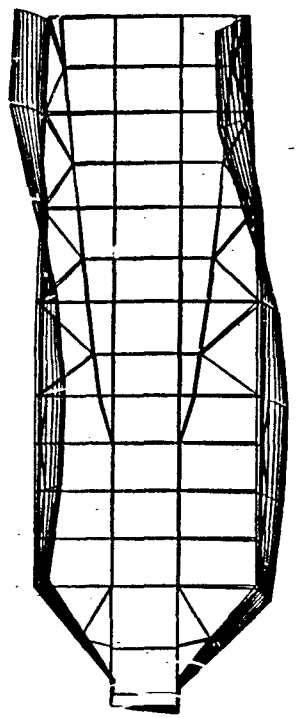

(b) MODE 2, 20.58 Hz

Figure 28. Continued.

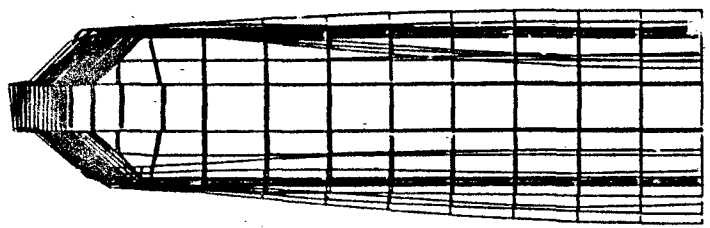

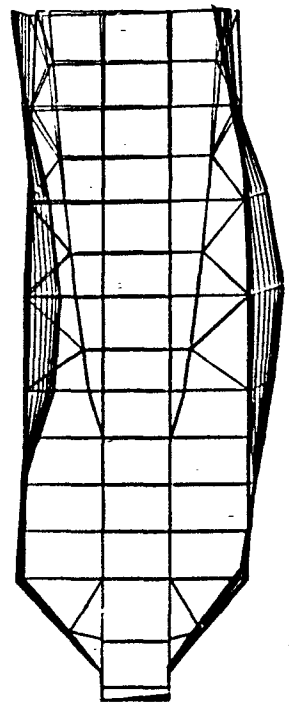

(c) MODE 3, 24.90 Hz

Figure 28. Continued.

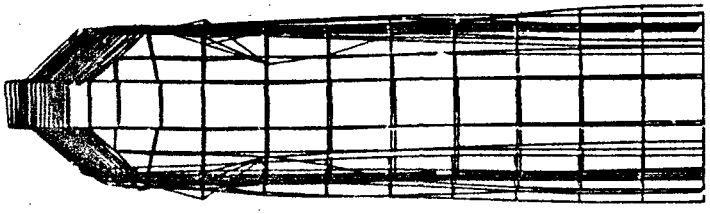

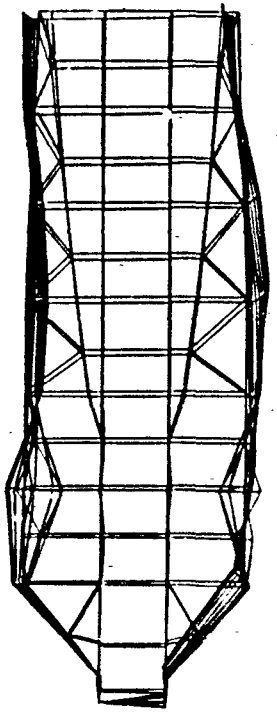

(d) MODE 4, 24.91 Hz

Figure 28. Continued.

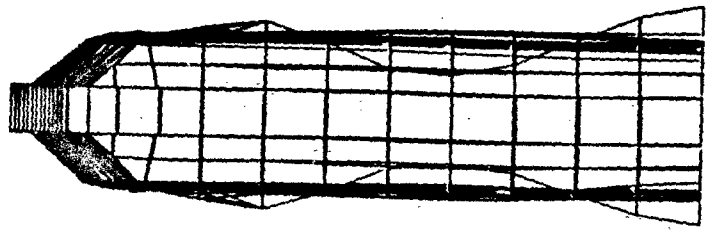

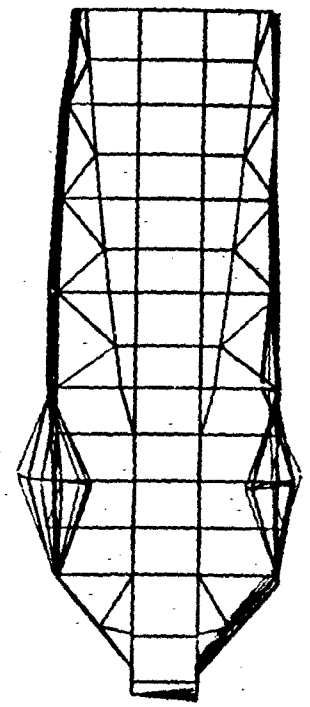

(e) MODE 5, 24.92 Hz

Figure 28. Continued.

Drydock Model Study

A simplified three-dimensional finite element model of drydock No. 6 at Puget Sound was constructed to demonstrate the fundamental nature of the natural modes of deformation inherent in the dynamic response of a drydock. One- and two-dimensional models, as discussed in previous sections of this report, yielded limited information in this respect. Despite the inability to effectively construct a fully three-dimensional model (with substructure-level detail) in a reasonable length of time, a simplified model was constructed which was sufficient to demonstrate the natural frequencies and natural mode shapes of a large, thin-walled drydock.

Plate Bending Finite Element Model of a Drydock. The three-dimensional model of the drydock is based on the cross-sectional idealization of drydock 6 (see Figure 1) used to construct the one-dimensional continuous beam model of the drydock. This latter model was discussed in the first section of this report where its natural frequencies and mode shapes were presented; these data will, therefore, be comparable with the calculated values of natural frequencies and mode shapes for the present three-dimensional model.

The present model was developed and analyzed using the GIFTS general purpose finite element program. The model is shown in Figure 29 and consists of over 780 four-node quadrilateral plate bending finite elements. A summary of the model is presented in Table 10. These data have been described and used in defining models previously discussed for the concrete drydock and for the steel caisson. The three-dimensional model is consistent with the one-dimensional continuous beam model with tip masses that represent the inertia of the endwall and caisson. The caisson section of the model is consistent with the plate bending finite element model used to study door seal loads. The overall stiffness distribution and mass distribution of drydock No. 6 is reasonably well replicated with this simple three-dimensional structural idealization.

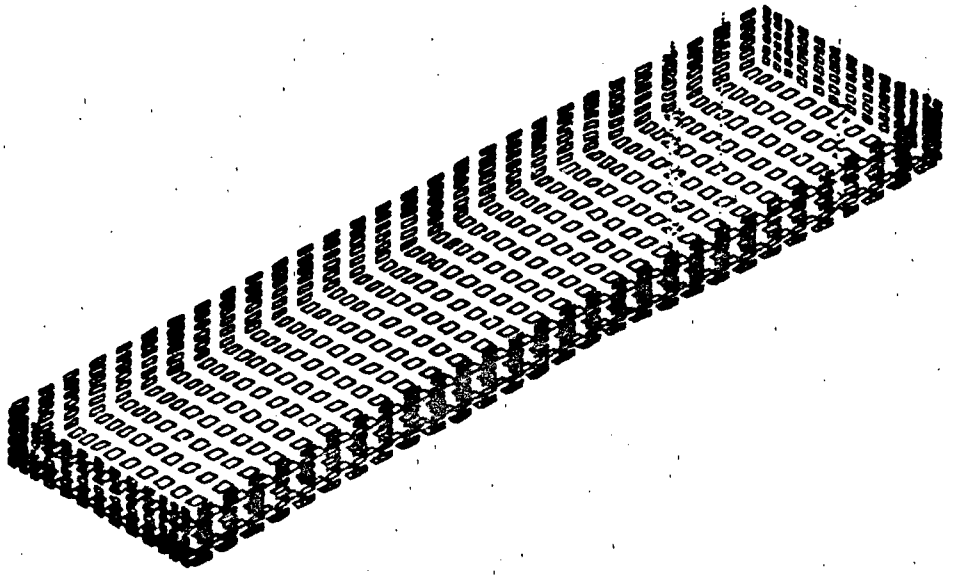

Figure 29. Three-Dimensional Plate Bending Finite Element Model of Drydock 6 at Puget Sound NSY.

A similar, simple idealization of the surrounding soil and foundation of the drydock is omitted from the three-dimensional model for the sake of expediency. From the previous study of one-dimensional models, it was shown that the natural mode shapes (not natural frequencies) of the model were independent of the soil foundation. It may be expected that an approximately similar situation exists for the present three-dimensional model.

Table 10. Summary of Three-Dimensional Finite Element Model Data for Drydock No. 6, Puget Sound NSY

Size:	650 in. high x 2,250 in. wide x 9,120 in. long
Drydock Wall Thicknesses:	
Top of Wall:	70 in.
Corner of Wall:	120 in.
Corner of Floor:	120 in.
Center of Floor:	110 in.
Equivalent Caisson Thickness:	56.5 in.
Material Properties:	
Concrete Dock	
Modulus of Elasticity:	4×10^6 psi
Mass Density:	2.25×10^{-4} lb-s^2/in. per in.^{3}
Steel Caisson	
Modulus of Elasticity:	29.5×10^6 psi
Mass Density:	7.339×10^{-5} lb-s^2/in. per in.^{3}

Natural Frequencies and Natural Mode Shapes. The first 10 nonzero natural frequencies and natural mode shapes are shown in Figures 30(a) through 30(j). Each figure includes four views of the mode shape information along with the value of the natural frequency. These different views aid in determining the nature of the deformation in each mode. Recall that bending moment magnitude is proportional to magnitude of curvature in the walls and floor of the deformed drydock. Thus, the location and relative intensity and direction of bending moment in the drydock walls and floor associated with each mode shape can be detected by scanning the deformed finite element mesh for areas of high curvature.

The main observation is that these natural mode shapes are primarily composed of longitudinal deformation modes. These modes are somewhat similar to the modes obtained from the one-dimensional continuous beam model, but they are entirely different from those obtained from the two-dimensional, plane strain finite element model.

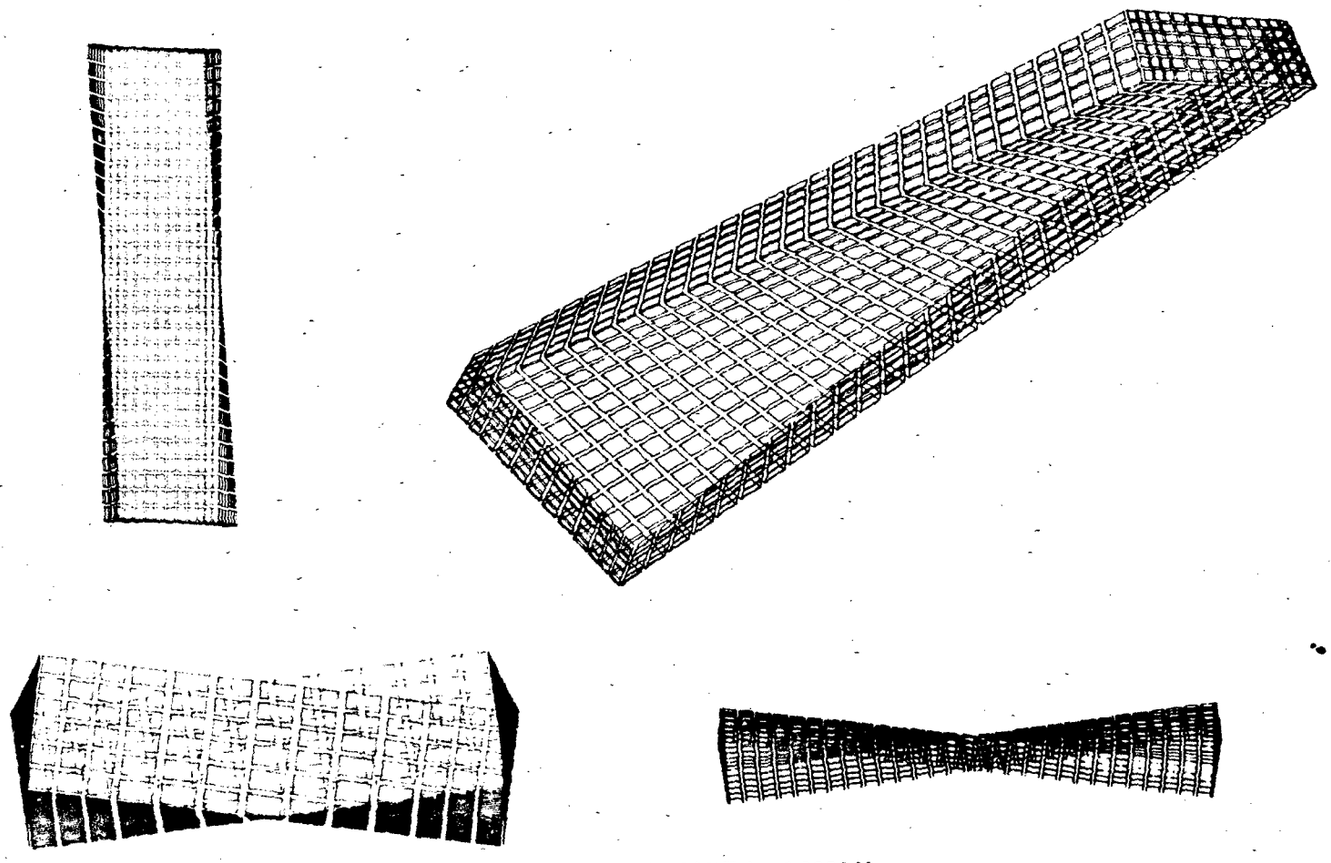

(a) MODE 1, 0.3806 Hz

Figure 30. Natural Frequencies and Mode Shapes - 3-D Drydock Model.

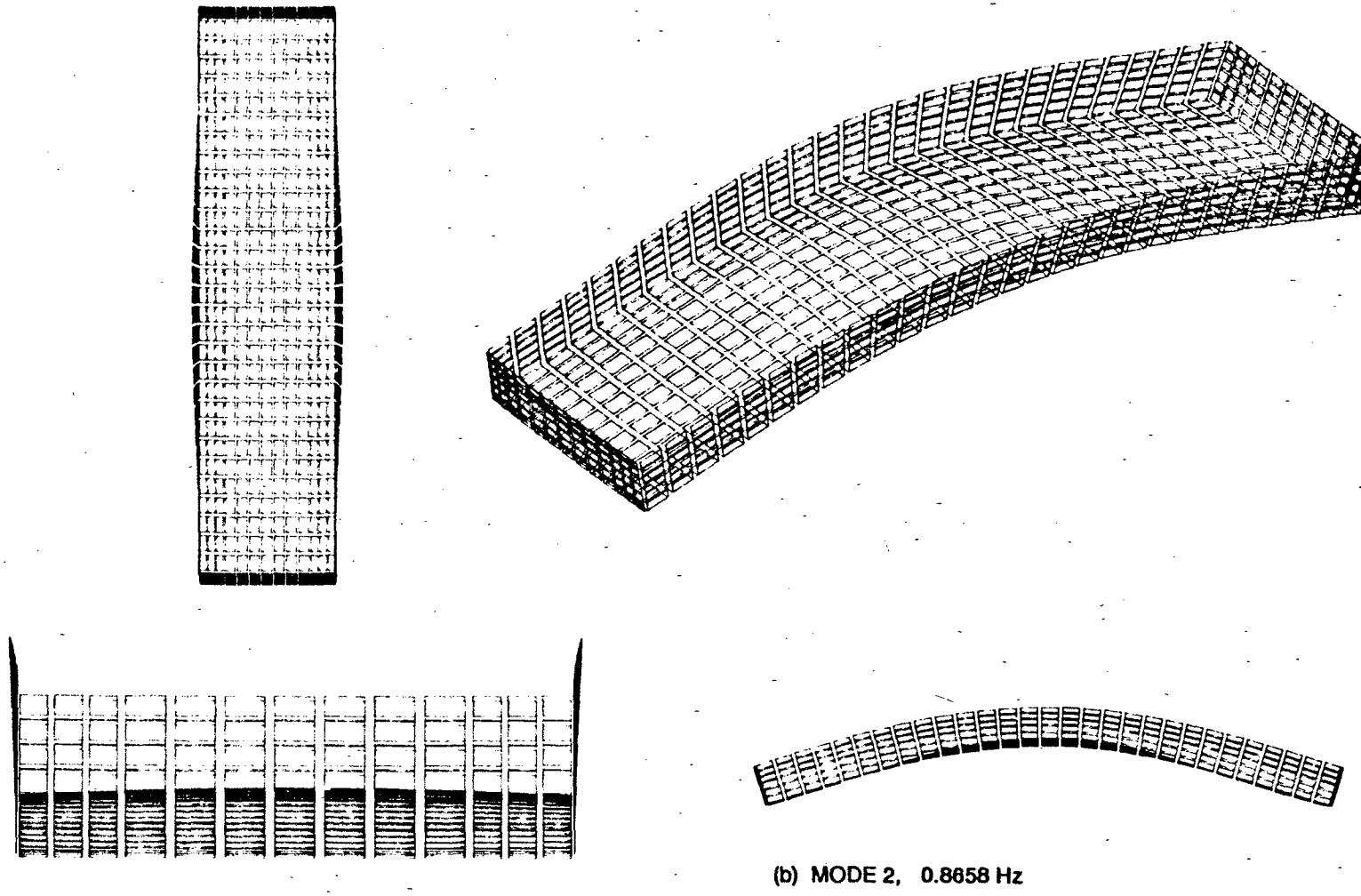

(b) MODE 2, 0.8658 Hz

Figure 30. Continued.

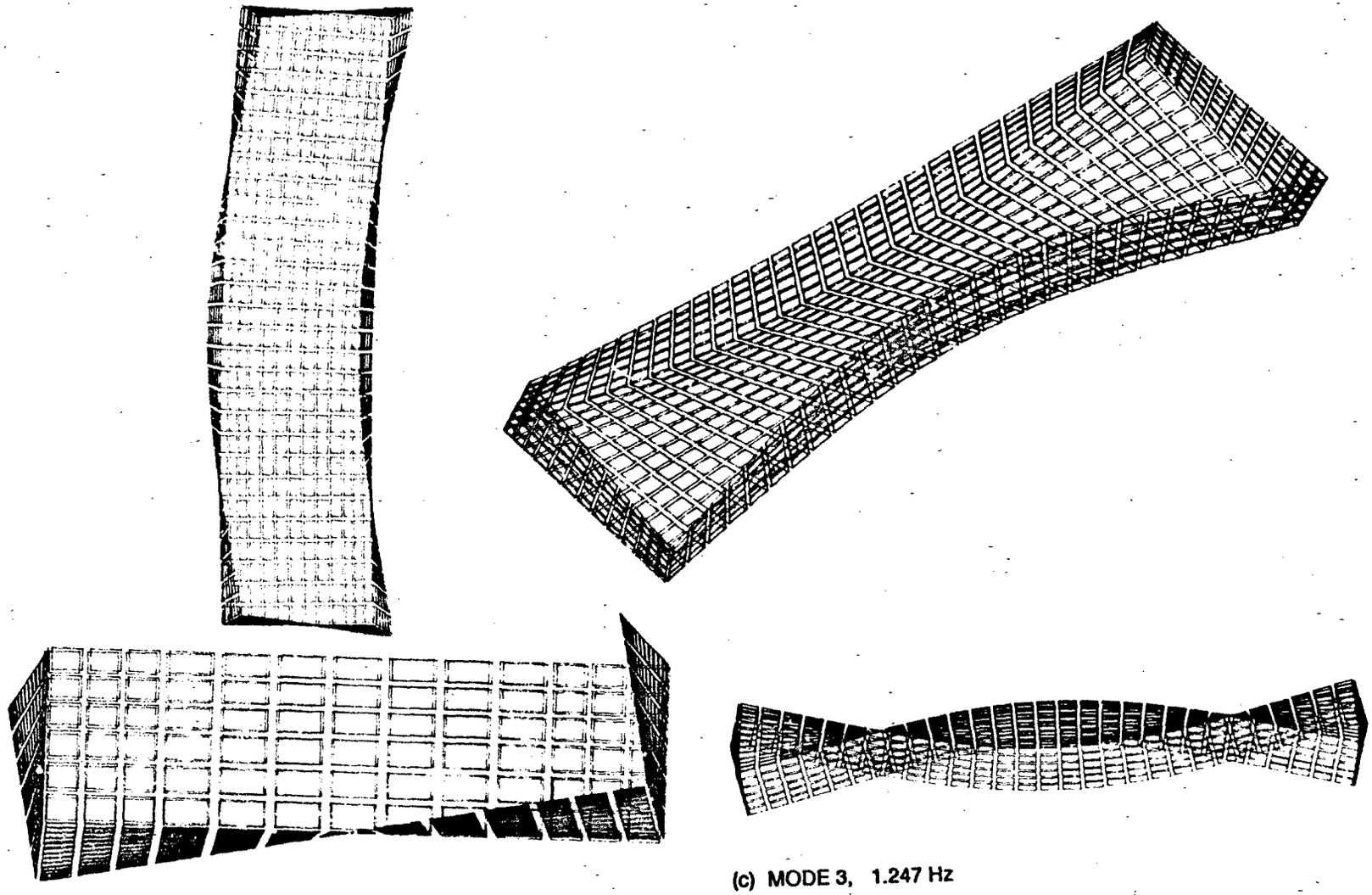

(c) MODE 3, 1.247 Hz

Figure 30. Continued.

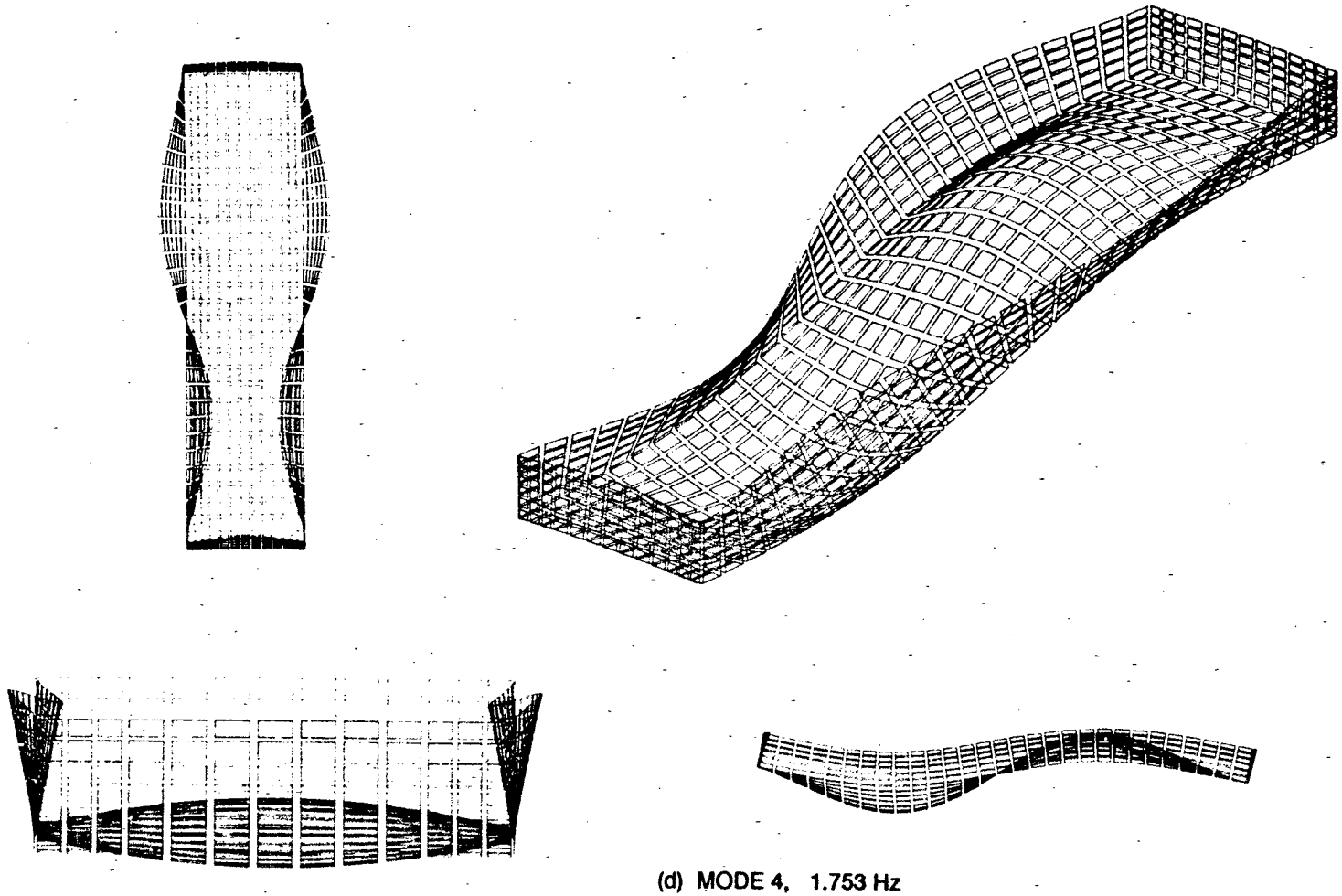

(d) MODE 4, 1.753 Hz

Figure 30. Continued.

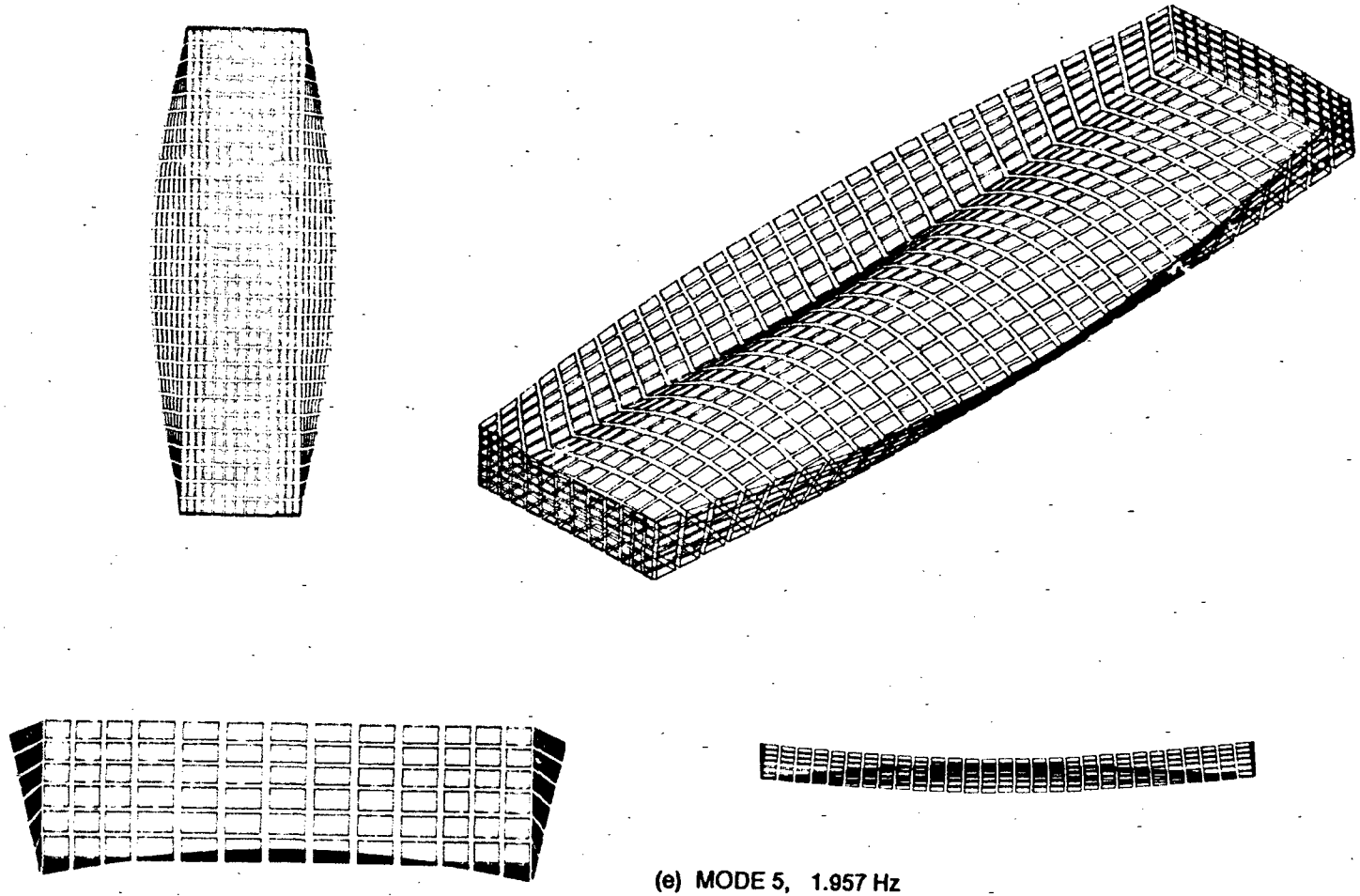

(e) MODE 5, 1.957 Hz

Figure 30. Continued.

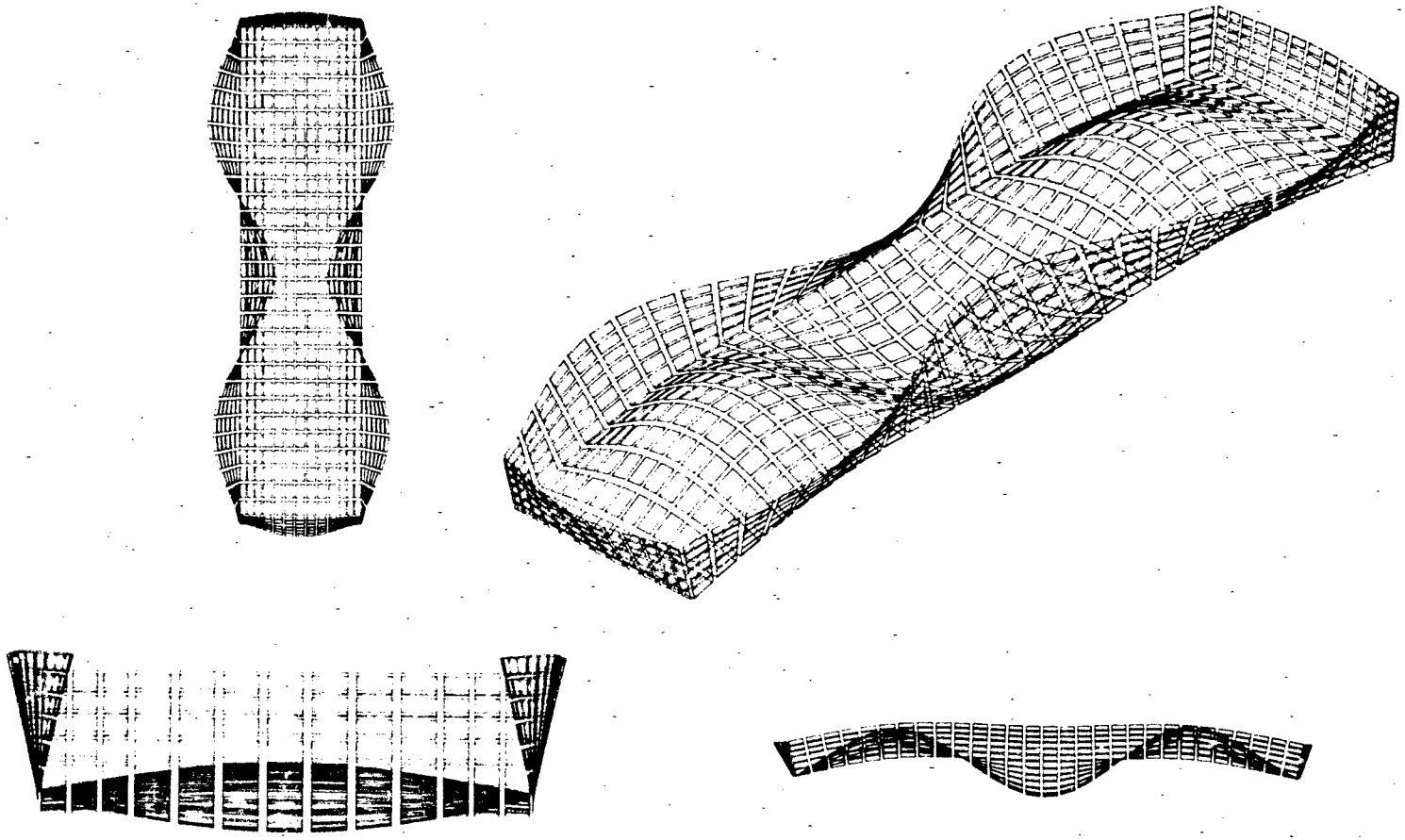

(f) MODE 6, 2.404 Hz

Figure 30. Continued.

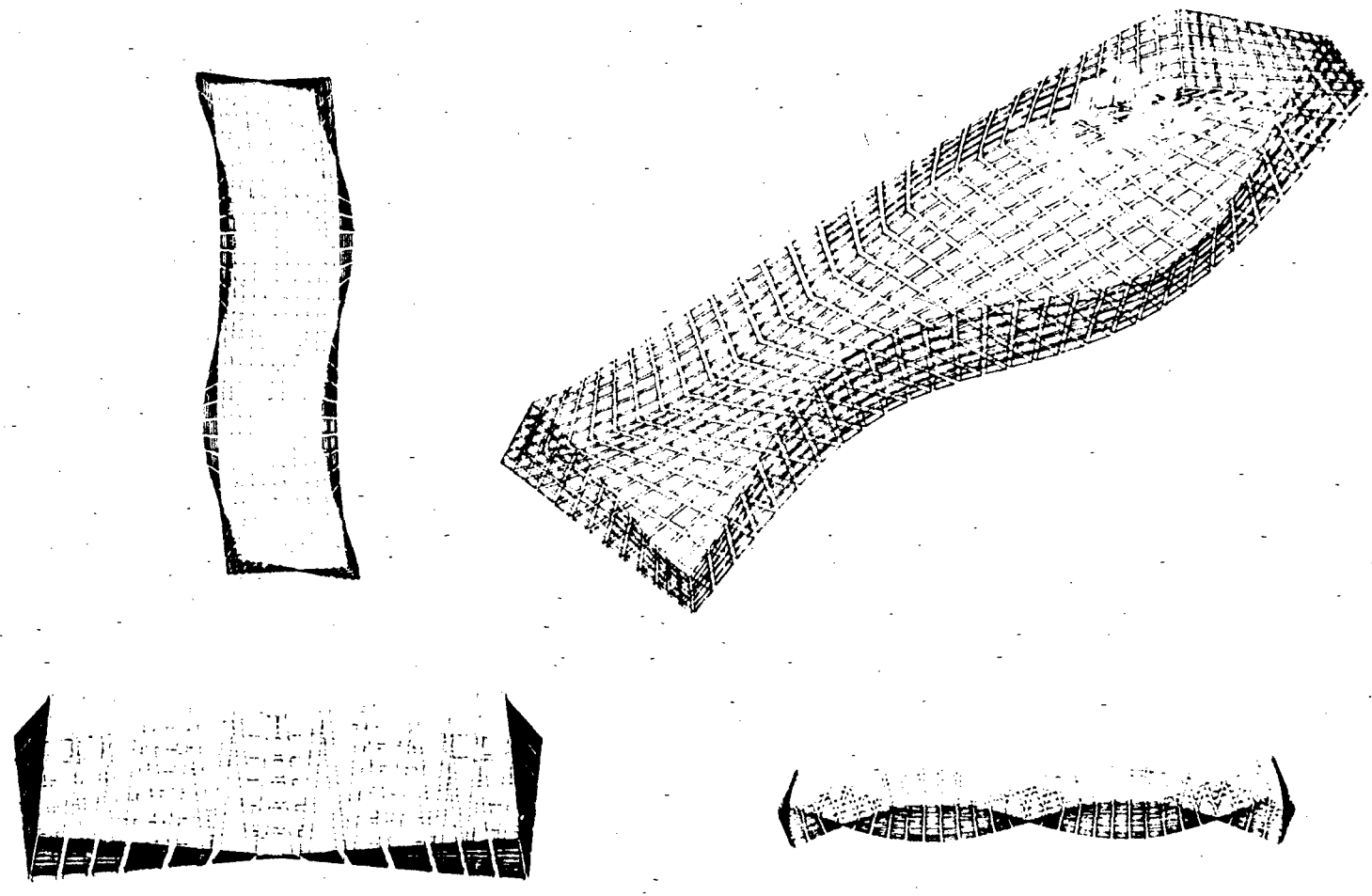

(g) MODE 7, 2.852 Hz

Figure 30. Continued.

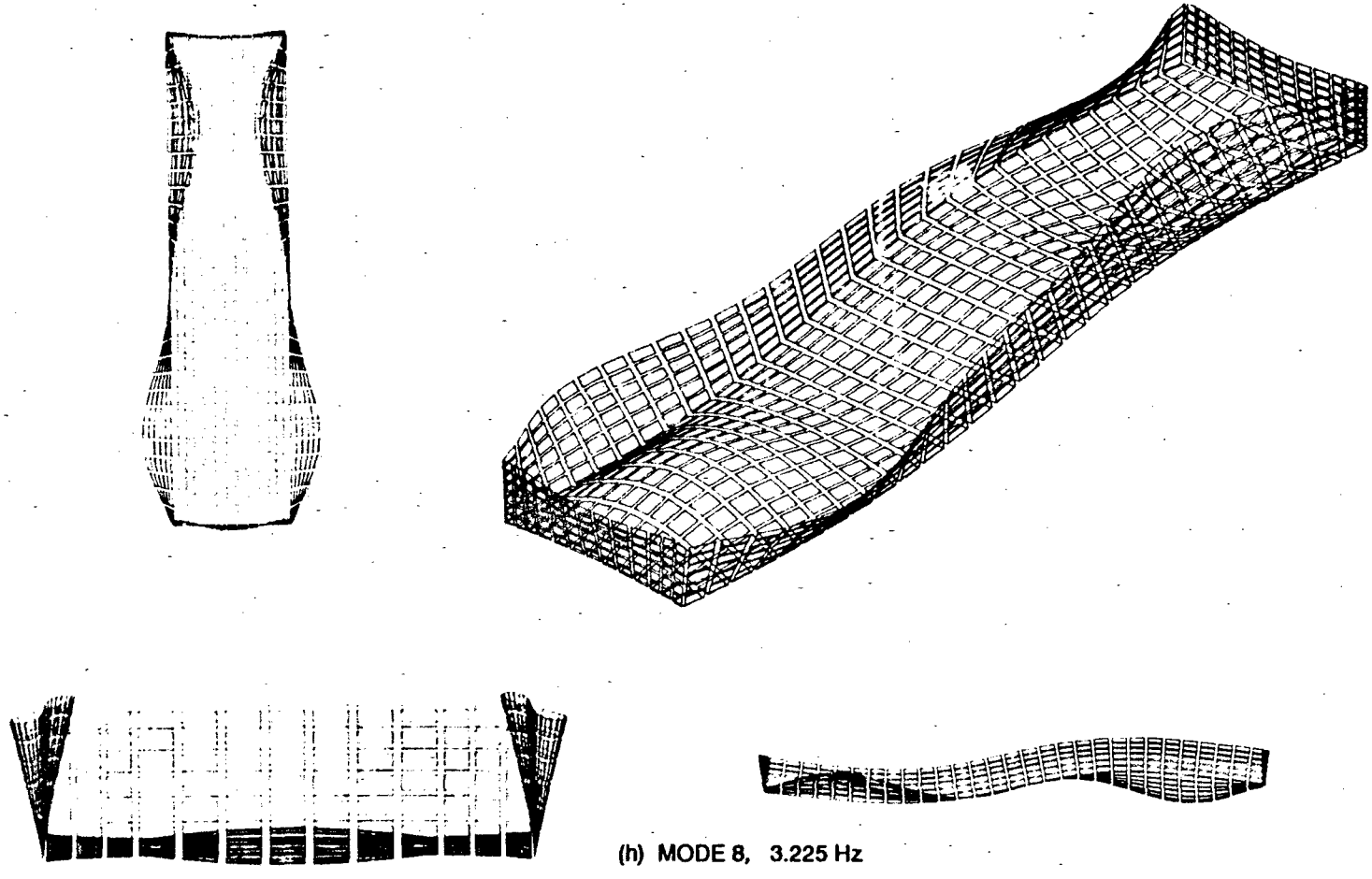

(h) MODE 8, 3.225 Hz

Figure 30. Continued.

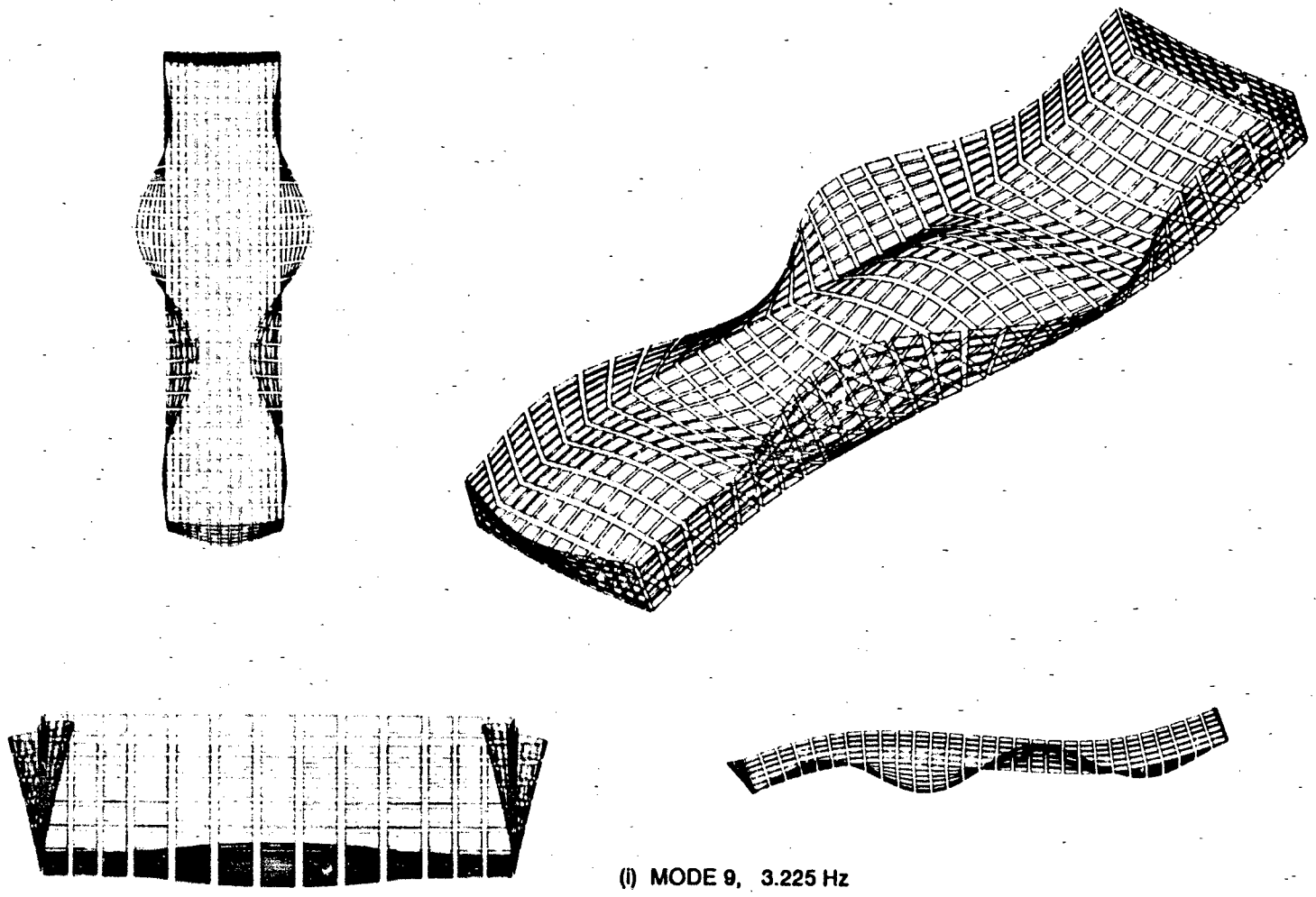

(i) MODE 9, 3.225 Hz

Figure 30. Continued.

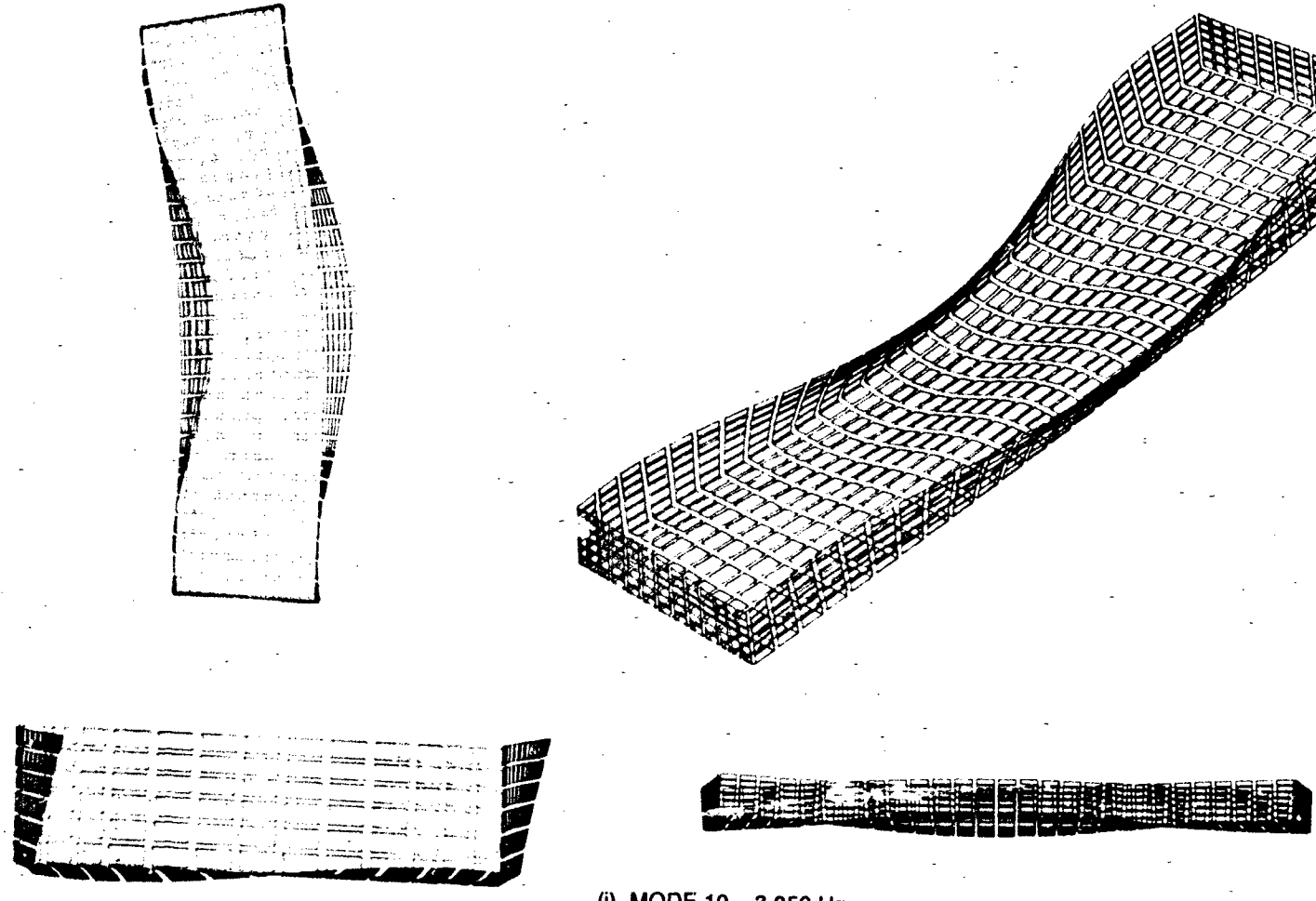

(j) MODE 10, 3.259 Hz

Figure 30. Continued.

The first, and fundamental, mode of vibration for the drydock model occurs at a frequency of 0.38 hertz, which is very low. Notice that all the generators in the deformed mesh are straight lines indicating that very little or no bending occurs in the drydock for this mode. This mode is a longitudinal torsional mode in which shear forces predominate. Recall that the one-dimensional continuous beam model is incapable of predicting longitudinal torsional natural modes of vibration.

The second mode shape is a longitudinal bending mode which is very similar to the first fundamental mode shape calculated using the one-dimensional continuous beam model. It is of interest, therefore, to also compare their corresponding natural frequencies, 0.87 hertz versus 1.04 hertz. The former value from the finite element model should be more accurate. Thus, the one-dimensional model prediction of this natural frequency is about 20 percent high.

The higher modes are increasingly more localized combinations of longitudinal and cross-sectional bending modes.

THREE-DIMENSIONAL NONLINEAR FINITE ELEMENT ANALYSIS OF A PIER DECK SCALE MODEL

Finite element technology can provide structural assessment of other waterfront facilities that impact fleet readiness, such as piers and wharfs. The computer code ADINA (ADINA Engineering, Inc., 1987) is used to predict the response, including load-deflection, stress distribution, extent of cracking, and failure mode, of a 1/3-scale reinforced concrete pier deck model. A three-dimensional nonlinear reinforced concrete model is required to accurately represent the progressive crack formation during loading, and to reflect the consequent stiffness degradation.

Agreement with experimental data is essential to the assessment of accuracy of analytical predictions. Fortunately, extensive data are available for a 1/3-scale model of a Navy reinforced concrete pier deck recently built and tested to failure in related exploratory research in structural assessment at NCEL. In the following, these data are used to assess the accuracy of three-dimensional nonlinear finite element technology for reinforced concrete structures.

Pier Deck Scale Model

Description. The model has five spans supported by six pile bents, and is shown in Figure 31. Dimensions and reinforcement used are detailed in Figure 32. The deck depth is 5.375 inches, representing a 16-inch prototype depth. The main reinforcement consists of #3 grade bars and D5 deformed wire, representing #9 and #6 bars in the prototype pier. The pier is designed for one-way action, hence the main reinforcing is longitudinal. Secondary transverse steel is also included at top and bottom.

Material Properties. The concrete mix is indicated in Table 11. The maximum aggregate size was scaled down to 3/8 inch. A higher relative content of lime aggregate and the use of a high-range water-reducing admixture (superplasticizer) allowed the concrete to be pumped. Concrete and steel properties are indicated in Table 12. The maximum concrete compressive stress of 7,700 psi was reached at a strain of 0.0027. The content of fine measured modulus of elasticity was found to be slightly lower than the traditional value of 57,000 $\sqrt{f'_c}$ for normal weight concretes. The measured Poisson ratio was 0.15 (typical values range from 0.15 to 0.22, ASCE, 1982).

Test Setup. A single centered patch load was applied to the center span. Patch dimensions were 8 by 8 inches, simulating a 24- by 24-inch crane outrigger load in the prototype pier. The load was applied in four steps, up to 30, 60, and 90 kips, then to failure. At each of the first three steps, the specimen was loaded then unloaded ten times. The load was applied through a 100-ton, hollow ram, hydraulic jack pushing on a 8- by 8- by 1-1/2-inch steel plate, and reacting against a high-strength steel rod anchored to the laboratory floor. The rod had been previously calibrated to 150 kips.

Deflections were measured at the center of the load patch using linear variable differential transformers (LVDTs).

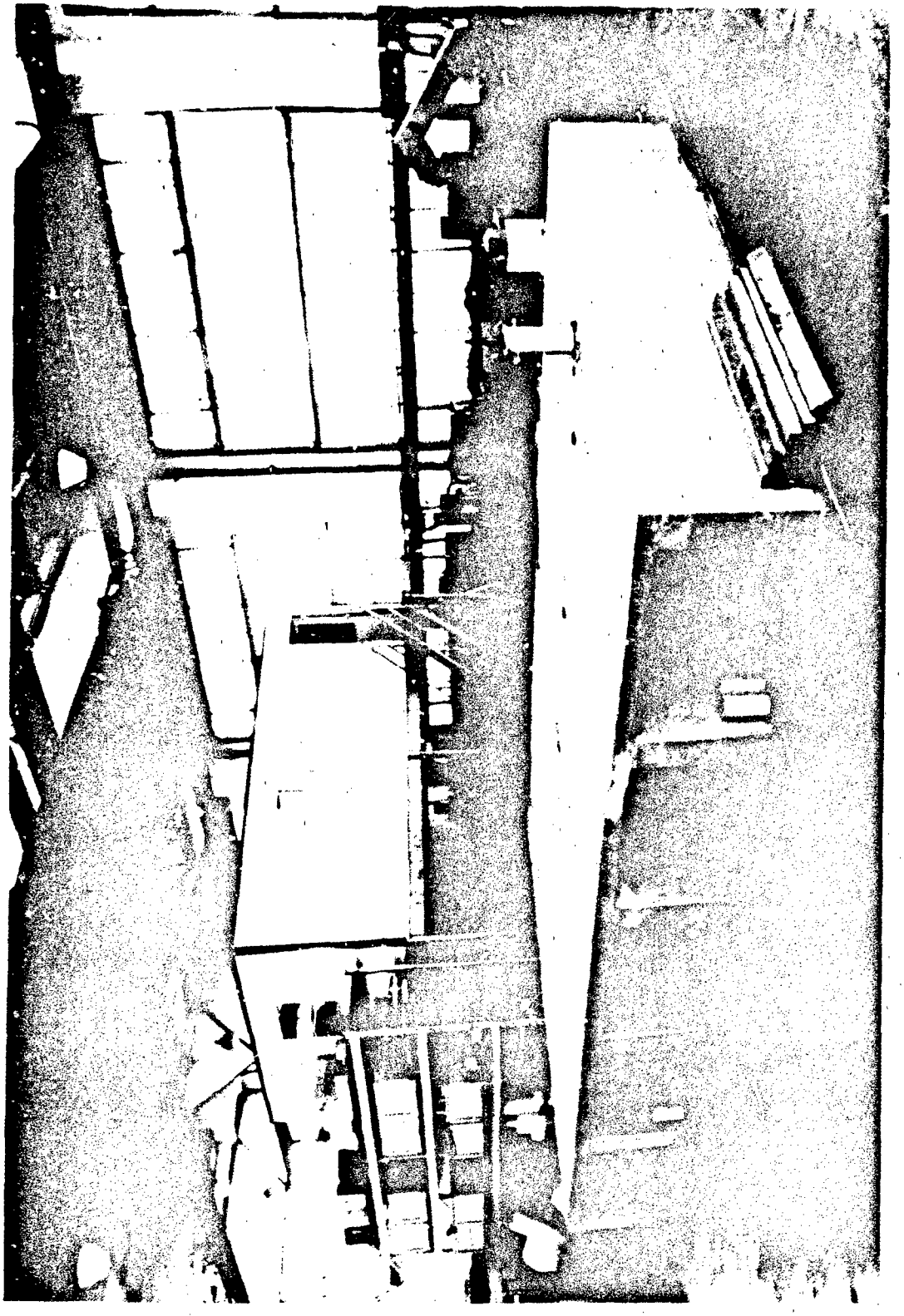

Figure 31. Reinforced Concrete Pier Deck.

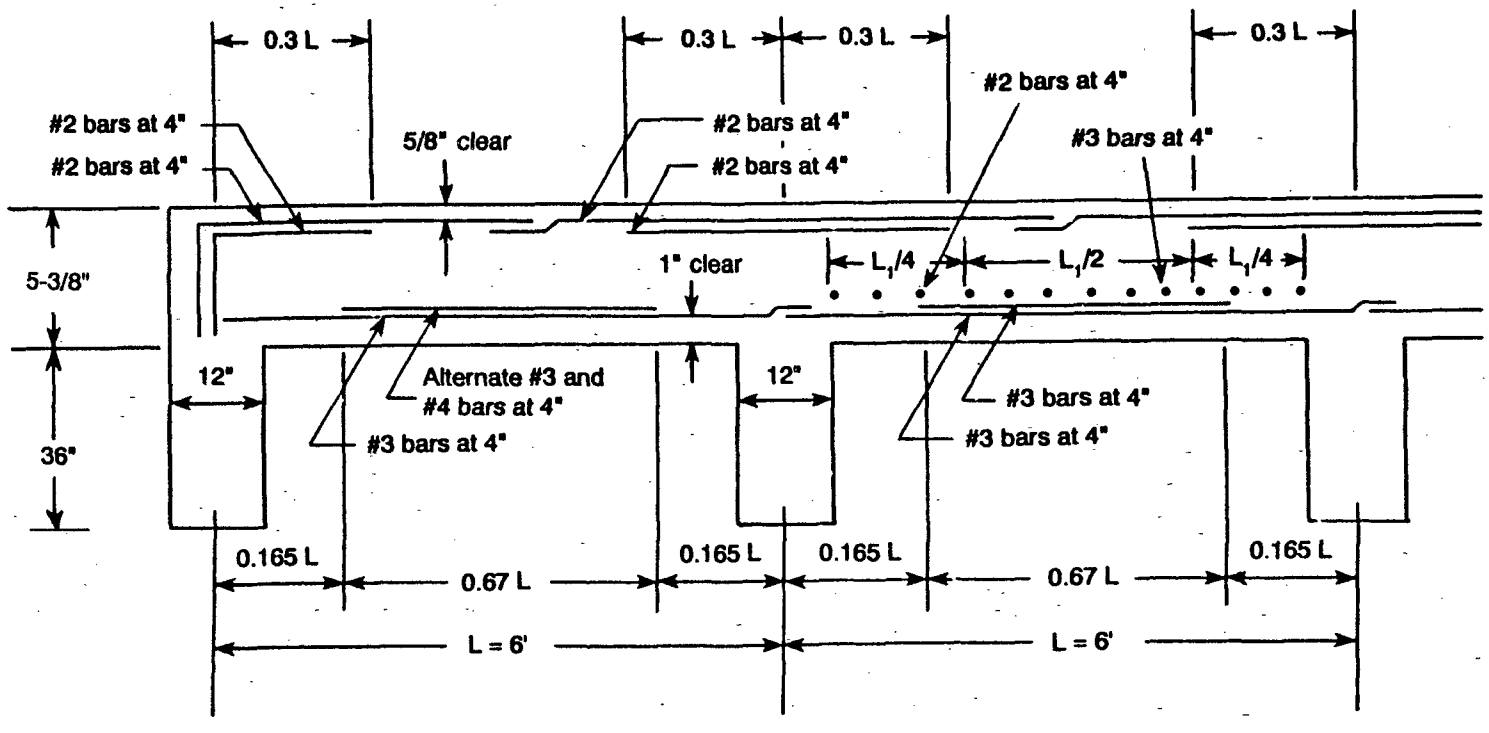

Note: Drawing not to scale

Figure 32. Pier Deck Shop Drawing.

Table 11. Concrete Mix[a]

Material	Weight Per Cubic Yard
Type I Cement	658 lb/y^3
Fly Ash	100 lb/y^3
Water	350 lb/y^3
3/8" Gravel	1,080 lb/y^3
Sand	1,740 lb/y^3

[a]Water reducing admixture (Sikament 86) per manufacturer.

Table 12. Concrete and Steel Properties

Concrete Properties		
Compressive strength	f'_c = 7,700 psi	
Tensile strength	f_t = 600 psi	
Modulus of elasticity	E = 4,020 ksi	
Poisson's ratio	μ = 0.15	
Steel Properties		
D5 wire	f_y = 81 ksi	f_u = 85 ksi
#3 rebar	f_y = 69 ksi	f_u = 109 ksi

SR-4 paper-backed concrete strain gages were epoxied to the compression face of the deck slab near the load point (1 inch away from the bearing plate). Weldable strain gages were attached to the tension reinforcement opposite the compression gages. These strain gage pairs provided a measure of the strain field across the deck depth.

Numerical Model

Due to the existing symmetry, only one quarter of the physical pier deck model is modeled numerically. The finite element mesh used is shown in Figures 33 and 34. Concrete in the center span was discretized using five layers of low-order 3-D isoparametric elements, with eight nodes, 3 degrees of freedom per node, and a 2x2x2 integration order. The mesh used is shown in Figure 35.

The material model used is a nonlinear elastic concrete model with compression crushing and tensile cracking cut-off with strain softening behavior. Reinforcing bars are represented using simple truss elements. This method is referred to as a discrete reinforcement model. Top and bottom reinforcement meshes are also shown in Figure 35. A nonlinear elastic-plastic material model was used for the steel.

Contiguous spans were modeled using linear four-node shell elements with 5 degrees of freedom per node, and uncracked concrete properties. In this way the confinement of the adjacent spans on the center span could be adequately represented without excessively increasing the computational effort. Transition shell elements were used around the center span to connect the shell to the 3-D elements. The model had a total of 4,083 degrees of freedom.

Owing to symmetry, only 1/4 of the concentrated vertical load needs to be considered in the analysis. This load is distributed on the top corner element, which has dimensions of 4x4x1 inch.

The pile bents rested on plywood sheets, which were also included in the finite element model (see Figure 33).

Concrete Constitutive Laws in the Post Cracking Range

Reinforced concrete structural failures primarily evolve from tensile cracking. Thus it is important to check the behavior and performance of any nonlinear concrete material model, especially with regard to its tensile cracking behavior, before the model is employed in the analysis of a structure.

REINFORCED CONCRETE PIER DECK

Finite Element Mesh

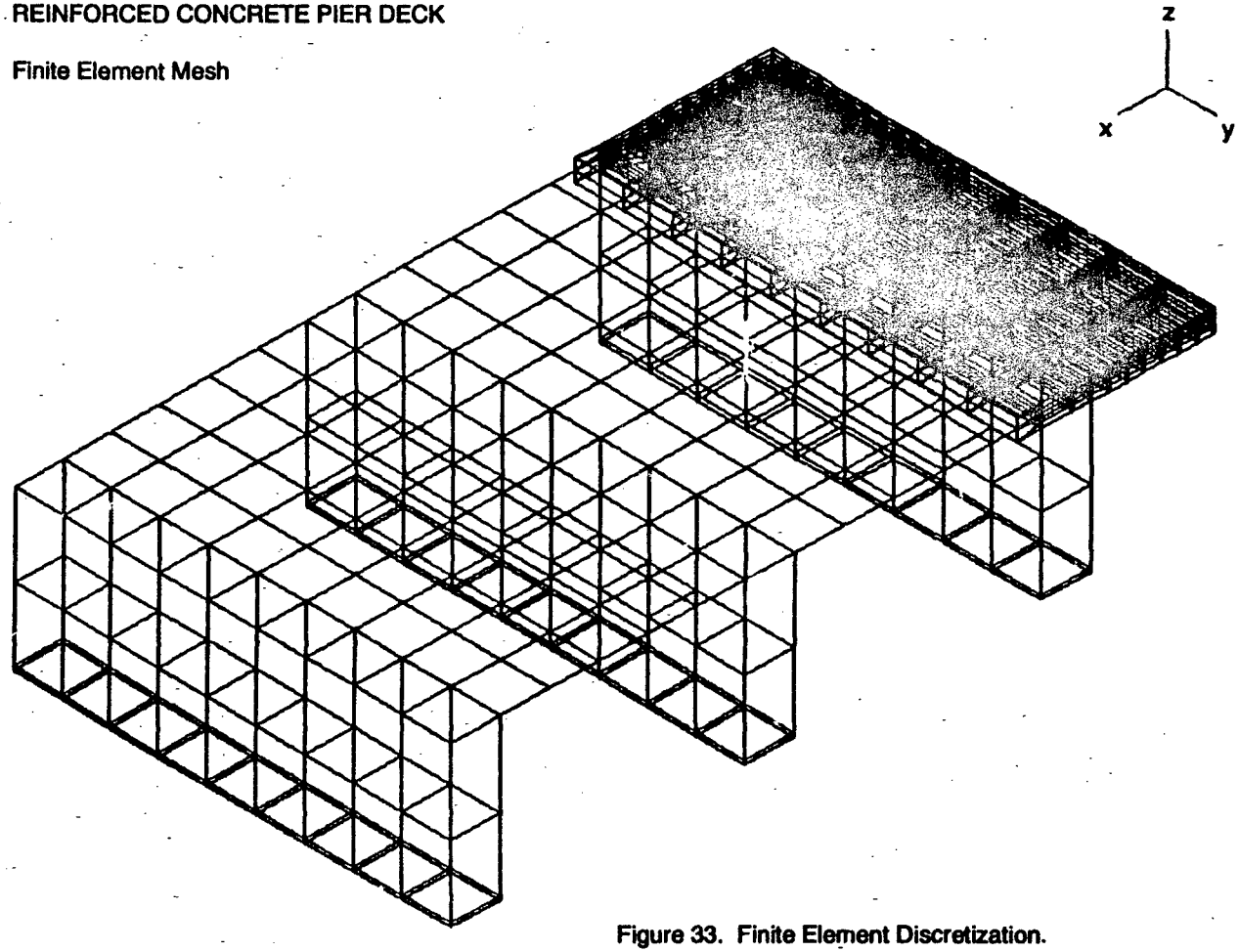

Figure 33. Finite Element Discretization.

REINFORCED CONCRETE PIER DECK

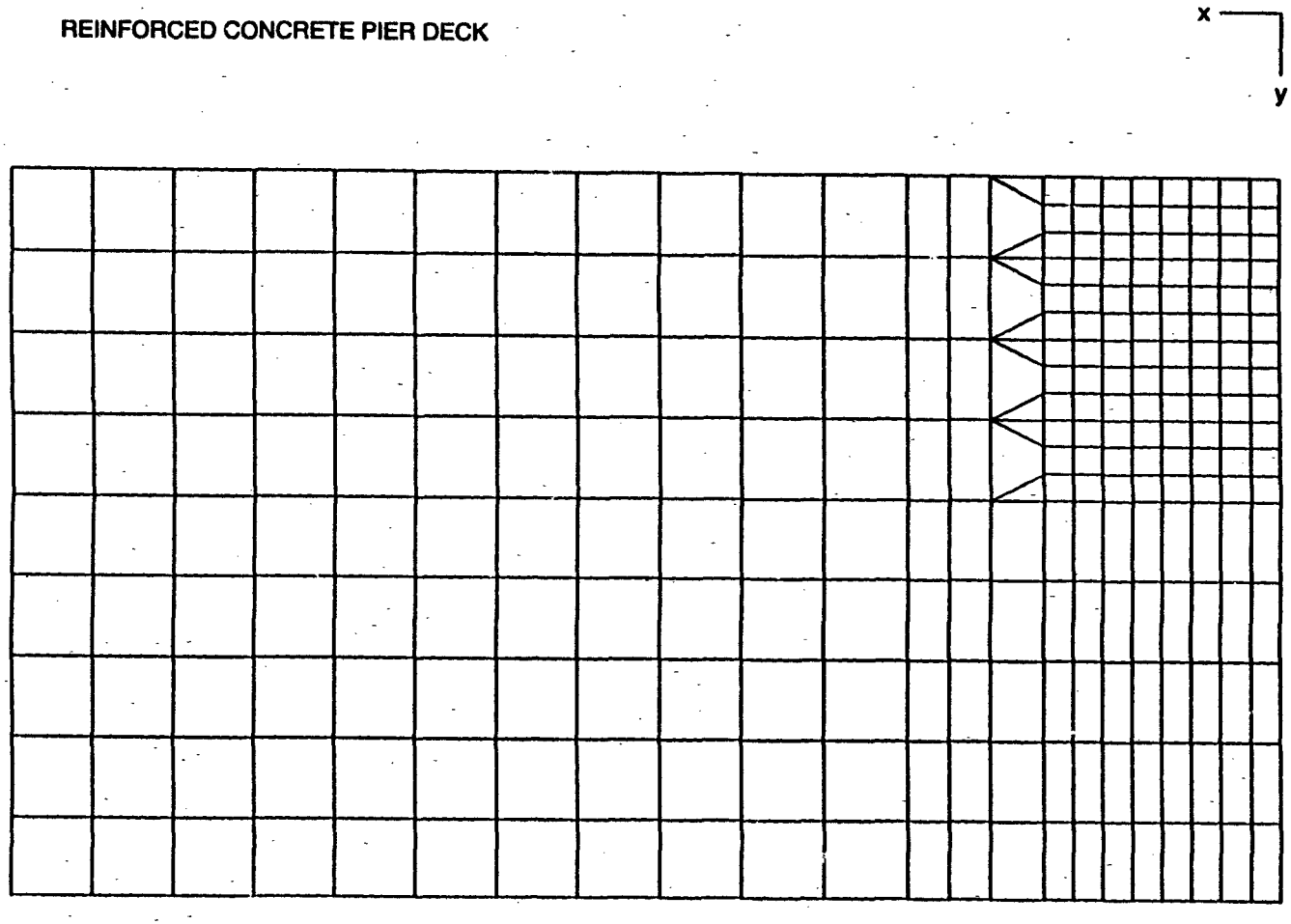

Figure 34. Finite Element Mesh, Top View.

NONLINEAR CONCRETE ELEMENTS

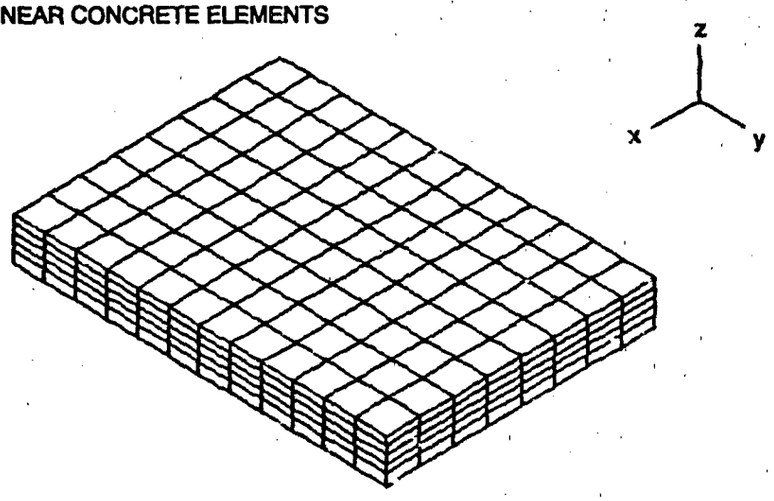

ELASTIC PLASTIC STEEL ELEMENTS

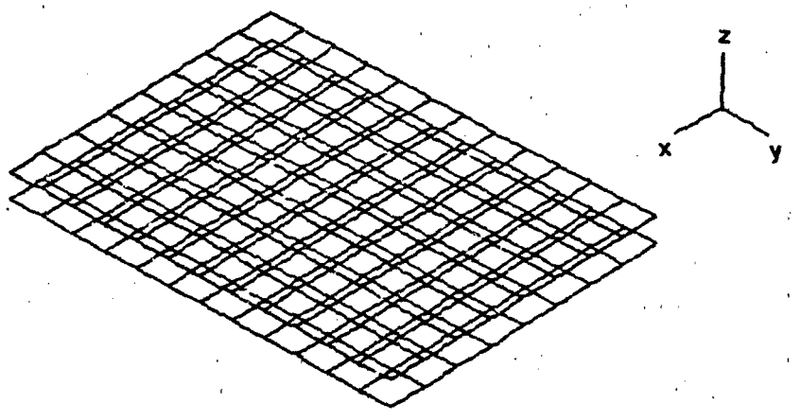

Figure 35. Concrete and Steel Meshes, Center Span.

Preliminary Material Model Testing. As part of the preliminary computer program evaluation, a simple tensile test on a single four-node 2-D concrete element was carried out. The element was pulled vertically from the top two nodes, then unloaded, then pulled until no more tensile stresses were transferred. All other degrees of freedom were deleted. From Figure 36a it may be observed that the unloading branch is incorrect because it is not directed at the origin. Since the ADINA source code is provided, it was possible to correct this deficiency as Figure 36b demonstrates. The same corrections were made to the 3-D concrete element.

The tensile test was repeated, this time allowing for lateral contraction (Poisson deformation) by releasing two lateral displacement degrees of freedom. No solution was obtained when the usual energy convergence criterion in ADINA was used. This problem was circumvented by switching to a force and moment convergence criterion in ADINA.

Constitutive Laws. For concrete in monotonic uniaxial tension beyond the cracking point, ADINA provides a linear release of the tensile stresses (Figure 36). This part of the stress-strain curve is referred to as strain softening. Related basic research in NCEL's Structural Modeling project has shown that a nonlinear tensile stress release is more realistic. The normalized strain softening relationship used is shown in Figure 37a. In this figure, limit strain is the strain beyond which no tensile stresses are transferred. This relationship was implemented in ADINA as an option (Malvar and Warren, 1989; Malvar and Fourney, 1990). A fracture energy of 0.57 lb/in. (100 N/m) was also assumed.

Accepted behavior after concrete cracking provides for shear stresses to be transferred across the crack. However, they decay quickly with increasing crack opening. To account for this in ADINA, the shear modulus is decreased linearly with increasing strain perpendicular to the crack, down to a minimum value which remains constant.

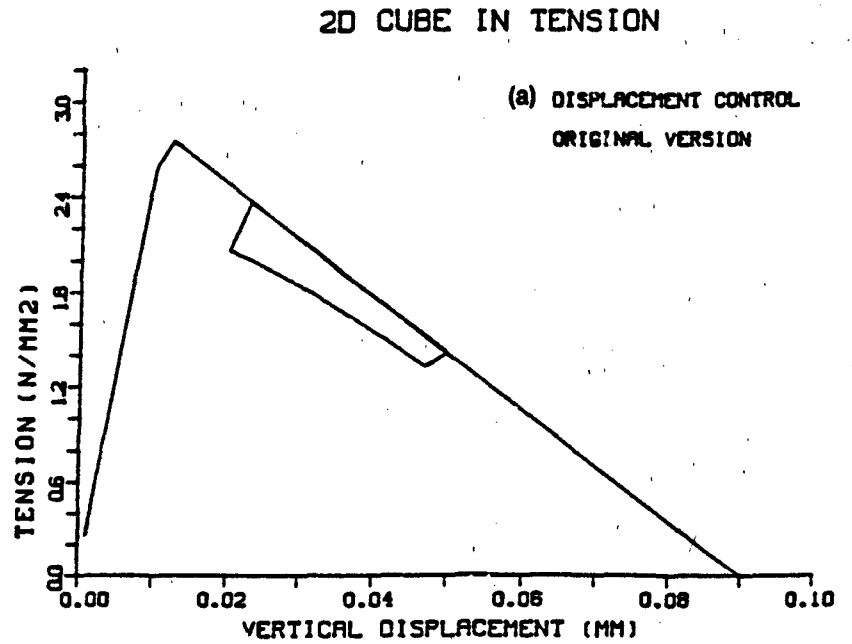

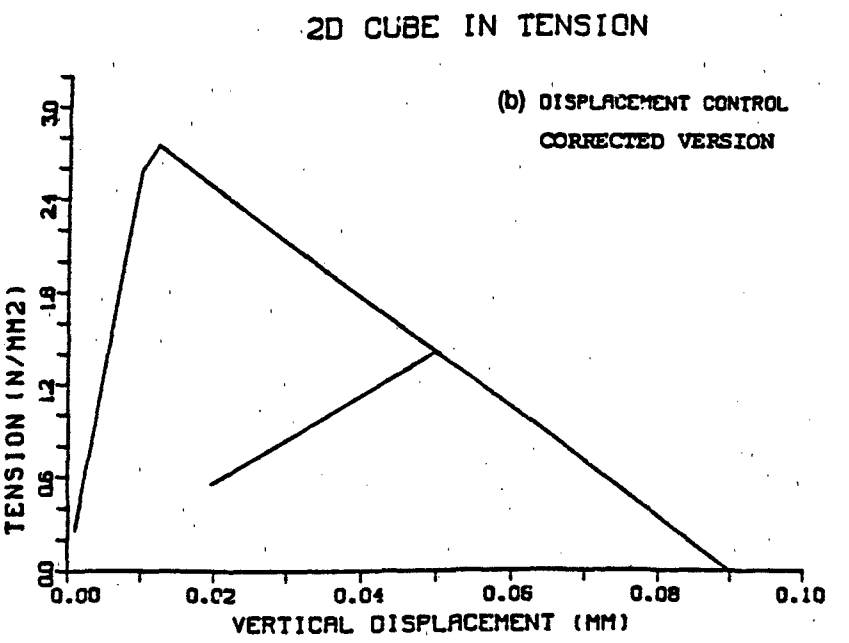

Figure 36. Tensile Behavior Correction of ADINA Concrete Model.

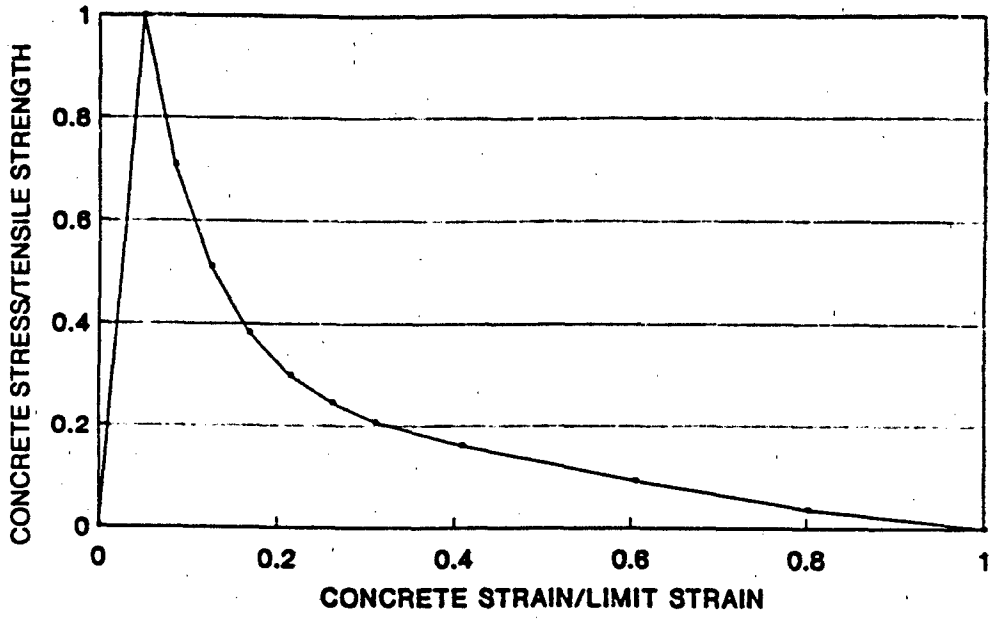

(a) Tensile strain softening normalized stress versus strain law

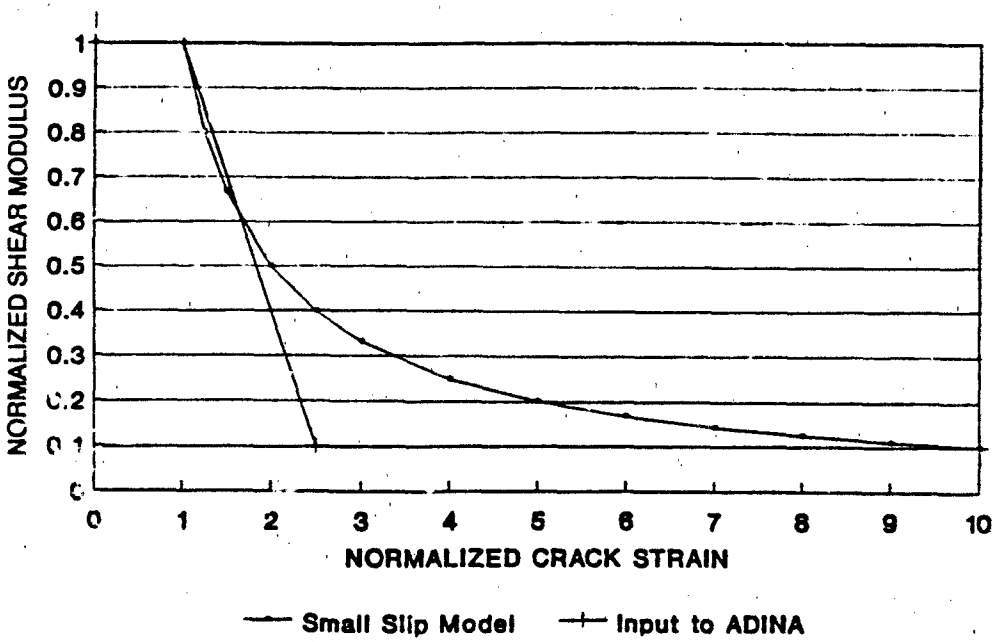

(b) Post cracking shear modulus

Figure 37. Tensile Strain Softening and Post Cracking Shear Modulus.

Experimental observations show that the shear stiffness decays exponentially. For small slip values in particular, the decrease in shear modulus G can be derived from Bazant and Gambarova (1987):

$$\sigma_{nt} = A_2 \frac{\delta_t}{\delta_n}$$

where: σ_{nt} = shear stress transferred across crack

δ_t = crack slip

δ_n = crack opening

$A_2 = a_3 \tau_u$

$a_3 = 2.45/\tau_o$

$\tau_o = 0.245 f'_c \qquad (N/mm^2)$

$\tau_u = \tau_o a_o /(a_o+\delta_n^2)$

$a_o = 0.01 D_a^2$

D_a = maximum aggregate size

For small crack openings, this can be simplified to:

$$\sigma_{nt} = 2.45 \frac{\delta_t}{\delta_n} \qquad (N/mm^2)$$

Further, if it is assumed that $\varepsilon_n = \delta_n/s$ and $\varepsilon_t = \delta_t/s$,

where s is a prescribed crack spacing, then the degradation of the shear modulus with crack opening is governed by:

$$G = \frac{\sigma_{nt}}{\varepsilon_t} = \frac{2.45}{\varepsilon_n}$$

This is equivalent to an exponential shear stiffness decay with increasing crack width, as shown in normalized form in Figure 37b. The bilinear approximation used as input to ADINA attempts to match the rapid shear stiffness decay at small crack openings. The ratio of cracked shear stiffness to the initial uncracked value is often termed the shear retention factor.

Experimental Results

Measured Load-Deflection Behavior. For the first load-unload cycle at each load step, the ascending part of load-deflection curve is shown in Figure 38. The slope of the curve (stiffness) shows a sharp decrease at around 30 kips, representative of extensive concrete cracking. Each successive loading or unloading is linear if the load is smaller than the maximum load previously attained. If this maximum load is exceeded, the load-deflection path shows a further decrease in slope and follows an envelope similar to a monotonic loading test.

In the final cycle to failure, a maximum load of 121 kips was obtained, at a deflection of 0.32 inch.

Observed Crack Patterns and Failure Mode. Crack maps were recorded at different load levels, and at failure. Cracks at the top and bottom of the deck are reported in Figures 39 and 40, respectively. Top cracks are almost circular and concentric around the load point. Bottom cracks are radial until punching failure takes place.

Brittle punching shear failure occurred at 121 kips. On the deck top, section cracks developed just around the load footprint at an initial angle of about 45 degrees with the vertical. Figure 40 shows the intersection of these cracks with the deck bottom. Deflections in the slab at failure were not high enough to develop membrane forces.

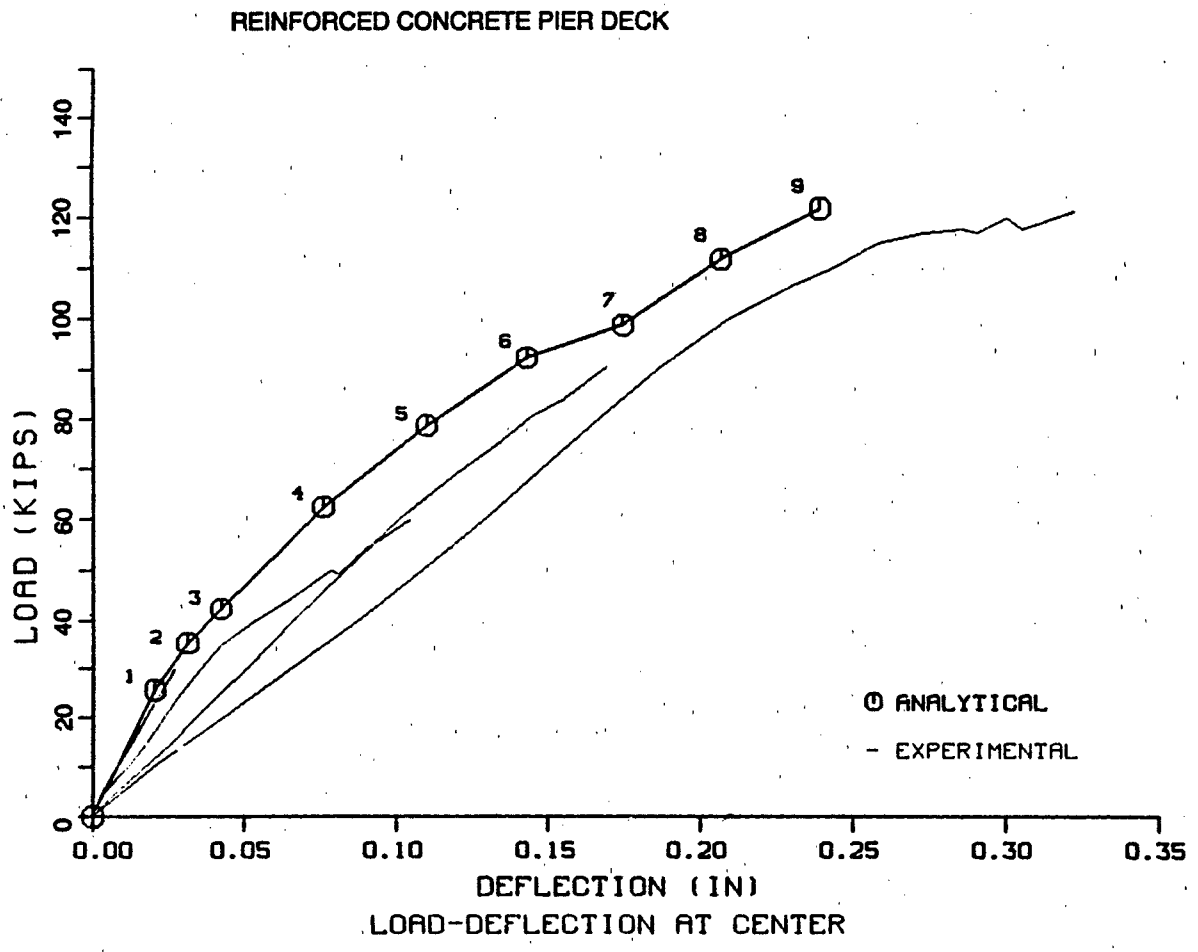

Figure 38. Load Deflection History at Center.

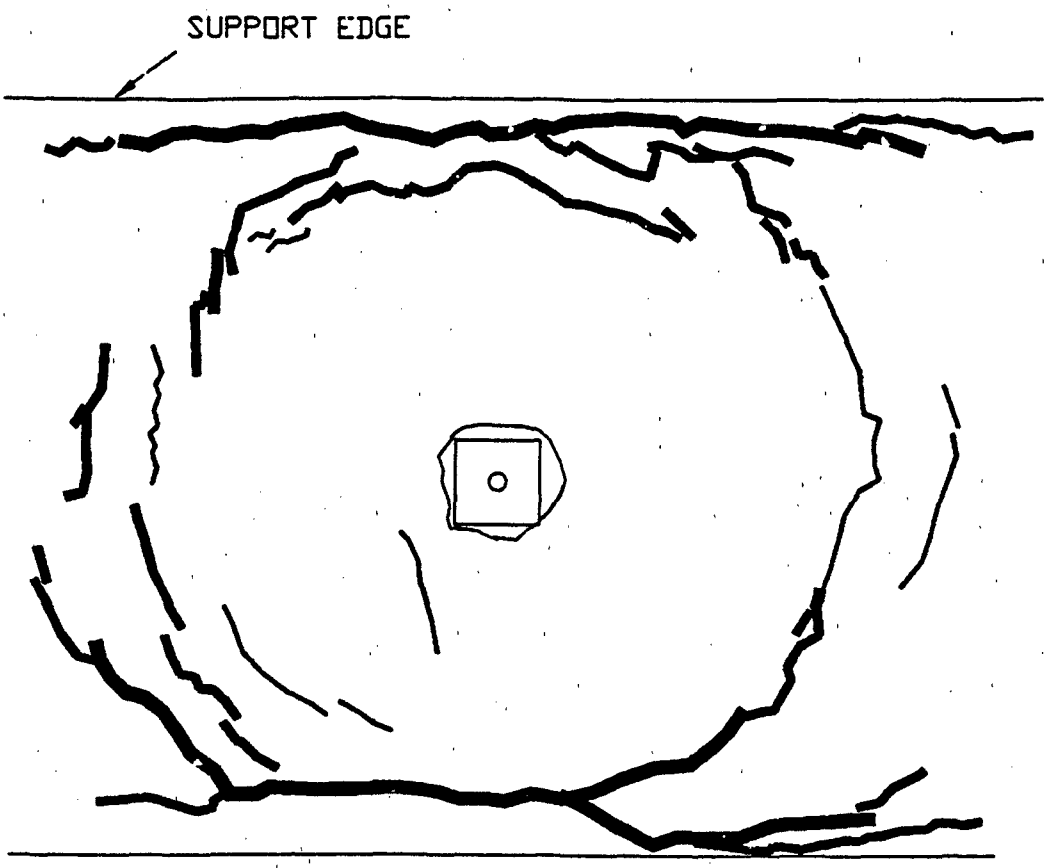

Figure 39. Experimental Crack Patterns on Deck Top.

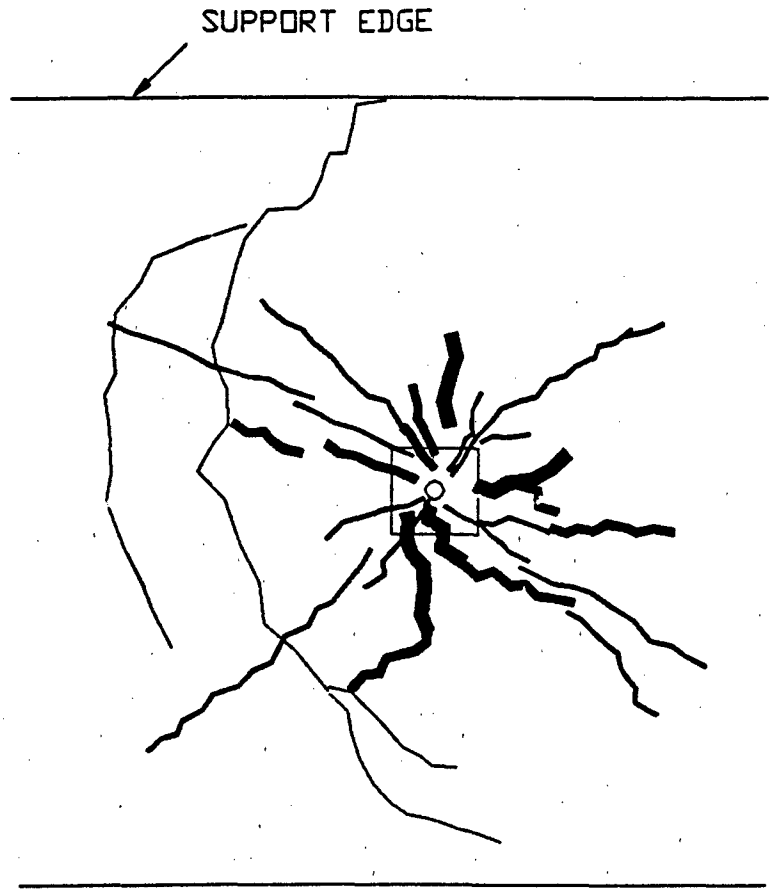

Figure 40. Experimental Crack Patterns on Deck Bottom.

Measured Concrete and Steel Strain. For the first cycles to 30, 60, and 90 kips, as well as for the cycle to failure, the strain in the extreme concrete compression fiber (deck top) and the strain in the tension steel next to the load point were recorded (Figures 41 and 42, respectively). Values for both strains kept close to each other during testing, indicating that the neutral axis in that section remained approximately equidistant from the deck top and the tension steel.

Numerical Results

Predicted Load-Deflection Behavior. In the predicted load-deflection graph (Figure 35), a marked variation in the slope at load step 2 reflects a prediction of extensive cracking of the concrete elements. After load step 6, the numerical response is totally dependent on the shear retention factor (i.e., the prescribed degradation of the shear modulus, G). When the shear retention factor was set to zero, brittle failure was predicted at load step 6. When post cracking shear retention was introduced (according to Figure 37), the remainder of the curve was obtained with a brittle failure mode predicted at a load of 122 kips (load step 9), which is within 1 percent of the measured failure load.

Predicted Crack Patterns and Failure Mode. The numerical crack maps at the deck top and bottom are shown in Figures 43 through 45. Crack surfaces and their orientation at integration points are represented by two parallel circles. On the deck top (Figures 43 and 44), horizontal in-plane cracks indicate delamination of the concrete compression zone near the load due to shear stresses. Away from the load, vertical cracks due to flexural stresses form almost circular patterns about the load. On the bottom, radial surface cracks eminate from the load point outward prior to failure, as shown in Figure 45.

At load step 6, Figure 46 indicates the initiation of a conical section crack around the load, typical of the punching shear failure observed experimentally (the load is applied on the top right element in Figure 46).

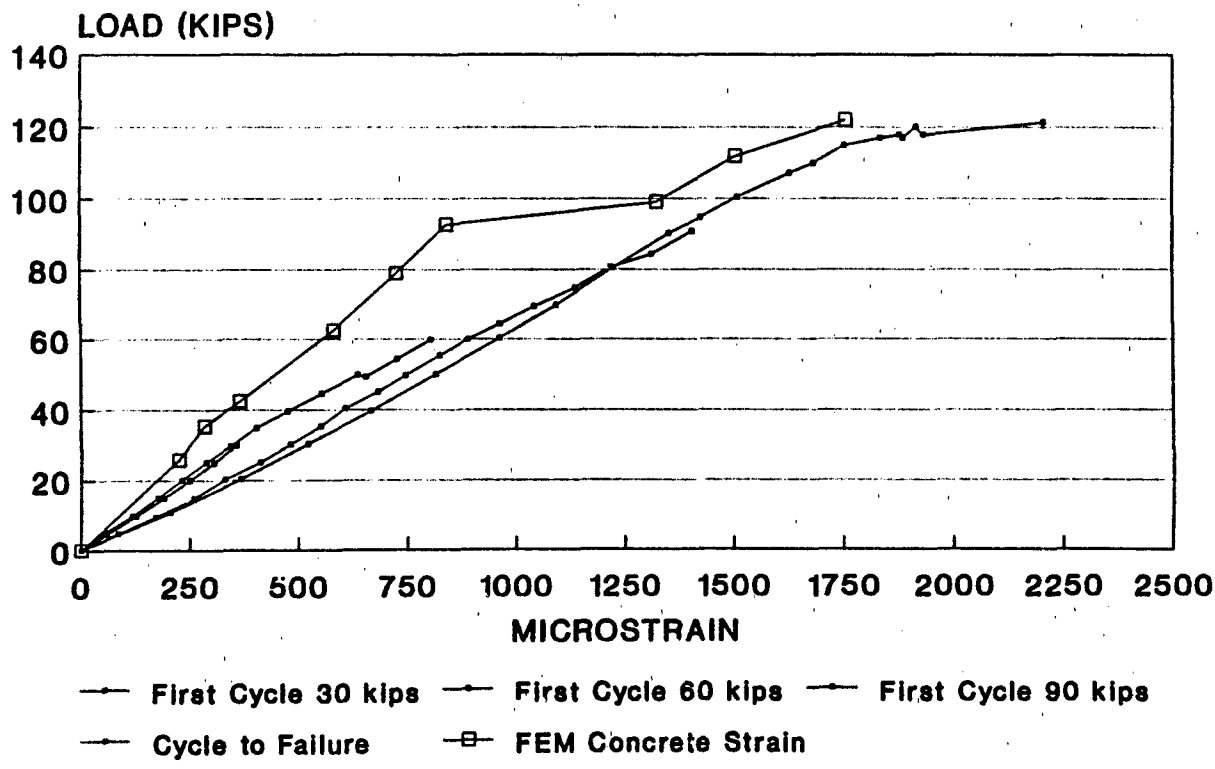

Figure 41. Measured Versus Computed Concrete Strain History.

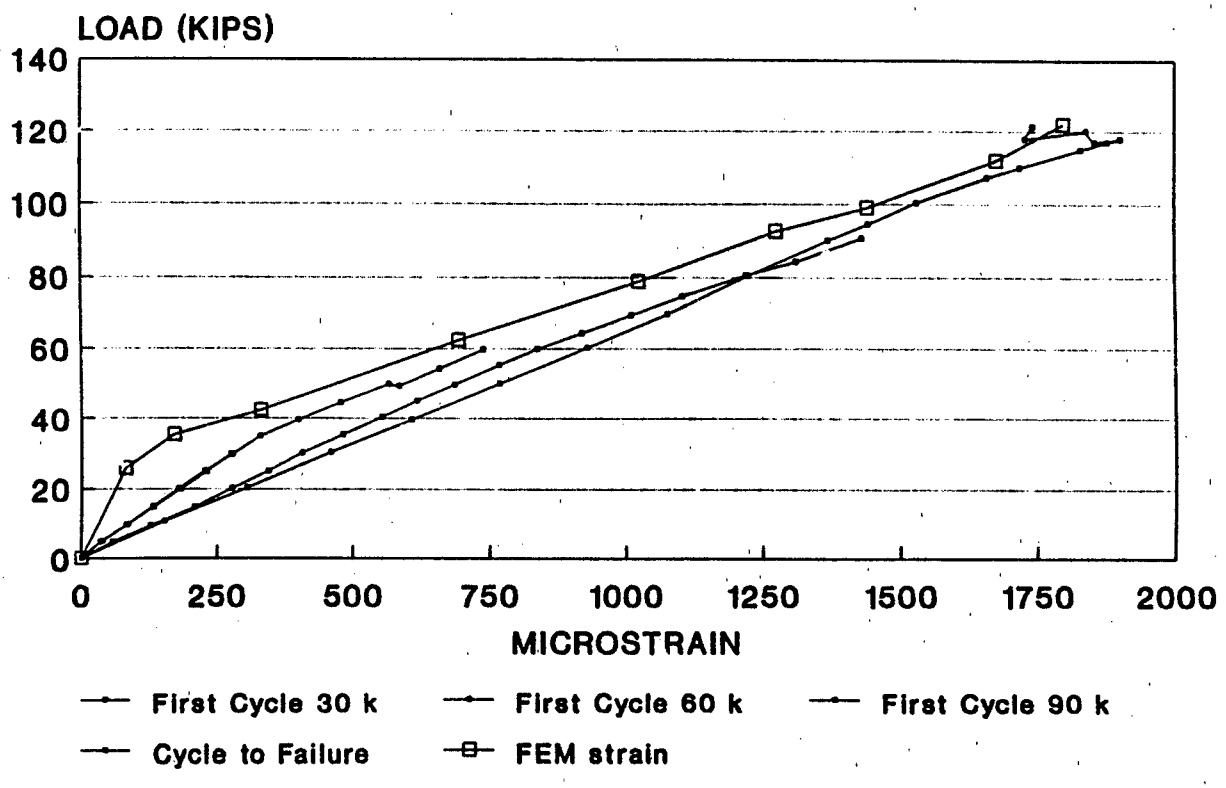

Figure 42. Measured Versus Computed Steel Strain History.

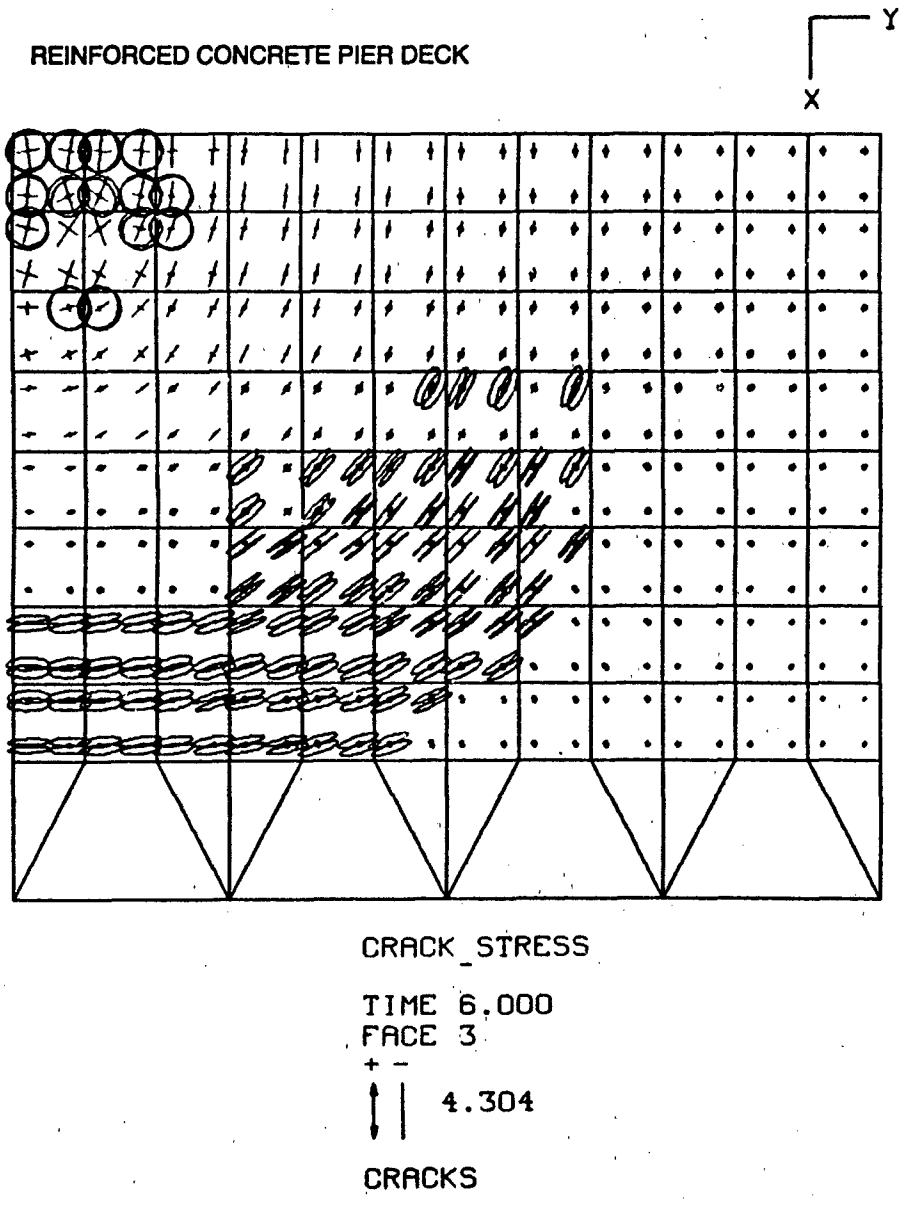

Figure 43. Predicted Crack Patterns on Deck Top at 90 Kips.

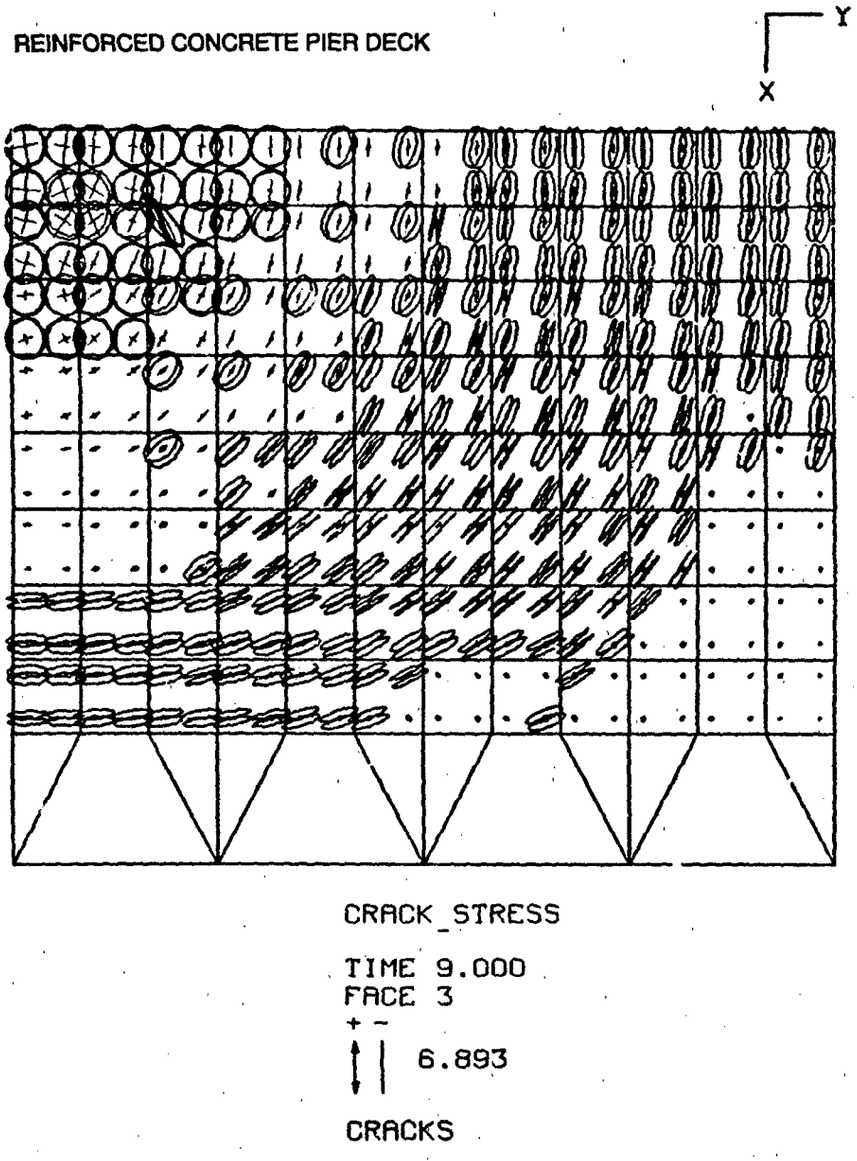

Figure 44. Predicted Crack Patterns on Deck Top at Failure.

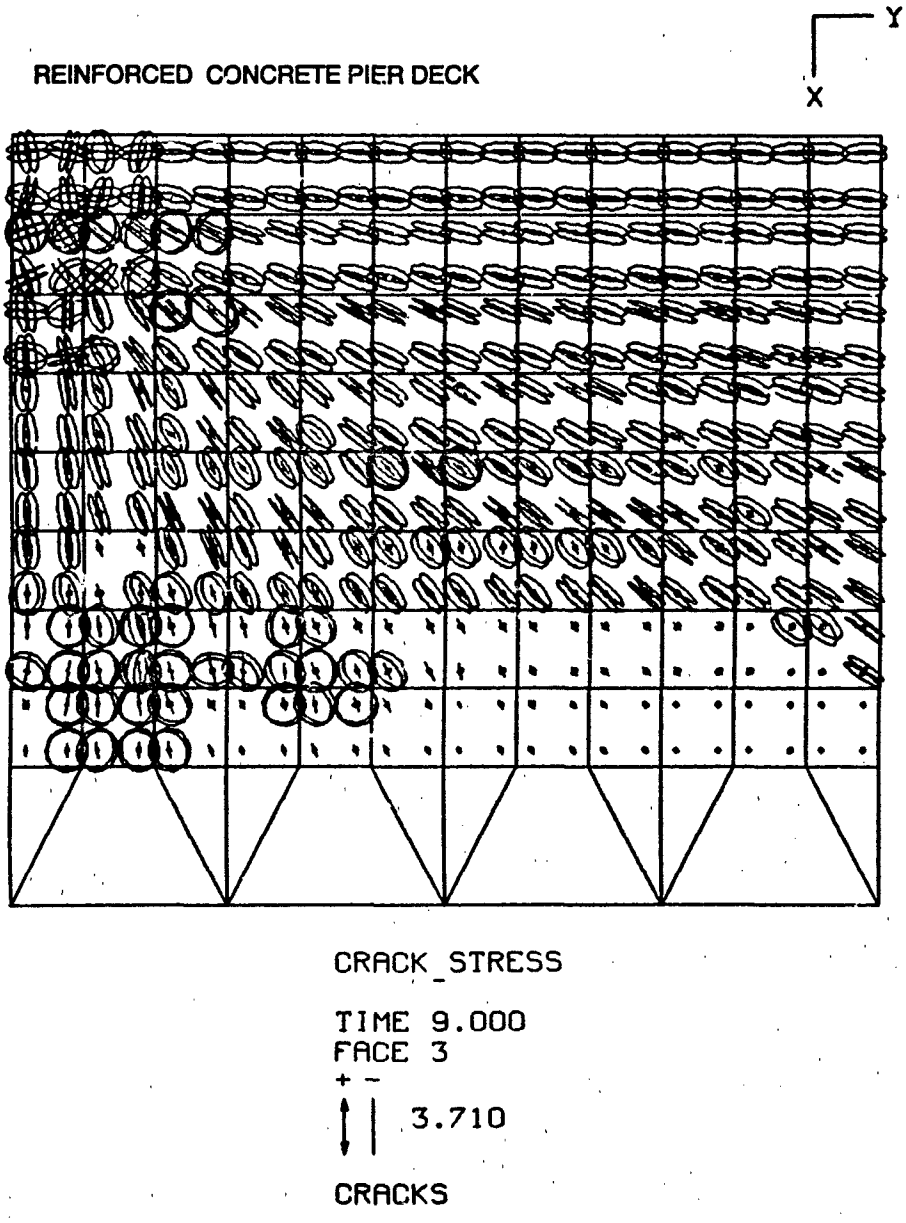

Figure 45. Predicted Crack Patterns on Deck Bottom at Failure.

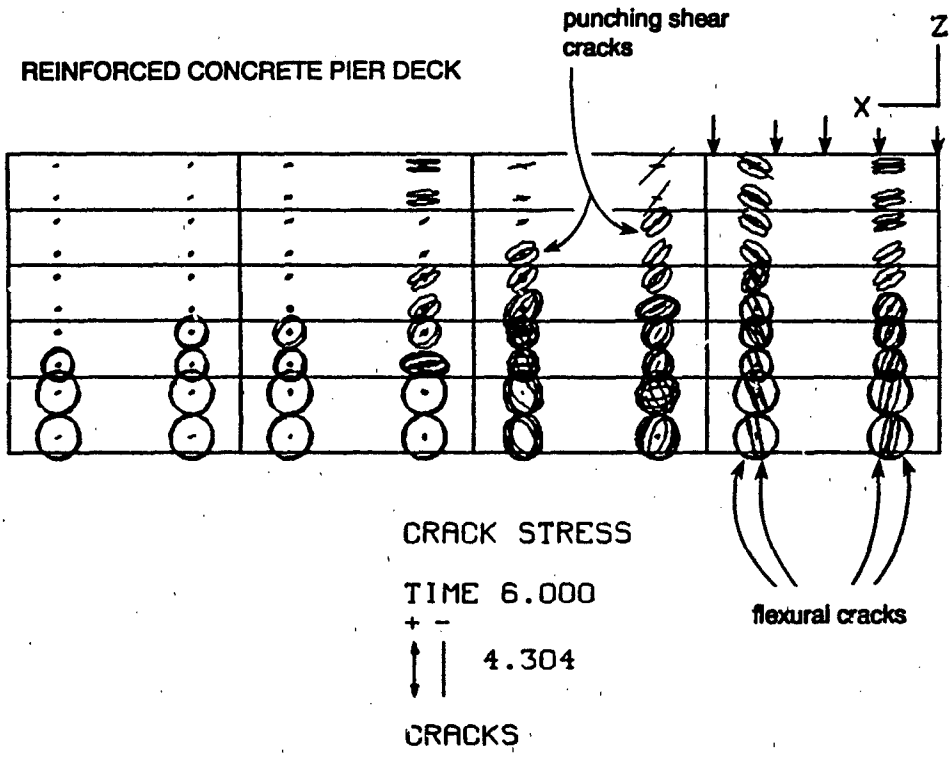

Figure 46. Punching Shear Cracks.

Predicted Concrete and Steel Strain. The computed concrete strain on the deck top, near the load point, and for monotonic loading, is compared with measured strain (Figure 41, FEM concrete strain). At step 6, quasi-horizontal cracking occurred in this location (upper right element in Figure 43), with corresponding large element deformations. Figure 42 shows the tension steel strain for the same case. Prior to concrete cracking in tension, the steel deformation is constrained.

The three-dimensional finite element model also allows for convenient evaluation of stress and strain distributions through the thickness of the pier deck, as indicated in Figure 47 for the pier deck center. The concrete compression stress is shown to decrease almost linearly down to the neutral axis, below which tension stresses and cracking are apparent. The steel stress is also indicated.

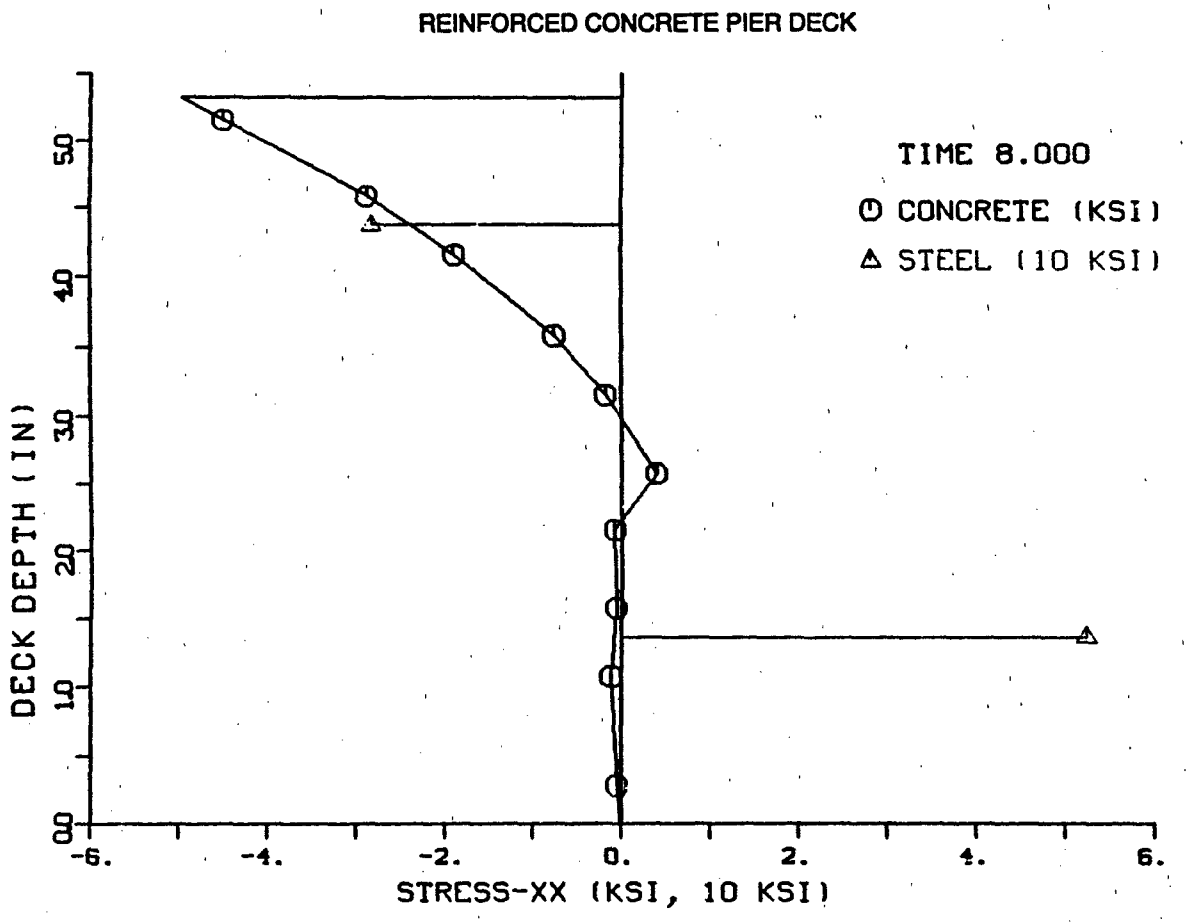

Figure 47. Computed Stress Profile at Center.

Discussion

Load-Deflection Behavior. The computed precracking branch (up to 30 kips) follows the experimental results very closely. Beyond cracking, the finite element model is consistently stiffer (see Figure 38). Three causes may account for this discrepancy. First, the limited amount of stiffness reformations performed around the cracking point may not be sufficient to represent all the cracking that occurs simultaneously. The prescribed relative closeness of load steps 1, 2, and 3 is an attempt at preventing this problem. Second, the low-order isoparametric elements used typically yield a somewhat stiffer response. Third, if the assumed fracture energy is larger than the actual value, the response beyond the cracking point will be stiffer.

At a load of 90 kips (load step 6), the finite element model shows a strong softening of the response. The experimental results show a rapid stiffness degradation under cycling at that same load.

At ultimate, the numerical solution did not converge, and the model was unable to represent the deformation at constant load which preceded brittle failure. The failure load was, however, accurately predicted by the finite element model.

Crack Patterns and Failure Mode. For the deck top, the crack formation in the finite element model simulates very closely the actual patterns (compare Figures 43 and 44 with Figure 39). The higher numerical crack density is due to the assumption of perfect bond between concrete and steel reinforcement. If bond-slip effects were to be simulated, these cracks would merge into fewer, wider cracks, which would be more realistic. Coalescence of the cracks when considering bond-slip effects has been demonstrated (Rots, 1985; RILEM Technical Committee, 1987).

The finite element model also indicates the presence of horizontal cracks under the load, due to the high horizontal compression in the concrete. These cracks could cause failure by delamination of the concrete cover.

The finite element model was able to successfully predict the type of failure, and to show the effects of shear retention on the pier deck response.

Concrete and Steel Strain. Experimental concrete strain readings on the deck top (Figure 41) show a progressive softening with successive load cycles. The finite element results show a similar, though stiffer behavior in the first few steps, and then a sudden softening after step 6. The excess stiffness may be attributed to the use of low-order isoparametric elements, and to a reduced number of stiffness reformations around cracking. The sudden softening after step 6 indicates the formation of a horizontal crack beneath the load, representative of delamination in the compression zone. This is not apparent in the test data. It may be an artifice due in part to the coarse discretization around the load patch, where the entire load is distributed over the surface of only one element.

The finite element tension steel strain prediction forms a reasonably accurate envelope to the maximum experimental readings (Figure 42). The finite element model shows a constrained deformation prior to concrete cracking in tension which is not apparent in the test data. This may be attributed to phenomena which were not modeled such as the prior existence of tension cracks in the concrete due to shrinkage, and to some low load tests (up to 8 kips) carried out initially.

SUMMARY AND CONCLUSIONS

A set of Naval civil-structural engineering problems involving waterfront facilities was considered to demonstrate the appropriateness of advanced three-dimensional structural analyses for the statics and dynamics of large structural/geotechnical systems. A drydock is a primary example of such a facility. There is a continuing Navy requirement to certify ship safety while it is in drydock. Thus, a drydock system is an appropriate subject for the technology demonstration contained in this report. In particular, drydock No. 6 at Puget Sound NSY was selected because it is a relatively modern, fully relieved drydock design having thin wall and thin floor sections. It is therefore a more suitable subject for advanced analysis methods than an older drydock constructed monolithically.

Natural mode shapes and natural frequencies are fundamental to structural dynamics of engineering systems. Previous analyses of Navy drydocks were not three-dimensional, and could not, therefore, predict longitudinal natural modes of vibration. Therefore, a fully three-dimensional finite element model was constructed to determine the natural modes and natural frequencies of the drydock. The results showed that these longitudinal modes are most important because they occur at the low end of the frequency spectrum for drydocks, and are thus more apt to be excited by typical earthquake ground motion. Natural modes, calculated using a two-dimensional model in this study, were generally higher frequency modes. The two-dimensional model clearly does not provide the same richness of information on natural modes of deformation and on dynamic response of drydocks. Further, the closeness of lower longitudinal mode frequencies and frequencies typical of earthquake spectra, indicate that full, three-dimensional dynamic analysis is necessary for investigating earthquake response of drydocks.

Since establishing ship safety is a paramount goal of the Navy's drydock certification program, inclusion of a simple blocked ship model as a substructure model together with the drydock structural model was proposed in this study. A simplified blocked ship model was developed and used to predict the natural mode shapes and natural frequencies as

well as the dynamic response of a blocked submarine subjected to a simulated floor motion excitation. The importance of knowing the drydock floor motion for reliable prediction of the blocked vessel's dynamic response was emphasized.

Measured earthquake-induced drydock floor motion data available to the Navy are scant. The 1987 Whittier-Narrows earthquake excited drydock No. 1 at Long Beach NSY and the induced motion was measured. Analysis of the data indicated that the drydock sustained primarily rigid body motion, and therefore it would not have been exposed to any significant structural action. The drydock did not experience a strong-motion earthquake during this event. Nonetheless, the blocking system supporting a Naval vessel in an adjacent drydock did experience some damage. In general, it is expected that substantial ground motion will induce both dynamic stresses in a drydock, and motion of any blocked vessels. Earthquake analysis procedures supporting drydock certification should therefore consider the interaction between the dynamic response of blocked vessels and the dynamic response of the drydock.

A three-dimensional nonlinear finite element analysis demonstration of a steel drydock caisson substructure has provided new insight into the behavior of forces acting on the door seal due to hydrostatic loads. This behavior is different from that which underlies current caisson design methods, and could improve caisson design methods and maintenance procedures. Further, a natural vibration analysis using the three-dimensional finite element model of the caisson was conducted to suggest how the caisson's vulnerability to earthquake and blast loads could be appropriately investigated with this technology.

A three-dimensional nonlinear finite element model of a reinforced concrete pier deck was developed and employed to demonstrate the accuracy of the technology in predicting the response of the structure to static load. Concrete and steel bars were modeled using a nonlinear concrete constitutive model and a discrete reinforcement model, respectively. Model predictions for the following detailed responses were in good agreement with experimental measurements and observations: monotonic load-displacement history; progressive crack formation and final crack

patterns; progressive stiffness degradation due to cracking; a punching shear failure mode; and concrete and steel strain histories through the deck depth.

Three-dimensional linear and nonlinear finite element technology is appropriate for engineering projects aimed at analysis and design, and aimed at understanding and improving serviceability, vulnerability, and survivability of drydocks and other large structural/geotechnical systems along the waterfront.

ACKNOWLEDGMENTS

Mr. Jim Sullivan and co-workers of the Computer-Aided Design Division, Pacific Missile Test Center (PMTC), Point Mugu, California, participated in the preparation of the two- and three-dimensional finite element models of drydocks. Dr. George Warren of NCEL provided the experimental results for the pier deck scale model.

REFERENCES

ADINA Engineering Incorporated (1985). ADINA User's Manual. Watertown, MA, Dec 1985.

_____ (1987). ADINA: A finite element program for automatic dynamic incremental nonlinear analysis. Watertown, MA, Dec 1987.

American Society of Civil Engineers (1982). State-of-the-art report: Finite element analysis of reinforced concrete, Task Committee on Finite Element Analysis of Reinforced Concrete Structures. New York, NY, 1982.

_____ (1983). Seismic response of buried pipes and structural components, ASCE Committee on Seismic Analysis. New York, NY, 1983.

_____ (1987). The effects of earthquakes on power and industrial facilities and implications for nuclear power plant design, ASCE Committee on Dynamic Analysis. New York, NY, 1987.

Bayo, E. (1983). Numerical techniques for the evaluation of soil-structure interaction effects in the time domain, Ph.D. thesis, University of California. Berkeley, CA, 1983.

Bayo, E. (1987). An evaluation of numerical algorithms for the nonlinear dynamic analysis of large soil structure systems, Naval Civil Engineering Laboratory, CR 88.002. Port Hueneme, CA, Dec 1987.

Bayo, E. and Stubbe, J. (1988). CAL-80 User's Manual, Department of Mechanical Engineering, University of California. Santa Barbara, CA, Sep 1988.

Bazant, Z.P. and Gambarova, P. (1987). "Rough cracks in reinforced concrete," Journal of Structural Engineering, American Society of Civil Engineers, vol 106, no. ST4, Jan 1987, pp 1-19.

Blevins, R.D. (1979). Formulas for natural frequency and mode shape. New York, NY, Van Nostrand Reinhold Co., 1979.

Bowles, J.E. (1977). Foundation analysis and design. New York, NY, McGraw-Hill Book Co., 1977.

CASA/GIFTS,Inc. (1988). GIFTS User's Manual, Release 6.2.8, DOS Version. Tucson, AZ, 1988.

Chelapati, C.V. and Takahashi, S.K. (1982). Evaluation of structural calculations in facility certification report of drydock 3, Mare Island Naval Shipyard, Vallejo, California and detailed structural analysis of drydock 3 using finite element methods, Naval Civil Engineering Laboratory, memorandum to files. Port Hueneme, CA, May 1982.

Clough, R.W. and Penzien, J. (1975). Dynamics of Structures. New York, NY, McGraw-Hill, Inc., 1975.

Craig, R. (1981). Structural dynamics - An introduction to computer methods. New York, NY, John Wiley and Sons, 1981.

Dhatta, S.K., O'Leary, P.M. and Shah, A.H. (1985). "Three-dimensional dynamic response of buried pipelines to incident longitudinal and shear waves," Paper No. 85-WA/APM-13, American Society of Mechanical Engineers (ASME), WAM, Miami, FL, Nov 17-21, 1985.

Furuike, T. (1972). "Computerized multiple level substructuring analysis," Computers and Structures, vol 2, 1972, pp 1063-1073.

Gallagher, R.H. (1975). Finite element analysis fundamentals. Eaglewood Cliffs, NJ, Prentice-Hall, Inc. 1975.

Hepburn, D., Luchs, J.K., Karr, D.G. and Haith, R.L. (1988). "Potential failure of surface ship and submarine drydock blocking systems due to seismic loadings and recommended design improvements," in SNAME, Paper No. 6, Annual Meeting, New York, NY, Nov 2-9, 1988.

Hibbitt, Karlsson and Sorenson, Inc. (1988). ABAQUS User's Manual. Providence, RI, 1988.

Holland, T.J. and Takahashi, S.K. (1984). Analysis of drydock No. 5 at Charleston Naval Shipyard, Naval Civil Engineering Laboratory, memorandum to files. Port Hueneme, CA, Sep 1984.

Jennings, P.C. and Wu, M. (1984). "Effect of embedment on foundation-soil impedances," ASCE Journal of Engineering Mechanics, vol 110, no. 7, July 1984.

Landers, J.A. (1990). A software development specification for nonlinear structural analysis, Naval Civil Engineering Laboratory, CR 90.016. Port Hueneme, CA, Jul 1990.

Lew, T.K. (1988). Personal communication, Naval Civil Engineering Laboratory, Port Hueneme, CA, Dec 1988.

Luco, J. Enrique (1982). "Linear soil-structure interaction: A review," in Earthquake Ground Motion and Its Effects on Structures, Ed. S.K. Dhatta, AMD-vol 53, ASME, New York, NY, Nov 1982.

Malvar, L.J. and Warren, G.E. (1989). Analytical modeling of reinforced concrete in tension, Naval Civil Engineering Laboratory, Technical Report R-926. Port Hueneme, CA, Apr 1989.

Malvar, L.J. and Fourney, M.E. (1990). "A three-dimensional application of the smeared crack approach," Engineering Fracture Mechanics, vol 35, no. 1/2/3, 1990, pp 251-260.

Moffat and Nichol, Engineers (1981). Phase I report: Feasibility study and budget estimate for alterations to drydock No. 3, Volume I, Mare Island Naval Shipyard, Vallejo, California. Long Beach, CA, Aug 1981.

Naval Sea System Command (1984). MIL-STD 1625(SH): Drydocking facilities certification criteria for docking U.S. Navy ships, 31 Aug 1984.

PATRAN, A Division of PDA Engineering (1988). PATRAN Plus User's Manual. Costa Mesa, CA, 1988.

Prime Computer, Inc. (1986). ComputerVision User's Manual. CADDS AX Finite Element Modeling Reference, Revision 5.0. Rockville, MD, 1986.

Przemieniecki, J.S. (1968). Theory of matrix structural analysis. New York, NY, McGraw-Hill Book Company, 1968.

RILEM Technical Committee 90-FMA (1987). Fracture mechanics of concrete, applications, Second draft report over the state-of-the-art, Division of Structural Engineering, Lulea University of Technology, S-951 87. Lulea, Sweden, May 1987.

Rogers, G.L. (1959). Dyanmics of frame structures. New York, NY, John Wiley and Sons, Inc., 1959.

Rots, J. (1985). Bond-slip simulations using smeared cracks and/or interface elements, Delft University of Technology, Structural Mechanics, Department of Civil Engineering, Research Report 85-01. Delft, The Netherlands, Nov 1985.

Seed, H.B. and Whitman, R.V. (1970). "Design of earth retaining structures for dynamic loads," Lateral Stresses in the Ground and Design of Earth Retaining Structures, ASCE, Cornell University. Ithaca, NY, 1970.

Shugar, T.A., Holland, T.J., Malvar, J. and Cox, J.V. (1992). Three-dimensional structural analysis methodology for Navy explosive safety facilities -- A technology assessment, Naval Civil Engineering Laboratory, Technical Note N-____ (in preparation). Port Hueneme, CA (1992).

Stafford, J.W. (1967). "Natural frequencies of beams and plates on an elastic foundation with a constant modulus," Journal of the Franklin Institute, no. 284, 1967, pp 262-264.

Timoshenko, S.P. and Woinosky-Krieger, S. (1959). Theory of plates and shells. New York, NY, McGraw-Hill Book Company, 1959.

URS/John A. Blume and Associates, Engineers (1978). Facility certification report for drydock number 3, Mare Island Naval Shipyard, Vallejo, California. San Francisco, CA, 1978.

Wolf, J.P. (1985). Dynamic soil-structure interaction. Eaglewood Cliffs, NJ, Prentice-Hall, Inc., 1985.

Woodward-Clyde Consultants and Moffat and Nichol Engineers (1979). Facilities certification report, Long Beach Naval Shipyard, drydock no. 1. Los Angeles, CA, Apr 1979.

Wu, A.H., Yachnis, M. and Brooks, E.W. (1984). "Structural analysis of graving drydocks by the finite element method," Fourth International Conference of Applied Numerical Modeling and Computational Mechanics, Taiwan, Dec 28-31, 1984.

Wu, A.H. (1985). "Structural analysis of graving drydocks by the finite element method," NAVFAC Structural Workshop, NBS, Gaithersburg, MD, 20-22 May 1985.

Wu, T.N. (1967). Soil mechanics, Ch. 1, Allyn and Bacon, Inc. Boston, MA, 1967.

Yachnis, M. (1985). "Point paper - Certification of graving docks, marine railways, and vertical lifts," NAVFAC Structural Workshop, NBS, Gaithersburg, MD, 20-22 May 1985.

Zola, S.P. and Boothe, P.M. (1960). "Design and Construction of Navy's Largest Drydock," Journal of the Waterways and Harbors Division, ASCE, vol WW1, Mar 1960.

Appendix A

STRUCTURAL DYNAMICS BIBLIOGRAPHY (BY DATE)

J.W.S. Rayleigh (1896). Theory of Sound. Vol 1, Dover Publications, New York, NY.

K. Hohenemser and W. Prager (1933). Dynamic der Stabwerke. Julius Springer, Berlin, Germany.

G.L. Rogers (1959). Dynamics of Frame Structures. John Wiley and Sons, Inc., New York, NY, 355 p.

J.M. Biggs (1964). Introduction to Structural Dynamics, McGraw-Hill, New York, NY.

W.C. Hurty and M.F. Rubenstein (1964). Dynamics of Structures. Prentice-Hall, Englewood Cliffs, NJ.

L. Meirovitch (1967). Analytical Methods in Vibration. The MacMillan Co., New York, NY, 555 p.

C. Lanczos (1970). The Variational Principles of Mechanics. University of Toronto Press, Toronto, 418 p.

W.T. Thomson (1972). Theory of Vibration With Applications, Prentice-Hall, Englewood Cliffs, NJ, 467 p.

R.D. Cook (1974). Concepts and Applications of Finite Element Analysis. John Wiley and Sons, Inc., New York, NY, 402 p.

R. W. Clough and J. Penzein (1975). Dynamics of Structures. McGraw-Hill, New York, NY, 634 p.

K.-J. Bathe and E. L. Wilson (1976). Numerical Methods in Finite Element Analysis. Prentice-Hall, Inc., Englewood Cliffs, NY, 528 p.

R.D. Blevins (1979). Formulas for Natural Frequency and Mode Shape. Van Nostrand Reinhold Co., New York, NY, 492 p.

Mario Paz (1980). Structural Dynamics Theory and Computation. Van Nostrand Reinhold Co., New York, NY, 446 p.

Roy R. Craig (1981). Structural Dynamics - An Introduction to Computer Methods. John Wiley and Sons, New York, NY, 527 p.

K.-J. Bathe (1982). Finite Element Procedures - Engineering Analysis. Prentice-Hall, Inc., Englewood Cliffs, NJ, 735 p.

T. Belytschko and T.J.R. Hughes (1983). Computational Methods for Transient Analysis. North-Holland, Amsterdam, 523 p.

John P. Wolf (1985). Dynamic Soil-Structure Interaction. Prentice-Hall, Inc., Englewood Cliffs, NJ, 466 p.

Mario Paz (1986). Microcomputer-Aided Engineering Structural Dynamics, Van Nostrand Reinhold Co., New York, NY, 321 p.

T.J.R. Hughes (1987). The Finite Element Method. Prentice-Hall, Inc., Englewood Cliffs, NJ, 803 p.

Appendix B

A BRIEF REVIEW OF SOLIDS MODELING RELATED TO 3-D FINITE ELEMENT MODEL CONSTRUCTION

The wireframe geometric model is the simplest of the modeling schemes and requires no sophisticated finite element preprocessing. In fact, determining the size and distribution of finite elements requires much ingenuity on the part of the analyst. An example of a wireframe modeler is the ComputerVision system. The boundaries of the geometric model are outlined using wireframes. The simplest wireframe element consists of two nodes connected by a line, scaled, and given some spacial orientation. Two or more nodes can occupy the same point in space but in general these wireframe elements have no connection (or connectivity) with other wireframe elements. The amount of time to assemble a geometric model is greatest for the wireframe method since each line has to be individually inserted. Shaded imaging for subsequent visualization requires additional work since surfaces also have to be defined and inserted.

Development of finite element meshes from the wireframe model generally requires additional work. The finite element modeler generates meshes using primitive shapes (i.e., cubes, boxes, cylinders, spheres, etc.). The wireframe model is subdivided into these primitive shapes to facilitate generation of the finite element mesh. Once the shapes or volumes are created, the mesh is developed by defining the number of elements or nodes along the wireframe edges of the primitive shapes. This volume is filled with elements and nodes that have complete connectivity within itself but is otherwise unrelated to other volumes. An adjacent shape is chosen for the next finite element discretization but now, in addition, it requires a strategy on how it connects to the previous volume. The number of nodes (or element projections) on the common surface must match the discretization of the new volume. If the volumes are different sizes (the common surface is only part of the surface of the larger volume), then the wireframe model must be further modified (so that the size of the surfaces matches) or, via a trick, the larger volume must be discretized so that the nodes match up at the common surface. The meshing is not complete, however, because the two volumes with their complete connectivities and matching common surface have no connectivity between themselves. A further step of merging the duplicate nodes (nodes occupying the same point in space) finally establishes a connectivity between the elements on the common surface and, hence, the volumes.

A second scheme is called the surface geometric model. It is a "solid-like" model because it uses solid primitives for assembly. Primitive shapes or volumes (i.e., cubes, boxes, cylinders, and spheres) are used to assemble models of more complicated shapes. These volumes, like

the wireframes, are scaled and given some spacial orientation which do not necessarily have any connectivity among them. With this scheme, the time needed for assembly of a geometric model is significantly decreased and shading for visual effect is straightforward, since surfaces exist naturally with this method.

The finite element mesh generation initially doesn't appear to be any easier than with the wireframe geometric model scheme. The mesh generation is restricted to the primitive volumes. There is some knowledge of the nodes and elements on the surface when working on the adjacent volume so generation of interface transitions is easier. The difficulty lies in the fact that transition meshes have to be created. The mesh generation is constrained at the common surfaces by the fact that the generation is only in the primitive volumes (i.e., nodes must lie on the surfaces). Therefore, the finite element meshes are easier to generate but still rely on generating oddly shaped elements for transition interfaces.

A third scheme is referred to as a true solids geometric model. It has the knowledge of what is solid and what is vacant. Although the assembly of the solid model may be by the use of primitive volumes, the common surfaces and, hence, the common surface restrictions are eliminated. The finite element mesh generation "flows" through the common surfaces (i.e., nodes are not restricted to lie on the common surface), thereby eliminating the use of transition meshes. The finite element mesh generation will be more susceptible to errors since the distribution of elements along the surfaces have to be thought out prior to data input.

Appendix C

SUBSTRUCTURE THEORY

It is convenient to partition a structural model along natural physical subdivisions called substructure models, although the definition of partitions is arbitrary. For example, a drydock may be partitioned as shown in Figure C-1. This figure illustrates the following quantities which are basic to substructure theory: substructures, boundary interface nodes, and interior nodes. There are five substructures constituting the drydock system. Node b is a boundary interface node between contiguous substructures 1 and 2, and node i is internal to substructure 3 which is contiguous only with substructure 2 as shown.

Following Przemieniecki (1968), we have the following vector or column matrix definitions:

$\underset{\sim}{D}_b$ = External displacements of boundary interface nodes between substructures.

$\underset{\sim}{D}_i$ = External displacements of internal nodes of substructures.

$\underset{\sim}{R}_b$ = External forces on boundary interface nodes.

$\underset{\sim}{R}_i$ = External forces on internal nodes.

The stiffness relations for the entire structure expressed in partitioned matrix form are:

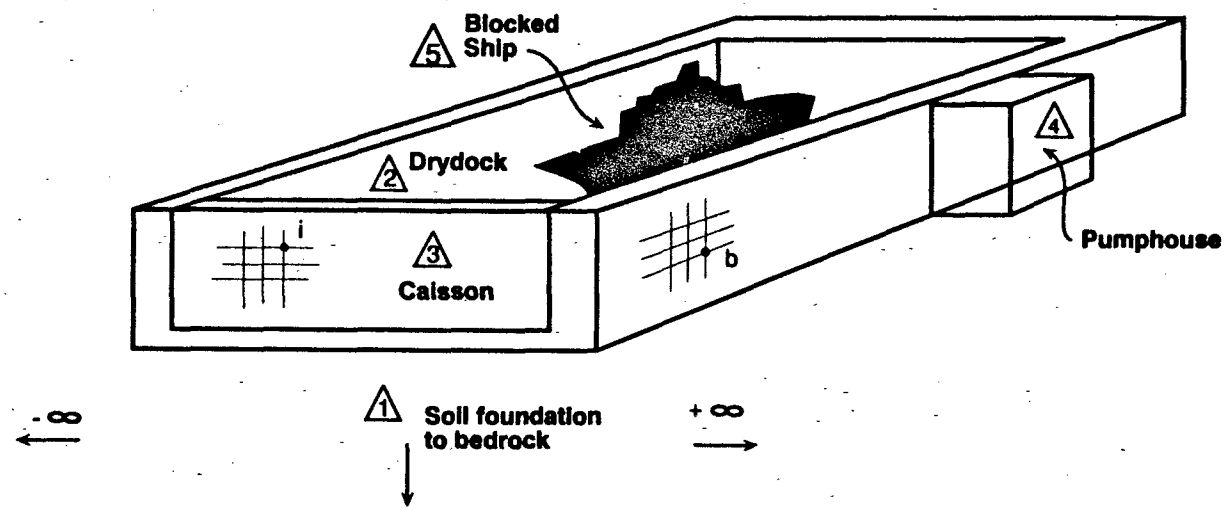

Figure C-1. Substructure Concept for Drydock System.

$$\left[\begin{array}{c|c} \underset{\sim}{K}_{bb} & \underset{\sim}{K}_{bi} \\ \hline \underset{\sim}{K}_{ib} & \underset{\sim}{K}_{ii} \end{array}\right] \left\{\begin{array}{c} \underset{\sim}{D}_b \\ \hline \underset{\sim}{D}_i \end{array}\right\} = \left\{\begin{array}{c} \underset{\sim}{R}_b \\ \hline \underset{\sim}{R}_i \end{array}\right\}$$

or, $\underset{\sim}{K}\ \underset{\sim}{D} = \underset{\sim}{R}$

Substructure analysis is separated into two distinct cases as follows:

I. Fixed boundary analysis, where all boundary interface dof are constrained to zero. The entire structure is subjected to external forces, $\underset{\sim}{R}_i$.

II. Correction analysis, where the boundary interface dof are relaxed. The structure is subjected to forces $(\underset{\sim}{R}_b - \underset{\sim}{R}^I_{br})$, where $\underset{\sim}{R}^I_{br}$ is the vector of boundary interface reaction forces at the artificial constraints, which are computed in Case I.

The total solution is the superposition* of the two solutions:

$$\left\{\begin{array}{c} \underset{\sim}{D}_b \\ \hline \underset{\sim}{D}_i \end{array}\right\}_{\text{Total}} = \left\{\begin{array}{c} \underset{\sim}{0} \\ \hline \underset{\sim}{D}^I_i \end{array}\right\}_{\substack{\text{Fixed} \\ \text{Boundary}}} + \left\{\begin{array}{c} \underset{\sim}{D}_b \\ \hline \underset{\sim}{D}^{II}_i \end{array}\right\}_{\text{Correction}}$$

$$\left\{\begin{array}{c} \underset{\sim}{R}_b \\ \hline \underset{\sim}{R}_i \end{array}\right\}_{\text{Total}} = \left\{\begin{array}{c} \underset{\sim}{R}^I_{br} \\ \hline \underset{\sim}{R}_i \end{array}\right\}_{\substack{\text{Fixed} \\ \text{Boundary}}} + \left\{\begin{array}{c} (\underset{\sim}{R}_b - \underset{\sim}{R}^I_{br}) \\ \hline \underset{\sim}{0} \end{array}\right\}_{\text{Correction}}$$

*If superposition is used within the context of linearized steps of a nonlinear analysis procedure, then substructure theory is also valid for nonlinear analysis.

Considering the n^{th} substructure as a free body (i.e., considering constrained coordinates), and writing the partitioned substructure stiffness relations, we get:

$$\left[\begin{array}{c|c} \underset{\sim}{K}_{bb}^{(n)} & \underset{\sim}{K}_{bi}^{(n)} \\ \hline \underset{\sim}{K}_{ib}^{(n)} & \underset{\sim}{K}_{ii}^{(n)} \end{array}\right] \left[\begin{array}{c} \underset{\sim}{D}_{b}^{(n)} \\ \hline \underset{\sim}{D}_{i}^{(n)} \end{array}\right] = \left[\begin{array}{c} \underset{\sim}{R}_{b}^{(n)} \\ \hline \underset{\sim}{R}_{i}^{(n)} \end{array}\right]$$

By applying the procedure known as static condensation to eliminate the internal dof and retaining the boundary interface dof, we get the substructure stiffness relations (in constrained coordinates),

$$\underset{\sim}{K}_{b}^{(n)} \; \underset{\sim}{D}_{b}^{(n)} = \underset{\sim}{R}_{b}^{(n)}$$

where the substructure stiffness matrix is:

$$\underset{\sim}{K}_{b}^{(n)} = \underset{\sim}{K}_{bb}^{(n)} - \underset{\sim}{K}_{bi}^{(n)} \left(\underset{\sim}{K}_{ii}^{(n)}\right)^{-1} \underset{\sim}{K}_{ib}^{(n)}$$

and reaction forces are:

$$\underset{\sim}{R}_{b}^{(n)} = \underset{\sim}{K}_{bi}^{(n)} \left(\underset{\sim}{K}_{ii}^{(n)}\right)^{-1} \underset{\sim}{R}_{i}^{(n)}$$

The reaction forces may be considered a consistent redistribution of forces $\underset{\sim}{R}_{i}^{(n)}$ to the retained boundary interface nodes, and the substructure stiffness matrix may be considered a super element stiffness matrix. Now, apply the Case I conditions to each substructure, in turn. That is, fix the boundary interface dof, thereby isolating substructure n,

$$\underset{\sim}{D}_{b}^{(n)} = \underset{\sim}{0}$$

and apply any external forces acting on internal nodes $R_{i}^{(n)}$. The corresponding solution for internal displacements is:

$$\underset{\sim}{D}_{i}^{(n)} = \left(\underset{\sim}{K}_{ii}^{(n)}\right)^{-1} \underset{\sim}{R}_{i}^{(n)}$$

Also, the corresponding solution for boundary interface reactions is:

$$\underset{\sim}{R}_{br}^{(n)} = \underset{\sim}{K}_{bi}^{(n)} \left(\underset{\sim}{K}_{ii}^{(n)}\right)^{-1} \underset{\sim}{R}_{i}^{(n)}$$

These reactions are necessary to maintain the constraint condition $\underset{\sim}{D}_{b}^{(n)} = \underset{\sim}{0}$.

The structure stiffness relations expressed in the boundary interface coordinates are obtained by the direct stiffness procedure using the substructure super elements as the basic building blocks. In effect, a substructure is used in the same way as an individual finite element whose internal dof have been statically condensed out (eliminated). Symbolically, the direct stiffness procedure is represented here for N substructures constituting the entire structural system by the expressions:

$$\underset{\sim}{K}_{b} = \sum_{n=1}^{N} \underset{\sim}{K}_{b}^{(n)}$$

and

$$\underset{\sim}{\bar{R}}_{b} = \underset{\sim}{R}_{b} - \sum_{n=1}^{N} \underset{\sim}{R}_{br}^{(n)}$$

where $\underset{\sim}{\bar{R}}_{b}$ is the resultant external force on boundary interface nodes of the structure. The minus sign converts the substructure reaction forces to external forces.

Coupling of substructure stiffness matrices occurs only where substructures have common boundaries (contiguous). In the case of the numbered substructures for the drydock system in Figure C-1, $\underset{\sim}{K}_{b}$ would have the form:

$$\underset{\sim}{K}_b = \begin{bmatrix} (1,1) & (1,2) & \underset{\sim}{0} & (1,4) & \underset{\sim}{0} \\ (2,1) & (2,2) & (2,3) & (2,4) & (2,5) \\ \underset{\sim}{0} & (3,2) & (3,3) & \underset{\sim}{0} & \underset{\sim}{0} \\ (4,1) & (4,2) & \underset{\sim}{0} & (4,4) & \underset{\sim}{0} \\ \underset{\sim}{0} & (5,2) & \underset{\sim}{0} & \underset{\sim}{0} & (5,5) \end{bmatrix}$$

Now, apply the Case II conditions to the structure boundary interface dof as follows:

a. Relax the constraints on the boundary interface nodes, i.e., $\underset{\sim}{D}_b$ becomes unknown.

b. Apply the resultant external force $\bar{\underset{\sim}{R}}_b$ to the boundary interface nodes.

c. Note that $\underset{\sim}{R}_i = \underset{\sim}{0}$ for Case II since the interior nodes are not accessible.

Upon solving the linear system:

$$\underset{\sim}{K}_b \underset{\sim}{D}_b = \bar{\underset{\sim}{R}}_b$$

the total displacements of the structure boundary interface nodes, $\underset{\sim}{D}_b$, are obtained. The values associated with each substructure, $\underset{\sim}{D}_{bi}^{(n)}$ can be picked from $\underset{\sim}{D}_b$ using code numbers for substructure n that are used in the direct stiffness assembly procedure.

The interior node displacements for each substructure can be found from the substructure stiffness relations:

$$\underset{\sim}{K}_{ib}^{(n)}\ \underset{\sim}{D}_{b}^{(n)} + \underset{\sim}{K}_{ii}^{(n)}\ \underset{\sim}{D}_{i}^{(n)} = \underset{\sim}{R}_{i}^{(n)}$$

$$\underset{\sim}{K}_{ii}^{(n)}\ \underset{\sim}{D}_{i}^{(n)} = \underset{\sim}{R}_{i}^{(n)} - \underset{\sim}{K}_{ib}^{(n)}\ \underset{\sim}{D}_{b}^{(n)}$$

$$\underset{\sim}{D}_{i}^{(n)} = \left(\underset{\sim}{K}_{ii}^{(n)}\right)^{-1} \left(\underset{\sim}{R}_{i}^{(n)} - \underset{\sim}{K}_{ib}^{(n)}\ \underset{\sim}{D}_{b}^{(n)}\right)$$

$$\underset{\sim}{D}_{i}^{(n)} = \left(\underset{\sim}{K}_{ii}^{(n)}\right)^{-1}\ \underset{\sim}{R}_{i}^{(n)} - \underset{\sim}{K}_{ii}^{-1}\ \underset{\sim}{K}_{ib}^{(n)}\ \underset{\sim}{D}_{b}^{(n)}$$

Appendix D

EQUIVALENT PLATE THICKNESS FOR A STEEL CAISSON

The caisson for drydock No. 6, Puget Sound NSY, consists of an internal frame cladded with plates stiffened in the long direction. It was decided to develop an equivalent thickness based upon I, the moment of inertia (as a beam) instead of D, the plate stiffness. In determining I, the internal structure is ignored since it is difficult to incorporate the internal structure in a rational way. The stiffened outer shell has been designed to carry the bending along the long direction and is used in establishing the equivalent thickness. The moment of inertia is calculated for this section via the parallel axis theorem using the centerline of the structure. The resulting moments of inertia are given in Table D-1.

Table D-1. Moments of Inertia for Equivalent Plate Thickness

Description	I ($in.^4$)
Shell	652,051
Small Angles	90,476
Large Angle	104,044
Total	846,571

The equivalent I is taken as the total and the thickness is determined by assuming the equivalent solid section to be rectangular. The thickness is calculated as:

$$h^3 = 12I/b = 196,306$$

$$h = 58.1 \text{ inches}$$

DISTRIBUTION LIST

ADINA ENGRG, INC / WALCZAK, WATERTOWN, MA
AFOSR / NA (LT COL L.D. HOKANSON), WASHINGTON, DC
APPLIED RSCH ASSOC, INC / HIGGINS, ALBUQUERQUE, NM
ARMSTRONG AERO MED RSCH LAB / OVENSHIRE, WRIGHT PATTERSON AFB, OH
ARMY CORPS OF ENGRS / HQ, DAEN-ECE-D (PAAVOLA), WASHINGTON, DC
ARMY EWES / WES (NORMAN), VICKSBURG, MS; WES (PETERS), VICKSBURG, MS; WESIM-C (N. RADHAKRISHNAN), VICKSBURG, MS
CATHOLIC UNIV / CE DEPT (KIM), WASHINGTON, DC
CENTRIC ENGINEERING SYSTEMS INC / TAYLOR, PALO ALTO, CA
DOT / TRANSP SYS CEN (TONG), CAMBRIDGE, MA
DTIC / ALEXANDRIA, VA
DTRCEN / (CODE 1720), BETHESDA, MD
GEN MOTORS RSCH LABS / (KHALIL), WARREN, MI
GEORGIA INST OF TECH / MECH ENGRG (FULTON), ATLANTA, GA
HQ AFESC / RDC (DR. M. KATONA), TYNDALL AFB, FL
LOCKHEED / RSCH LAB (M. JACOBY), PALO ALTO, CA; RSCH LAB (P UNDERWOOD), PALO ALTO, CA
MARC ANALYSIS RSCH CORP / HSU, PALO ALTO, CA
MEDWADOWSKI, S. J. / CONSULT STRUCT ENGR, SAN FRANCISCO, CA
NAVFACENGCOM / CODE 04B2 (J. CECILIO), ALEXANDRIA, VA; CODE 04BE (WU), ALEXANDRIA, VA
NORTHWESTERN UNIV / CE DEPT (BELYTSCHKO), EVANSTON, IL
NRL / CODE 4430, WASHINGTON, DC
NSF / STRUC & BLDG SYSTEMS (KP CHANG), WASHINGTON, DC
NUSC DET / CODE 44 (CARLSEN), NEW LONDON, CT
OCNR / CODE 10P4 (KOSTOFF), ARLINGTON, VA; CODE 1121 (EA SILVA), ARLINGTON, VA; CODE 1132SM, ARLINGTON, VA
OHIO STATE UNIV / CE DEPT (SIERAKOWSKI), COLUMBUS, OH
OREGON STATE UNIV / CE DEPT (HUDSPETH), CORVALLIS, OR; CE DEPT (LEONARD), CORVALLIS, OR; CE DEPT (YIM), CORVALLIS, OR; DEPT OF MECH ENGRG (SMITH), CORVALLIS, OR
PORTLAND STATE UNIV / ENGRG DEPT (MIGLIORI), PORTLAND, OR
SCOPUS TECHNOLOGY INC / (B NOUR-OMID), EMERYVILLE, CA; (S. NOUR-OMID), EMERYVILLE, CA
SRI INTL / ENGRG MECH DEPT (GRANT), MENLO PARK, CA; ENGRG MECH DEPT (SIMONS), MENLO PARK, CA
STANFORD UNIV / APP MECH DIV (HUGHES), STANFORD, CA; CE DEPT (PENSKY), STANFORD, CA; DIV OF APP MECH (SIMO), STANFORD, CA
TRW / CARPENTER, SAN BERNARDINO, CA
TRW INC / CRAWFORD, REDONDO BEACH, CA
UNIV OF CALIF DAVIS / CHENEY, DAVIS, CA; SHEN, DAVIS, CA; CE DEPT (HERRMANN), DAVIS, CA; CE DEPT (KUTTER), DAVIS, CA; CE DEPT (ROMSTAD), DAVIS, CA; CE DEPT (WILSON), BERKELEY, CA; CTR FOR GEOTECH MODEL (IDRISS), DAVIS, CA; MECH ENGRG DEPT (BAYO), SANTA BARBARA, CA; MECH ENGRG DEPT (BRUCH), SANTA BARBARA, CA; MECH ENGRG DEPT (LECKIE), SANTA BARBARA, CA; MECH ENGRG DEPT (MCMEEKING), SANTA BARBARA, CA; MECH ENGRG DEPT (MITCHELL), SANTA BARBARA, CA; MECH ENGRG DEPT (TULIN), SANTA BARBARA, CA
UNIV OF COLORADO / CE DEPT (HON-YIM KO), BOULDER, CO; MECH ENGRG DEPT (FELLIPA), BOULDER, CO; MECH ENGRG DEPT (PARK), BOULDER, CO

UNIV OF ILLINOIS / CE LAB (ABRAMS), URBANA, IL; CE LAB (PECKNOLD), URBANA, IL
UNIV OF N CAROLINA / CE DEPT (GUPTA), RALEIGH, NC; CE DEPT (TUNG), RALEIGH, NC
UNIV OF TEXAS / CE DEPT (STPKOE), AUSTIN, TX
UNIV OF WYOMING / CIVIL ENGRG DEPT, LARAMIE, WY
WEBSTER, R / BRIGHAM CITY, UT
WEIDLINGER ASSOC / F.S. WONG, LOS ALTOS, CA

DISTRIBUTION QUESTIONNAIRE

The Naval Civil Engineering Laboratory is revising its primary distribution lists.

SUBJECT CATEGORIES

1 SHORE FACILITIES
1A Construction methods and materials (including corrosion control, coatings)
1B Waterfront structures (maintenance/deterioration control)
1C Utilities (including power conditioning)
1D Explosives safety
1E Aviation Engineering Test Facilities
1F Fire prevention and control
1G Antenna technology
1H Structural analysis and design (including numerical and computer techniques)
1J Protective construction (including hardened shelters, shock and vibration studies)
1K Soil/rock mechanics
1L Airfields and pavements
1M Physical security

2 ADVANCED BASE AND AMPHIBIOUS FACILITIES
2A Base facilities (including shelters, power generation, water supplies)
2B Expedient roads/airfields/bridges
2C Over-the-beach operations (including breakwaters, wave forces)
2D POL storage, transfer, and distribution
2E Polar engineering

3 ENERGY/POWER GENERATION
3A Thermal conservation (thermal engineering of buildings, HVAC systems, energy loss measurement, power generation)
3B Controls and electrical conservation (electrical systems, energy monitoring and control systems)
3C Fuel flexibility (liquid fuels, coal utilization, energy from solid waste)
3D Alternate energy source (geothermal power, photovoltaic power systems, solar systems, wind systems, energy storage systems)
3E Site data and systems integration (energy resource data, integrating energy systems)
3F EMCS design

4 ENVIRONMENTAL PROTECTION
4A Solid waste management
4B Hazardous/toxic materials management
4C Waterwaste management and sanitary engineering
4D Oil pollution removal and recovery
4E Air pollution
4F Noise abatement

5 OCEAN ENGINEERING
5A Seafloor soils and foundations
5B Seafloor construction systems and operations (including diver and manipulator tools)
5C Undersea structures and materials
5D Anchors and moorings
5E Undersea power systems, electromechanical cables, and connectors
5F Pressure vessel facilities
5G Physical environment (including site surveying)
5H Ocean-based concrete structures
5J Hyperbaric chambers
5K Undersea cable dynamics

ARMY FEAP
BDG Shore Facilities
NRG Energy
ENV Environmental/Natural Responses
MGT Management
PRR Pavements/Railroads

TYPES OF DOCUMENTS

D = Techdata Sheets; **R** = Technical Reports and Technical Notes; **G** = NCEL Guides and Abstracts; **I** = Index to TDS; **U** = User Guides; ☐ None - remove my name

Old Address:

_____

_____

_____

_____

Telephone No.: _____

New Address:

_____

_____

_____

_____

Telephone No.: _____

INSTRUCTIONS

The Naval Civil Engineering Laboratory has revised its primary distribution lists. To help us verify our records and update our data base, please do the following:

- Add - circle number on list
- Remove my name from all your lists - check box on list.
- Change my address - add telephone number
- Number of copies should be entered after the title of the subject categories you select.
- Are we sending you the correct type of document? If not, circle the type(s) of document(s) you want to receive listed on the back of this card.

Fold on line, staple, and drop in mail.

DEPARTMENT OF THE NAVY

Naval Civil Engineering Laboratory
Port Hueneme, CA 93043-5003

Official Business
Penalty for Private Use, $300

NO POSTAGE NECESSARY IF MAILED IN THE UNITED STATES

BUSINESS REPLY CARD

FIRST CLASS PERMIT NO. 12503 WASH D.C.

POSTAGE WILL BE PAID BY ADDRESSEE

CODE L34 (J LEDERER)
COMMANDING OFFICER
NAVAL CIVIL ENGINEERING LABORATORY
PORT HUENEME CA 93043-5003

NCEL DOCUMENT EVALUATION

You are number one with us; how do we rate with you?

We at NCEL want to provide you our customer the best possible reports but we need your help. Therefore, I ask you to please take the time from your busy schedule to fill out this questionnaire. Your response will assist us in providing the best reports possible for our users. I wish to thank you in advance for your assistance. I assure you that the information you provide will help us to be more responsive to your future needs.

R. N. STORER, Ph.D, P.E.
Technical Director

DOCUMENT NO. _____ TITLE OF DOCUMENT: _____

_____

Date: _____ Respondent Organization : _____

Name: _____ Activity Code: _____
Phone: _____ Grade/Rank: _____

Category (*please check*):

Sponsor ____ User ____ Proponent ____ Other (*Specify*) _____

Please answer on your behalf only; not on your organization's. Please check (*use an X*) only the block that most closely describes your attitude or feeling toward that statement:

SA Strongly Agree **A** Agree **O** Neutral **D** Disagree **SD** Strongly Disagree

---

		SA	A	N	D	SD
1.	The technical quality of the report is comparable to most of my other sources of technical information.	( )	( )	( )	( )	( )
2.	The report will make significant improvements in the cost and or performance of my operation.	( )	( )	( )	( )	( )
3.	The report acknowledges related work accomplished by others.	( )	( )	( )	( )	( )
4.	The report is well formatted.	( )	( )	( )	( )	( )
5.	The report is clearly written.	( )	( )	( )	( )	( )
6.	The conclusions and recommendations are clear and directly supported by the contents of the report.	( )	( )	( )	( )	( )
7.	The graphics, tables, and photographs are well done.	( )	( )	( )	( )	( )

Do you wish to continue getting NCEL reports? ☐ YES ☐ NO

Please add any comments (e.g., in what ways can we improve the quality of our reports?) on the back of this form.